Received: 25 January 2018 | Accepted: 27 January 2018

DOI: 10.1111/cid.12596

ORIGINAL ARTICLE

WILEY

Biocompatibility and osteoconductivity of PLCL coated and noncoated xenografts: An in vitro and preclinical trial

Yaniv Mayer DMD[1] | Ofir Ginesin DMD MSc[1] | Alaa Khutaba DMD MSc[1] | Eli E. Machtei DMD[1] | Hadar Zigdon Giladi DMD PhD[2]

[1]Department of Periodontics, School of Graduate Dentistry, Rambam Health Care Campus, Haifa, Israel

[2]Lab of Bone Regeneration, Department of Periodontics, School of Graduate Dentistry, Rambam Health Care Campus, Haifa, Israel

Correspondence
Dr Yaniv Mayer, DMD, Department of Periodontics, School of Graduate Dentistry, Rambam Health Care Campus, PO Box 9602, Haifa 31096, Israel.
Email: dr.yaniv.mayer@gmail.com

Abstract

Background: Cells, scaffolds, and growth factors are the key components in bone tissue engineering. Scaffold composition, topography, and architecture influence the amount of regenerated bone in the implantation site. The aims of the study were to compare viability and proliferation of mesenchymal stem cells (MSCs) seeded onto two commercial xenografts: Bio-Oss (BO) and bioactive bone bovine (BB). Next, these materials were compared for histomorphometric bone formation in a socket preservation model in rats.

Materials and Methods: MSCs were seeded onto monolayers of BO or BB granules. Cell viability and proliferation were evaluated after incubation of 0, 2, 20, and 48 h. A total of 24 Sprague Dawley rats underwent unilateral extraction of maxillary molars. Rats were randomly divided into three groups: natural healing (nongrafted socket) or socket preservation with either BO or BB. Rats were sacrificed after 8 weeks, and histomorphometric analysis was done to evaluate bone formation and residual scaffold at the extraction site.

Results: Differences in the metabolic activity of MSCs that were seeded onto BO or BB was observed at 2 h after seeding: the metabolic activity was elevated compared to baseline in the BB ($P = .046$) and not changed in the BO wells ($P = .84$). After 20 h, the metabolic activity of MSCs seeded onto BO was decreasing ($P = .005$), while cell viability was not changed in the BB group ($P = .356$). Intergroup comparison revealed higher metabolic activity of MSCs seeded on BB after 48 h compared with BO ($P = .016$). The in vivo results demonstrated differences in socket healing between the groups: percentage of new bone was higher in the BB compared to BO group (39.1 ± 14.3 vs. $23.7 \pm 10.8\%$, respectively, $P = .096$). Connective tissue portion was higher in the BO group compared with BB (73.7 ± 11.1 vs. $49.6 \pm 13.7\%$, respectively, $P = .018$). Residual grafting martial was higher in the BB (11.34 ± 4.18 vs. $2.62 \pm 1.23\%$, $P = .011$).

Conclusions: The results of this study demonstrating higher vitality and proliferation of MSCs seeded onto BB. Furthermore, following ridge preservation, higher percentage of new bone and lower residual scaffold were found in the BB compared with BO. This enhanced regenerative response might be the result of an enhancement of metabolic activity in cells attached to it. Further research will be needed to understand the precise mechanism.

KEYWORDS

alveolar bone, extraction, mesenchymal stem cells, regeneration, socket preservation, xenograft

1 | INTRODUCTION

Tooth extraction initiates several biological processes that one of the final outcomes is alveolar bone loss.[1,2] The loss occurs on all dimensions of the alveolar bone (ie, buccal, lingual, vertically, and horizontally) and is more prominent in the buccal aspect.[1,2] Changes in bone height may pose difficulties in restoring the function and the aesthetics of the extracted tooth. In order to diminish the rate of the alveolar ridge dimensional changes, several clinical and animal experiments were performed to evaluate the hypothesis that grafting of the socket immediately after tooth removal may represent of an advantages outcome following tooth extraction. There are numerous evidences that socket preservation can reduce the alveolar bone resorption after tooth extraction.[3–5] Multiple materials and methods have been tested with different success rate.[3–5] Today, deproteinized (anorganic) bovine bone is one of the most used biomaterials for socket preservation.[6–9] This extensive use in the different periodontal procedures in general and in socket preservation in particular owed to its large availability and his cost effectiveness compare to other products.

Cells, scaffolds, and growth factors are the key components required to generate engineered tissues. A scaffold can deliver growth factors and supports cell attachment. The material composition, topography, and architecture influence cell behavior and intercellular interactions and overall performance of the scaffolds including the angiogenesis and degradation rate. New xenograft-based material was introduced, with scaffold modification, cover by poly(L-lactide-co-ε-caprolactone) (PLCL) and polysaccharides.[10] The properties of this new xenograft suggest better cell adhesion[10] and as such may provide better outcomes in preserving bone after tooth extraction, compared to the current xenograft materials that are in use. Mesenchymal stem cells (MSCs) contribute to the maintenance of various tissues, especially bone, in adults.[11] Previous animal studies showed that transplantation of MSCs formed ectopic bone and improved healing of bone defects.[12,13]

Hence, the first aim of the present study was to compare the viability and proliferation of MSCs onto two commercial xenografts (with or without PLCL coating). The second aim was to compare the histomorphometric bone formation in a socket preservation model in rats. Our hypothesis is that PLCL coating of xenograft will increase MSCs' adherence to the scaffold in vitro and, therefore, stimulate bone formation in a rat extraction socket model.

2 | MATERIALS AND METHODS

2.1 | In vitro assay

To investigate cell proliferation on the examined scaffolds, MSCs were seeded on a monolayers of (BB) (Alpha Bio's Graft, Bioactive Bone; Industrie Biomediche Insubri SA, Mezzovico-Vira, Switzerland) or (BO) (Bio-Oss; Geistlich Pharma, Wolhusen, Switzerland) that covered the bottom of 96-well plates. Both materials were used with the same granules size (0.25-1 mm granules). Human MSCs were isolated and characterized as previously described.[14] A total of 3×10^3 bone marrow-derived human MSCs were suspended in DMEM (Sigma-Aldrich, Munich, Germany) and dripped (50 μl) over the granules layer. Cell proliferation kit (XTT) (Sigma-Aldrich) was used to quantify cell growth, viability, and proliferation after 0, 2, 20, and 48 h of incubation. The assay was performed twice in triplicates. Absorbance of the wells containing the cells (indicating on cell metabolic activity) and the blank background control wells were investigated at 450–500 nm wave length using a microtiter plate reader (BioTek, Winooski, Vermont).

2.1.1 | Fluorescent assay

Cells were labeled with fluorescent DII stain (D282; Thermo Fisher Scientific, Waltham, Massachusetts) and seeded onto BB or BO scaffolds. Twenty-four hours later, scaffolds without cells and scaffold loaded with cells were observed under a fluorescent microscope (Nikon eclipse TsTR).

2.2 | In vivo assay

The study protocol was approved by the Committee for the Supervision of Animal Experiments at the Faculty of Medicine, Technion, IIT (approval # B126111010).

A total of 24 Sprague-Dawley rats (300 g) were used. The rats were allowed to acclimate for 1 week before the first procedure.

Rats were anesthetized with isoflurane inhalation followed by intramuscular injection of ketamine (Ketaset, Fort Dodge, Iowa) (10 mg/100 g body weight) and xylazine. In addition, local anesthesia (2% lidocaine with epinephrine in the ratio of 1:100 000) was infiltrated to the surgical site (Figure 1A). Two right maxillary molars were extracted (Figure 1B), and the sockets of both molars were connected using a diamond bur with copious saline irrigation. Rats were randomly assigned using a designated allocation chart to one of the following three groups (eight rats in each group):

1. Experimental group (BB): the socket was grafted with coated bovine bone (Figure 1C).
2. Positive control (BO): the socket was grafted with uncoated bovine bone.
3. Negative control (NC): the socket was left to natural healing.

Flaps were coronally positioned to achieve primary closure and sutured using resorbable vicryl 5-0 sutures (Figure 1D). Postoperative treatment included buprenorphine (0.01 mg/kg) subcutaneously for 3 days.

The rats were housed and given water and solid diet until sacrificed. The rats were sacrificed 8 weeks postoperation with CO_2 inhalation. The right maxilla of each rat was retrieved for histological analysis.

2.2.1 | Histological preparation

All specimens were fixed in 4% paraformaldehyde for 2 days, decalcified in 10% EDTA, for 4 weeks, and cut into two halves in the midline. The water within the samples was removed by dehydration; the samples were washed in ethanol baths (in increasing concentrations) in order to remove residual water. This was followed by a hydrophobic clearing agent (Xylol) to remove the alcohol content. After the samples were dehydrated, cleared, and infiltrated with Paraffin wax, they

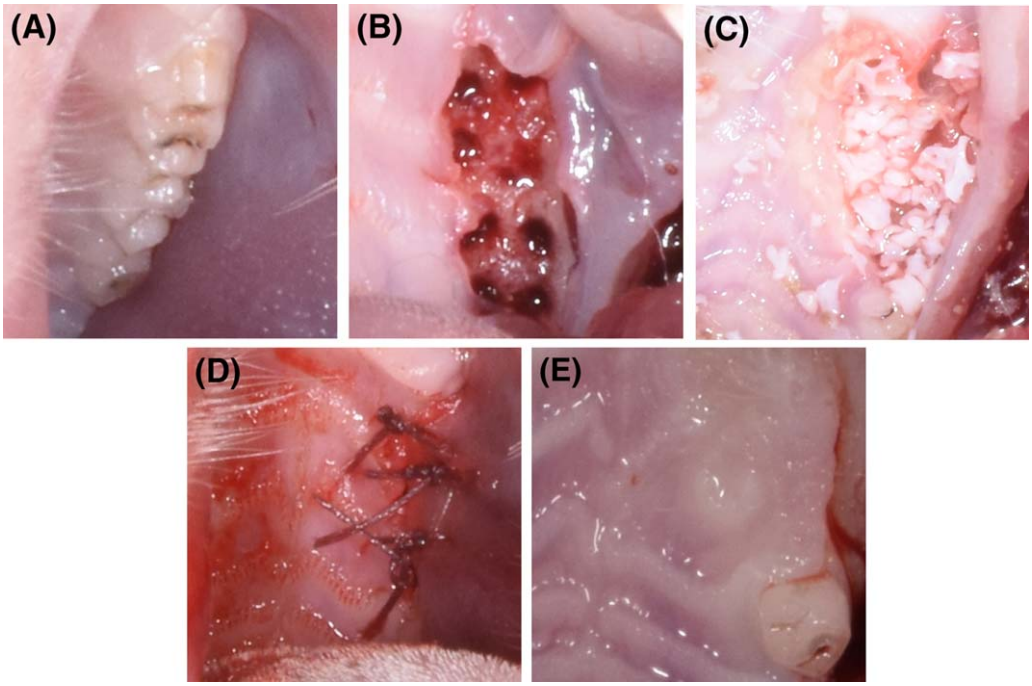

FIGURE 1 Clinical macroscopic view of the surgical procedure and healing. (A) Maxillary molars before extraction. (B) Extraction sockets of M1 + M2. (C) Filling the defect with xenograft. (D) Sutures for primary closure. (E) Healing of extraction and ridge preservation site, 8 weeks after surgical treatment

undergo external embedding. For light microscopy, the samples were sectioned using a steel knife mounted in a microtome (Leica RM 2135, Jung RM 2065; Leica Microsystems, Wetzlar, Germany) to a thickness of 8 μm and the sections were mounted on a glass microscope slides using paraffin section mounting bath (Electron Microscopy Sciences, Hatfield, England). For the determination of bone morphology, the mounted sections were stained with: hematoxylin and eosin and Masson's trichrome.

2.2.2 | Histomorphometric analysis

Histomorphometric evaluation of the socket preservation region was performed from each specimen, under a light microscope (Zeiss Axioskop; Carl Zeiss, Jena, Germany). Images were analyzed using software (ImageJ; National Institutes of Health, Bethesda, MD). The following values were measured: (1) total bone area, (2) connective tissue, and (3) residual bone graft. The measurements were expressed as percentages of the total sample area.

2.2.3 | Statistical analysis

To compare between the group regarding the metabolic activity and histomorphometric parameters, one-way analysis of variance was used. A *P*-value of $<.05$ was selected to determine statistical significance.

3 | RESULTS

3.1 | In vitro

Two hours after MSCs seeding onto the scaffold, the metabolic activity was not changed (compared to baseline) in the BO wells (0.277 ± 0.06, $P = .84$). However, in the BB, the metabolic activity was elevated significantly (0.359 ± 0.06, $P = .046$). A similar trend was observed after 20 h: the metabolic activity of MSCs seeded onto BO was decreasing significantly (0.144 ± 0.01, $P = .005$), while cell viability was not changed in the BB group (0.289 ± 0.1, $P = .356$). Forty-eight hours following incubation, metabolic activity continued to decrease in the BO group (0.129 ± 0.01, $P = .03$), whereas cells seeded onto BB presented increased metabolic activity (0.329 ± 0.08, $P = .12$). Intergroup comparison revealed higher metabolic activity of MSCs seeded on BB compared to BO after 20 h ($P = .08$) and after 48 h ($P = .016$) (Table 1).

3.1.1 | Fluorescent assay

Cells were dispersed over both scaffolds with a higher cell density on BB (Figure 2A,B)

3.2 | In vivo

No surgical complications were reported. All rats survived to the end of the study. Rats tolerated the surgical procedure and gained weight (Figure 1E). Six extraction sockets healed with secondary intention.

TABLE 1 Metabolic activity (fluorescent units) of bone-marrow derived human MSCs seeded on the scaffolds

Group	2 h	20 h	48 h
BB	0.359 ± 0.06	0.289 ± 0.1	0.329 ± 0.08
BO	0.277 ± 0.06	0.144 ± 0.01	0.129 ± 0.01
P value, BB vs BO at each time point	NS	.08	.016

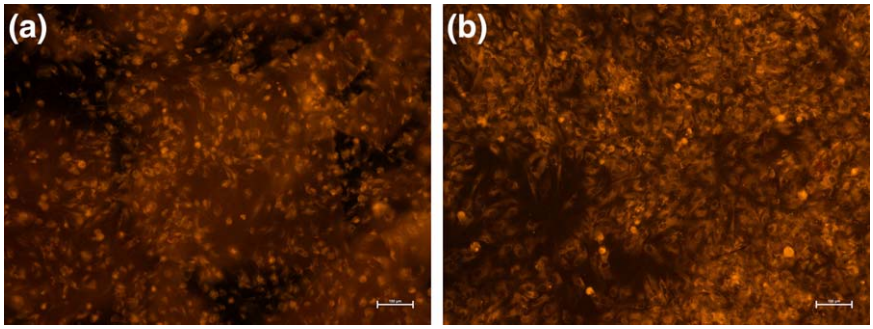

FIGURE 2 Adhesion of MSCs over BO scaffold (A) and BB scaffold (B)

3.2.1 | Histology

Histological sample from BO and BB groups presented direct contact between the residual bone substitutes and the newly formed bone, suggesting that the both xenografts have osteoconductive properties. The newly formed bone was vital and vascularized (Figure 3A,B).

3.2.2 | Histomorphometric analysis

Results for each type of treatment after 8 weeks of healing are presented in Table 2.

The amount of newly formed bone was 39.06 ± 14.26, 23.7 ± 10.77, and 48.86 ± 12.84% for BB group, BO group, and negative control group, respectively. The statistical comparison regarding the three different treatment modalities is presented in Table 3. Statistically significant difference was found between the negative control and BO group ($P = .021$), and borderline statistically significance was found between BB and BO group ($P = .096$). No statistical difference was found between BB and control ($P = .291$).

The amount of residual graft was significantly higher in the BO compared with BB groups (11.34 ± 4.17 vs. 2.62 ± 1.23%, respectively, $P = .011$).

The percentage of the connective tissue was 49.6 ± 13.67, 73.68 ± 11.05, and 51.14 ± 12.84 in the BB group, BO group, and negative control group, respectively. Comparison between the groups revealed statistically significant difference between BO and control ($P = .012$) and between BB and BO ($P = .018$), and no statistical difference was found between BB and negative control ($P = .86$).

4 | DISCUSSION

In the present study, we compared biocompatibility and osteoconductivity of two commercial xenograft scaffolds. According to the results, xenograft that was reinforced with PLCL showed superior in vitro and in vivo results. MSCs that were seeded on the PLCL reinforced xenograft showed higher viability and proliferation compared with the noncoated xenograft.

Socket preservation has been proven to be effective in reducing the bone loss postextraction.[15] Still studies report on bone resorption on all aspect with a range of 11–22% on vertical dimension and 29–63% on the horizontal dimension depends on the material and method of the preservation.[16] Currently, ideal grafting material is yet to be found. Xenograft is one of the most used materials that is in use for socket preservation, and it is biocompatible and osteoconductive. Two major flaws of the xenograft that are widely used are the poor cell adhesion[17] and different clinical behaviors depending on source.[18] Coating the xenograft scaffold might enhance cell adhesion and further maintain the bone volume after tooth extraction. Our findings further strengthen previous material characterization of PLCL reinforcement that was published.[10] Pertici and colleagues[10] showed that coating xenografts with degradable synthetic [PLCL] and natural (polysaccharides) polymers has increased their mechanical properties. Furthermore, PLCL coating was shown to improve cell adhesion due to improved hydrophilicity.

According to the in vitro results, MSCs adhere better to the PLCL-reinforced xenograft (BB) in comparison to the noncoated xenograft

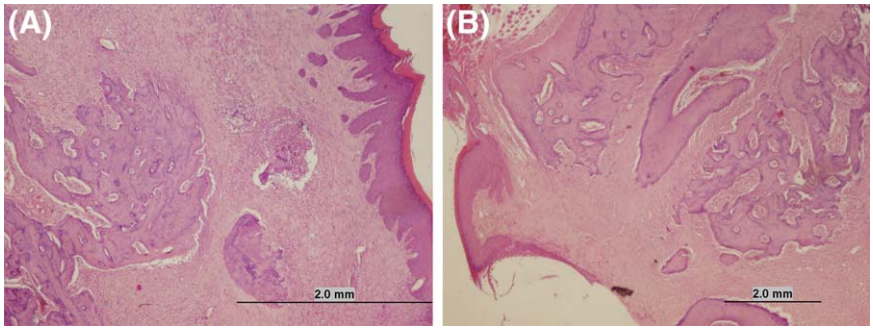

FIGURE 3 Histological sections of sockets grafted with BO scaffold (A) and BB scaffold (B). H&E staining

TABLE 2 Histomorphometric analysis (% total sample area, mean ± SD)

Group	% bone	% connective tissue	% residual graft
BB	39.06 ± 14.26**	49.6 ± 13.67*	11.34 ± 4.17*
BO	23.7 ± 10.77‡,**	73.68 ± 11.05*,‡	2.62 ± 1.23*
Negative control	48.86 ± 12.84‡	51.14 ± 12.84‡	–

*BB-BO $P < .05$.
**BB-BO $P < .1$.
‡BO-NC $P < .05$.

(BO). Furthermore, cells' viability and proliferation were higher when seeded on PLCL-reinforced xenograft. Since MSCs play a critical role in new bone formation,[19] the adherence and viability of MSCs to the scaffold may influence the amount of new bone formed in the implantation site. Previous studies prove the ability of MSCs to stimulate new bone formation in cases of bone loss,[20] and bone regeneration.[21] Indeed, the in vivo and in vitro results were in agreement as higher bone formation was found in the BB group compared to the BO group. Further studies are needed to explore the exact mechanism of bone formation around xenograft with PLCL coating.

Implantation of PLCL coated and noncoated xenograft into bone defect in a ridge preservation rat model showed that the extraction socket was filled with new bone, connective tissue, and residual graft. The ratio between these elements was different between the groups. Previous studies that used BO for ridge preservation demonstrated similar results.[22,23] A comparison between BO and BB revealed higher bone formation with lower percentage of connective tissue and residual scaffold in the BB group. These results can be attributed to the greater biocompatibility of the PLCL reinforced xenograft as well as to faster degradation of the scaffold. A previous study[10] found that the PLCL coating accelerates scaffold degradation and is in positive correlation to the thickness of the coating.

Vascularization and oxygenation are important process in order to create new bone formation.[24] Percentage of new bone formation was higher in the BB group compared to the BO group. This fact may be attributed to the large pores of the BB[10] that favor direct osteogenesis, as they allow vascularization and high oxygenation. Further studies are required to validate this assumption.

Secondary healing was found in six of the 24 animals. This phenomenon can be attributed to the flap design.[25] We did not raise the flap or vertical releasing incisions; thus, the primary closure might have had tension and was not passive. Another possible reason is the heat produced during the use of the bar although constant water irrigation was done. Previous studies[26–28] showed that excessive heat can harm the osteoblast.[28] Heating to 47°C for 1 min caused significantly reduced bone formation,[27] and this temperature or even higher one can be achieved by rotating dental cutting instruments.[26] We cannot exclude other causes as inflammatory reaction[29] due to the higher prevalence of secondary healing in the test and positive control groups compared to the negative control groups (only one in the latter out of all the cases).

TABLE 3 Comparison between groups—*P*-value (ANOVA)

Group	% bone	% connective tissue	% residual graft
BB/BO	0.096	**0.018**	**0.011**
BO/NC	**0.012**	**0.012**	–
BB/NC	0.291	0.88	–

Significant values in bold. $P < 0.05$.

This study has some limitations in terms of the relatively small sample size. Moreover, socket size in rat even though two of them were connected is still small volume that fact together with small amount of xenograft that was placed inside the defect might mask or lower some of the outcomes.

5 | CONLUSIONS

The results of this study demonstrating higher vitality and proliferation of MSCs seeded onto PLCL-coated xenograft (BB) compared with commonly used noncoated xenograft (BO). Furthermore, the greater percentiles of new bone formation with fewer residual scaffolds in the BB group would suggest potentially better regenerative capacity for the PLCL-coated xenografts. Further studies will be necessary to fully understand this mechanism.

ACKNOWLEDGMENT

We would like to thank Prof Samer Srouji, Galilee Medical Center, Nahariya, for kindly providing the bone-marrow-derived human MSCs.

CONFLICT OF INTEREST

The authors declare that they do not have conflict of interest regarding the present study. The study was supported by an educational grant from the Alpha Bio Tec Ltd. The funders had no role in the study design, data collection and analysis; decision to publish; or preparation of the manuscript.

ORCID

Yaniv Mayer DMD http://orcid.org/0000-0001-5500-7961

REFERENCES

[1] Van der Weijden F, Dell'Acqua F, Slot DE. Alveolar bone dimensional changes of post-extraction sockets in humans: a systematic review. *J Clin Periodontol*. 2009;36(12):1048–1058.

[2] Tan WL, Wong TL, Wong MC, Lang NP. A systematic review of post-extractional alveolar hard and soft tissue dimensional changes in humans. *Clin Oral Implants Res*. 2012;23(suppl 5):1–21.

[3] MacBeth N, Trullenque-Eriksson A, Donos N, Mardas N. Hard and soft tissue changes following alveolar ridge preservation: a systematic review. *Clin Oral Implants Res*. 2017;28(8):982–1004.

[4] Iocca O, Farcomeni A, Pardiñas Lopez S, Talib HS. Alveolar ridge preservation after tooth extraction: a Bayesian Network meta-

analysis of grafting materials efficacy on prevention of bone height and width reduction. *J Clin Periodontol*. 2017;44(1):104–114.

[5] Horváth A, Mardas N, Mezzomo LA, Needleman IG, Donos N. Alveolar ridge preservation. A systematic review. *Clin Oral Investig*. 2013;17(2):341–363.

[6] Avila-Ortiz G, Elangovan S, Kramer KW, Blanchette D, Dawson DV. Effect of alveolar ridge preservation after tooth extraction: a systematic review and meta-analysis. *J Dent Res*. 2014;93(10):950–958.

[7] Scheyer ET, Heard R, Janakievski J, et al. A randomized, controlled, multicentre clinical trial of post-extraction alveolar ridge preservation. *J Clin Periodontol*. 2016;43(12):1188–1199.

[8] Araújo MG, Liljenberg B, Lindhe J. Dynamics of Bio-Oss collagen incorporation in fresh extraction wounds: an experimental study in the dog. *Clin Oral Implants Res*. 2010;21(1):55–64.

[9] Lindhe J, Cecchinato D, Donati M, Tomasi C, Liljenberg B. Ridge preservation with the use of deproteinized bovine bone mineral. *Clin Oral Implants Res*. 2014;25(7):786–790.

[10] Pertici G, Carinci F, Carusi G, Epistatus D, Villa T, Crivelli F, Rossi F, Perale G. Composite polymer-coated mineral scaffolds for bone regeneration: from material characterization to human studies. *J Biol Regul Homeost Agents*. 2015;29(3 suppl 1):136–148.

[11] Fridenshteĭn A. I A, Piatetskiĭ-Shapiro II, Petrakova KV. Osteogenesis in transplants of bone marrow cells. *Arkh Anat Gistol Embriol*. 1969;56(3):3–11.

[12] Petite H, Viateau V, Bensaïd W, et al. Tissue-engineered bone regeneration. *Nat Biotechnol*. 2000;18(9):959–963.

[13] Bruder SP, Kraus KH, Goldberg VM, Kadiyala S. The effect of implants loaded with autologous mesenchymal stem cells on the healing of canine segmental bone defects. *J Bone Joint Surg Am*. 1998;80(7):985–996.

[14] Costa-Pinto AR, Correlo VM, Sol PC, et al. Chitosan-poly(butylene succinate) scaffolds and human bone marrow stromal cells induce bone repair in a mouse calvaria model. *J Tissue Eng Regen Med*. 2012;6(1):21–28.

[15] Mayer Y, Zigdon-Giladi H, Machtei EE. Ridge preservation using composite alloplastic materials: a randomized control clinical and histological study in humans. *Clin Implant Dent Relat Res*. 2016;18(6):1163–1170.

[16] Hämmerle CH, Araújo MG, Simion M, Osteology Consensus Group 2011. Evidence-based knowledge on the biology and treatment of extraction sockets. *Clin Oral Implants Res*. 2012;23(suppl 5):80–82.

[17] Tabatabaei FS, Samadi R, Tatari S. Surface characteristics of three commercially available grafts and adhesion of stem cells to these grafts. *Biomed Mater Eng*. 2017;28(6):621–631.

[18] Meng S, Zhang X, Xu M, et al. Effects of deer age on the physicochemical properties of deproteinized antler cancellous bone: an approach to optimize osteoconductivity of bone graft. *Biomed Mater*. 2015;10(3):035006.

[19] Zigdon-Giladi H, Rudich U, Michaeli Geller G, Evron A. Recent advances in bone regeneration using adult stem cells. *World J Stem Cells*. 2015;7(3):630–640.

[20] Yao W, Guan M, Jia J, et al. Reversing bone loss by directing mesenchymal stem cells to bone. *Stem Cells*. 2013;31(9):2003–2014.

[21] Lin T, Pajarinen J, Nabeshima A, et al. Preconditioning of murine mesenchymal stem cells synergistically enhanced immunomodulation and osteogenesis. *Stem Cell Res Ther*. 2017;8(1):277.

[22] Kuchler U, Keibl C, Fügl A, et al. Dimethyloxalylglycine lyophilized onto bone substitutes increase vessel area in rat calvarial defects. *Clin Oral Implants Res*. 2015;26(5):485–491.

[23] Araújo MG, Lindhe J. Ridge preservation with the use of Bio-Oss collagen: a 6-month study in the dog. *Clin Oral Implants Res*. 2009;20(5):433–440.

[24] Carlier A, Geris L, van Gastel N, Carmeliet G, Van Oosterwyck H. Oxygen as a critical determinant of bone fracture healing—a multiscale model. *J Theor Biol*. 2015;365:247–264.

[25] Plonka AB, Sheridan RA, Wang HL. Flap designs for flap advancement during implant therapy: a systematic review. *Implant Dent*. 2017;26(1):145–152.

[26] Hudson DC, Sweeney WT. Temperatures developed in rotating dental cutting instruments. *J Am Dent Assoc*. 1954;48(2):127–133.

[27] Eriksson RA, Albrektsson T. The effect of heat on bone regeneration: an experimental study in the rabbit using the bone growth chamber. *J Oral Maxillofac Surg*. 1984;42(11):705–711.

[28] Li S, Chien S, Brånemark PI. Heat shock-induced necrosis and apoptosis in osteoblasts. *J Orthop Res*. 1999;17(6):891–899.

[29] Girard B, Baker G, Mock D. Foreign body granuloma following placement of hard tissue replacement material: a case report. *J Periodontol*. 2000;71(3):517–520.

How to cite this article: Mayer Y, Ginesin O, Khutaba A, Machtei EE, Zigdon Giladi H. Biocompatibility and osteoconductivity of PLCL coated and noncoated xenografts: An in vitro and preclinical trial. *Clin Implant Dent Relat Res*. 2018;20:294–299. https://doi.org/10.1111/cid.12596

COMPOSITE POLYMER-COATED MINERAL SCAFFOLDS FOR BONE REGENERATION: FROM MATERIAL CHARACTERIZATION TO HUMAN STUDIES

G. PERTICI[1], F. CARINCI[2], G. CARUSI[3], D. EPISTATUS[4], T. VILLA[5,6], F. CRIVELLI[7], F. ROSSI[8] and G. PERALE[1,9]

[1]Industrie Biomediche Insubri SA, Mezzovico-Vira, Switzerland; [2]Department of Morphology, Surgery and Experimental Medicine, University of Ferrara, Ferrara, Italy [3]Private practice, Ponsacco, Italy; [4]Universitatea de Medicina si Farmacie "Carol Davila", Bucharest, Romania; [5]Politecnico di Milano, Laboratory of Biological Structure Mechanics, Department of Chemistry, Materials and Chemical Engineering "G. Natta", Milan, Italy; [6]IRCCS Istituto Ortopedico Galeazzi, Milan, ltaly; [7]Azienda Ospedaliera di Circolo, Busto Arsizio, Italy; [8]Politecnico di Milano, Physical Chemistry Laboratory, Department of Chemistry, Materials and Chemical Engineering "G. Natta", Milan, Italy; [9]Department of innovative Technologies, University for Applied Science and Art of Southern Switzerland, Manno, Switzerland

Bovine bone xenografts, made of hydroxyapatite (HA), were coated with poly(L-lactide-co-ε-caprolactone) (PLCL) and RGD-containing collagen fragments in order to increase mechanical properties, hydrophilicity, cell adhesion and osteogenicity. *In vitro* the scaffold microstructure was investigated with Environmental Scanning Electronic Microscopy (ESEM) analysis and micro tomography, while mechanical properties were investigated by means compression tests. In addition, cell attachment and growth within the three-dimensional scaffold inner structure were validated using human osteosarcoma cell lines (SAOS-2 and MG-63). Standard ISO *in vivo* biocompatibility studies were carried out on model animals, while bone regenerations in humans were performed to assess the efficacy of the product. All results from *in vitro* to *in vivo* investigations are here reported, underlining that this scaffold promotes bone regeneration and has good clinical outcome.

Evidence of clinical needs related to bone reconstruction dates back to ancient Egypt. A more rigorous scientific approach has been followed since 1889, when "modern" scientists started to focus their efforts on what can be defined as the early bone tissue engineering (1). In the wide framework of reconstructive orthopedics, a primary role is played by critical-sized bone defects, which are a large disruption, either a fracture or a hole, typically resulting from severe injuries or traumas, that cannot spontaneously heal because of their size and site (2-4). Both functional and aesthetical reasons make oral and maxillo-facial restorations critical operations: indeed, bone loss due to trauma, infection, or tumor and congenital deformity still remain heavy challenges for surgeons (5, 6).

Hence, the need of adequate bone substitutes for the remodeling of native bone tissue is evident and covers a wide spectrum of proposed solutions, belonging to academia, clinics and industry (7-9).

Key words: bone, cell growth, oral surgery, scaffold, tissue engineering

Mailing address: Prof. Francesco Carinci, Department of Morphology, Surgery and Experimental Medicine, University of Ferrara, Via Luigi Borsari 46, 44100 Ferrara, Italy
e-mail: crc@unife.it
Tel.: +39 0532 455874
Fax: +39 0532 455876

0393-974X (2015)

DISCLOSURE: ALL AUTHORS REPORT NO CONFLICTS OF INTEREST RELEVANT TO THIS ARTICLE.

The current clinical gold standard for treatment of critical sized and non-union bone defects still remain distraction osteogenesis and autograft bone: in particular, autografts are commonly considered the best option to restore defects in oral surgery (10, 11). Although advantageous for immunocompatibility and their self-evident capability to strongly support osteogenesis, osteoinduction and osteoconduction, autografts nevertheless carry a wide spectrum of risks (general anesthesia, second surgical field, infections, fractures, pain, etc.). In addition, there is quite a high percentage of failure (more than 20%); moreover, high costs increase the related to time of surgery (12). Furthermore, larger defects cannot be corrected by harvesting bone from the patient donor site, at least without morbidity in the second surgical field. These major drawbacks have led to the necessity of new methods for bone tissue regeneration (13-15) and today surgeons can choose from substitutes that can be divided into 3 main categories: i) allografts, *i.e.* bone segments taken from cadavers and duly deantigenized sterilized; ii) xenografts, *i.e.* bone segments taken from animal bones, duly processed and sterilized; and iii) synthetic scaffolds and biomaterials.

Allografts derived from cadavers bone have been an accepted alternative, but concerns related to disease transmission, immunologic rejection risks and very high sample variability are progressively leading to other alternatives, when these are available (16). The current focus and major research trends, thus, are on xenografts *vs* synthetic devices (4): naturally-derived materials provide structures extremely similar to living tissues, such as stimulating a specific cellular response, which sometimes supersedes the advantages of synthetic polymers (17, 18). Xenografts may also reduce the stimulation of chronic inflammation or immunological reactions and toxicity, often detected with synthetic polymers and minerals (such as *e.g.* bioglasses and bioceramics) (17-19).

On the other hand, material science, in conjunction with bio- and nano-technologies, can satisfy these requirements by developing novel grafting devices (8, 20, 21). In particular, bioresorbable scaffolds, as key artificial devices widely used in tissue engineering, aim to provide a desirable microenvironment that allows neo-tissue to be generated properly for repairing and replacing damaged tissues or organs (22, 23). Indeed, synthetic polymers can be tuned in terms of composition, rate of degradation, mechanical and chemical properties (17, 19). As a fundamental premise in tissue engineering, polymeric scaffold should provide: (a) host tissue-like mechanical support for promoting neo-tissue ingrowth and functioning (24); (b) adequate porosity and permeability for nutrient delivery and metabolite removal (25); and (c) controllable degradation rate of scaffolding matrix to allow proper substitution with natural functional new tissues (26). Significant progress in tissue engineering could yield more favorable outcomes than the current range of approaches used to repair bone defects (3, 10, 27).

For all these reasons, the goal of our approach was to combine the biocompatibility and tissue integration of natural materials with the possibility to tune mechanical and physical properties typical of synthetic ones: composite grafts best mimic the real nature of healthy human bone, being rigid and elastic, compact but porous, dense but viable to cells and vessels. A newly developed bone substitute, named SmartBone® (briefly SB), was designed following a new concept of bottom-up composite approach, starting from bovine bone-derived mineral matrix, reinforced with bioresorbable aliphatic polymers and RGD-containing collagen fragments as cell nutrients (28, 29).

The bovine-derived matrix is mineral and mainly made of calcium hydroxyapatite (HA, $Ca_5(PO_4)_3(OH)$) that presents a chemical structure and a morphology resembling human bone (30, 31). However, its physical properties have a rigid but not elastic structure, which makes it too fragile. In addition, sterilization processes destroy its natural porous structure, widening it further than natural limits, and does not consent either easy graft manufacturing or cell adhesion. For these reasons bovine structure was reinforced with the addition of an elastic component in terms of polymer coating, thus losing the fragility and reducing porosity to resemble healthy human bones (32). Finally, the addition of RGD-containing collagen fragments, increases the cell viability and hydrophilicity of the scaffold with consequent higher cell attachment, thus enhancing biocompatibility and osteointegration (7, 29, 32). The scaffold produced was firstly characterized in terms of chemistry, microstructure and physical

properties. Then material biocompatibility and suitability as cell growth matrix were studied *in vitro* with SAOS-2 and MG-63 cells. Animal implantation studies, on New Zealand white rabbits (33), and advanced biocompatibility tests were performed according to ISO10993 specifications. Lastly, human studies were performed on critical-sized maxillary and mandibular bone defects to verify SB suitability as scaffold for bone tissue engineering.

MATERIALS AND METHODS

Materials and scaffold preparation

The bovine-derived cancellous bone was sourced as previously described (28), being certified for human use and of BSE/TSE free origin. The choice of polymers was suggested by their potential applicability within the pharmaceutical and biomedical industry and the necessity to obtain scaffolds with suitable mechanical properties. A commercially available copolymer of poly(L-lactic acid) and poly(ε-caprolactone), PLCL, already used in medical applications, was chosen (Purac Biomaterials, Gorinchem, The Netherlands). RGD-containing collagen fragments were also chosen to improve cell viability, hydrophilicity of the matrix and biocompatibility in general, and were sourced in their pharmaceutical grade formulation (Merck, Darmstadt, Germany). All materials were used as received. SB grafts were then obtained by the reinforcement of bovine bone derived matrix with the mixture of PLCL and (Merck, Darmstadt, Germany) through a proprietary process.Validated ethylene oxide sterilization (at BioSter SpA, Bergamo, Italy) was applied after final double layer packing.

Environmental scanning electron microscopy (ESEM) analysis

Environmental scanning electron microscopy analysis and energy dispersive analysis (EDS) were performed on unseeded samples at 10 kV with Evo 50 EP Instrumentation (Zeiss, Jena, Germany) before cell seeding. Each sample was first analyzed on the side surfaces and then halved with a sharp scalpel and the two inner exposed surfaces were finally analyzed (34). Then, at the end of the cell culture studies, scaffolds were fixed with 2.5% (v/v) glutaraldehyde solution in 0.1 M sodium cacodylate buffer for 1 h at 4°C, washed with sodium cacodylate buffer, and then dehydrated at room temperature in a gradient ethanol series up to 100%. The samples were kept in 100% ethanol and then analyzed, again, both on external surfaces and internal ones (35).

Porosity evaluation

Micro computer-assisted tomographic (μ-CT) scan were performed on SB cubic blocks to investigate internal porosity and to numerically evaluate the geometric characteristics of the average SB, *i.e.* free volume and surface to volume ratio (*s/v*). Scan were performed on 10 samples, sized about 8x8x8 mm^3 (*i.e.* ≈ 0.5cc) for analytic reasons, using a VTomEx-s tomograph (Phoenix|x-ray, a GE company, Germany) (34).

Mechanical testing

Uniaxial test was performed using a MTS 858 MiniBionix (Eden Praire, MN, USA) testing machine equipped with a 10 kN calibrated load cell, compressing the specimen between two parallel plates at a constant speed of 1 mm/min: displacement of the upper plate and force were acquired at 10 Hz frequency (28).

Cell culture

The human osteosarcoma cell line SAOS-2 was obtained from the American Type Culture Collection (HTB85, ATCC, Rockville, MD, USA). Following the method used by Pertici et al. (35), cells were cultured in Dulbecco's Modified Eagles Medium DMEM (Sigma-Aldrich, Germany) modified medium with L-glutamine, HEPES (Cambrex Bio Science Baltimore, Baltimore, USA), supplemented with 15% fetal bovine serum, 2% sodium pyruvate, 1% antibiotics, and 0.1 μM puromycin (Invitrogen, Carlsbad, CA, USA). The cells were cultured at 37°C with 5% CO_2, routinely trypsinized after confluence, counted, and seeded. From many cell lines that exhibited osteoblastic features, SAOS-2 cells were selected because they exhibited the most mature osteoblastic phenotype among different osteoblast-like cell lines (36, 37). SB samples were then seeded (6 x 10^4 cells each sample) with SAOS-2 cells by micro seeding technique and incubated at 37°C and 5% CO_2. Cells, at the same concentration, were also seeded on standard polystyrene cell culture plates as control group (CTRL). At different time points, on days 1, 4, 7, 12, 18, 25 and 32, cellular metabolic activity was assessed using an Alamar Blue™ assay (AbD Serotec, UK) where absorbance was measured by spectrophotometry (Genius Plus, Tecan, Italy) at 570 nm.

Histological studies on in vitro cultured samples

At day 25, samples were removed from culture dishes and dipped quickly into liquid nitrogen, then placed in histological common carriers and embedded in paraffin (Paraplast®, 56°C fusion point; SPI supplies, West Chester, PA, USA) following standard histological embedding techniques. Samples were then cut with a microtome, into 3-μm slices, which were placed on microscope slides (SuperFrost®; Menzel-Gläser, Braunschweig, Germany), and stained with hematoxylin and eosin (H&E).

ISO10993 studies

The complete biocompatibility and biological evaluation of SB scaffolds was performed under ISO-10993 standards, particularly addressing: cytotoxicity (with cell culture method); sensitization (applying Guinea pig maximization test); intracutaneous reactivity (on New Zealand rabbits), systemic toxicity test (on lab. mice), implantation (on New Zealand rabbits, with explanations at 4 and 8 weeks post grafting); genotoxicity.

Clinical study

All clinical investigations were carried out after having received specific ethics committee approval (made available to the editor) and under strict observance of the Declaration of Helsinki.

A female patient, 55 years old, good initial health condition underwent surgical intervention, in January 2012, on two different sites, for bone volume recovery for implantation purposes. Specifically: A) surgical site 45-46 was suffering from bone atrophy and was treated with SB 10x10x10 mm blocks, manually sized to fit defect to achieve thickness transverse recovery; B) a post-extractive bone gap was present in site 23, filled with shaped-to-size 7x7x7mm bone block, while the bone loss in neighboring area 24-25 was cross-increased with 10x10x10 mm SB blocks, duly shaped to match bone profile, and SB microchips (1-2mm) to maintain final volume. Surgical follow-up was monitored via intraoral x-ray imaging at month 2; after 4 months, a CT scan was performed to check bone regeneration, and histological sampling was then performed during site preparation for implantation. Further follow-up included controls at months 12 and 24. A final control was carried out by X-ray out after 3 years from SB grafting to prove the healthy and solid structure of newly formed bone.

The second patient was a female, aged 52 years, treated in area 24 for a large bone loss due to fracture: the patient underwent bone reconstruction with SB granules (1 - 2 mm) in January 2012, underwent implant surgery after 5 months and was followed-up at months 8 and 24 with intraoral X-ray.

Bone block regenerative surgery always requires the use of membranes to cover grafts and hence provide separation from soft tissues, mainly to avoid fibroblast proliferation and competition in the graft and to finally maintain tissue separation during the early healing stage. Here, the composite intimate nature of SB called for the strict avoidance of enzymatic-processed membranes, specifically to avoid the eventual activation of residual enzymes by degradation products of the polymers used. Clinical investigations were, hence, performed with regenerated collagen membranes (Resodont Forte, Resorba GmbH, Germany).

Statistical analysis

Experimental data were analyzed using Analysis of Variance (ANOVA); statistical significance was set to P value < 0.05; results are presented as mean ± SD (19).

RESULTS

ESEM analysis and porosity

Native bovine-derived bone scaffold was analyzed from a microstructural point of view using SEM (Fig. 1A): pores were well distributed along the sample but they were extremely larger in respect to those present in healthy human iliac crest bones, (Fig. 1B). Comparing the SB scaffold (Fig. 1C) with human cortical iliac crest bone sample (Fig. 1B) a strong resemblance between them is clearly visible: both exhibited a similar porous structure confirming the obtained SB scaffold as suitable for bone tissue engineering.

MicroCT scans supported these statements as they confirmed a strong resemblance with human cortical bone in terms of open and interconnected mid-sized porosity, with an average 27% (±2%) of free volume and an average s/v of 4.46mm^{-1} (*i.e.* a free surface of about 2.3mm^2 out of a volume of 512mm^3, as also previously shown (34).

Analyzing the inner surface of the sample (Fig. 1D), the porous structure and the two parts were more evidently visible: mineral and polymer were easily distinguishable; furthermore EDS spectrum of zone 1 in Fig. 1E was characterized by strong element signals of C and O confirming the presence of the polymeric film, while in the cavity (zone 2) the presence of Ca and P showed the mineral part of the sample corresponding to HA (Fig. 1F). In addition, Fig. 1G evidenced the inner surface of SB scaffold after being cut, exhibiting great evidence of mineral matrix coated with polymeric film. Structural differences between mineral fraction and polymer were highlighted by backscatter image (Fig. 1G, left). The corresponding EDS analysis, performed (yellow line) from the surface to the inner part of the sample, is presented in Fig. 1H: it highlighted C (red) as polymer presence on the surface of the scaffold while the increasing presence of Ca (blue) moving to its inner part highlighted the mineral nature of the matrix.

Compressive properties

Compressive tests were performed to evaluate the

Table I. *Compressive properties of the SB and native bone scaffold scaffolds: maximum stress, compressive modulus and fracture strength.*

Mechanical properties	SB scaffold	Native bone scaffold
Maximum compression stress [MPa]	28	7.5
Compressive modulus [GPa]	0.5	0.07
Fracture strength [MPa]	14	7

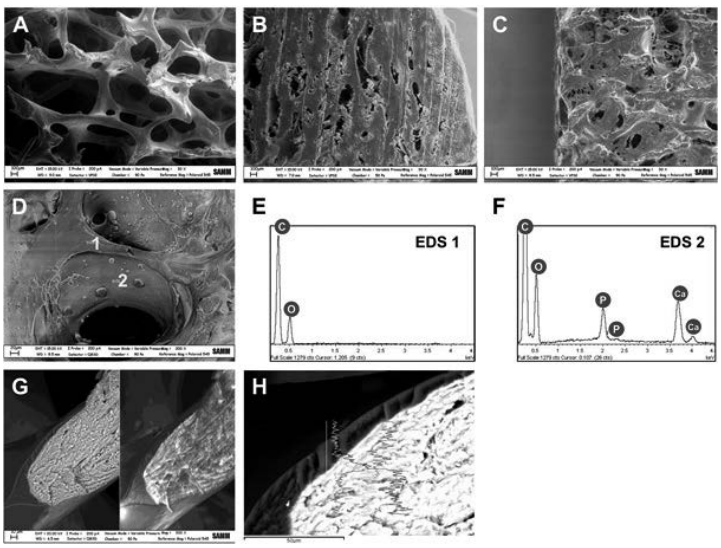

Fig. 1. A, B, C) *ESEM images at the same magnitude (bar scales = 100 µm) of bovine scaffold (A), healthy human iliac crest bone sample (B) and polymer coated SB scaffold (C).* ***D, E, F)*** *SB scaffold ESEM image (scale bar = 20 µm) and corresponding EDS spectra. Spot 1 is characterized only by the strong signals of C and O, typical of the presence of polymer film and spot 2 characterized by the presence of Ca and P, confirming the mineral nature of the matrix.* ***G, H)*** *SB scaffold ESEM image (scale bar = 10 µm) and corresponding EDS spectrum (scale bar = 50 µm). It evidences the outer polymer film while signal of Ca indicates the inner mineral part of the sample.*

mechanical properties of the SB scaffold in terms of maximum stress, compressive modulus and fracture strength: stress was obtained dividing the recorded force by the initial cross-section area while strain was calculated as the recorded displacement divided by the initial height of the specimen. Moreover, the effect of polymer coating and reinforcement was investigated comparing SB with native bone scaffold. As shown in Fig. 2 and Table I, the maximum stress, compressive modulus and fracture strength of the modified SB scaffolds were higher than those of the native bone scaffold. In detail, compression of SB scaffolds evidenced a maximum stress resistance (28 MPa av.) and a Young's modulus (0.5 GPa av.). From a mechanical point of view, SB scaffolds were found to be more rigid and comparable with human bone ones, underlining the necessity of the previously described reinforcement process (Table I).

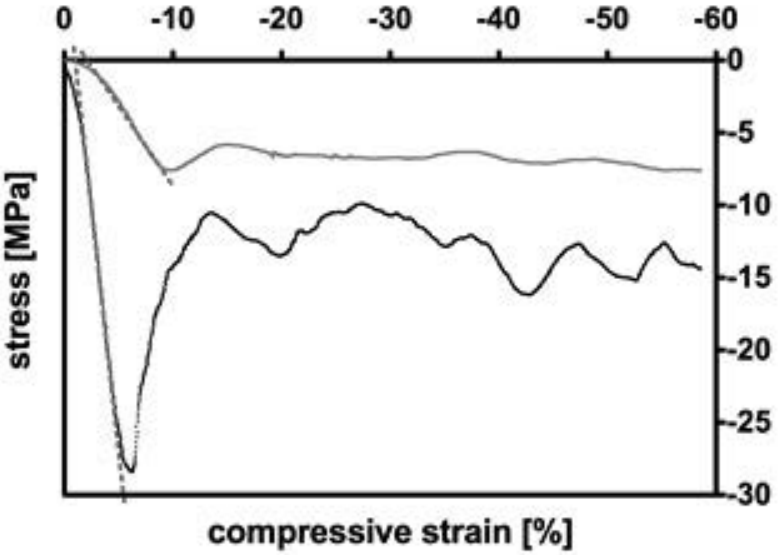

Fig. 2. *Compressive stress vs. strain plot of native bone (grey and upper line) and SB (black and lower line) scaffolds.*

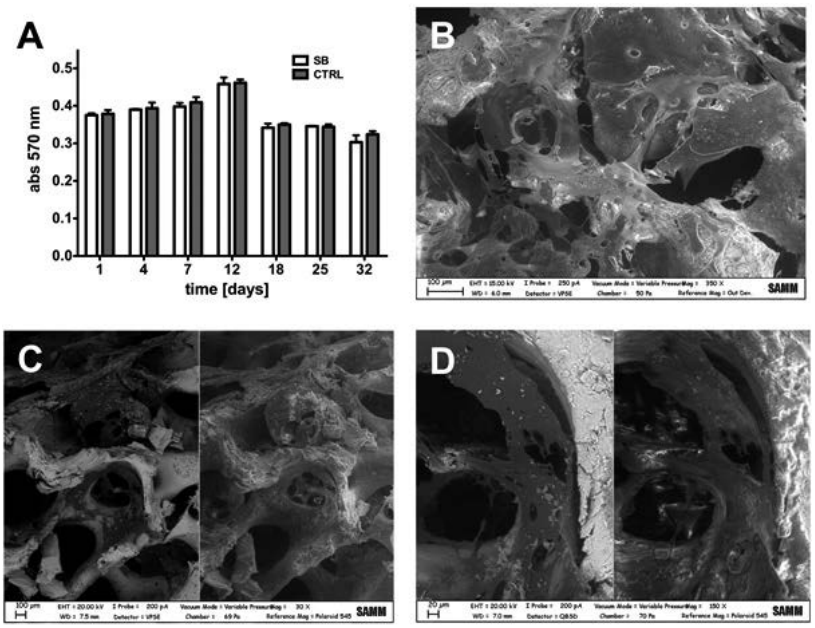

Fig. 3. A) *Alamar BlueTM staining indicating comparable values and profiles between P-BS and control (CTRL) groups at each time point (p > 0.005) for SAOS-2 cells seeded within SB scaffolds;* ***B, C, D)*** *ESEM images at different magnification of SAOS-2 cells seeded on SB scaffold after 25 days.* ***E)*** *Alamar BlueTM staining indicating comparable values and profiles between SB and control (CTRL) groups at each time point (p > 0.005) for MG-63 cells seeded within SB scaffolds;* ***F)*** *ESEM image of MG-63 cells seeded within SB scaffold after 8 days. Bar scales: 100 µm (B), 100 µm (C), 20 µm (D) and 100 µm (F).*

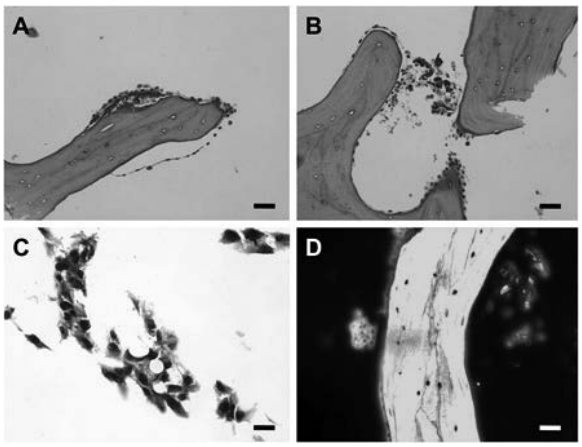

Fig. 4. *Histologic images of SAOS-2 after 25 days culture within SB scaffold. (A, B, D) H&E staining shows cell morphology and spread inside SB scaffold; the massive cell proliferation onto the thin polysaccharide and copolymer coating, thus confirmed its importance as enhancer of cell adhesion; (C) H&E staining shows cell morphology and spread inside SB scaffold. Bar scales: 200 µm (A), 200 µm (B), 50 µm (C) and 100 µm (D).*

In vitro cell morphology and viability

SAOS-2 cell morphology, within SB scaffolds, was firstly visualized by ESEM images (Fig. 3B, C, D). Fig. 3B is a representative image of 25 days within SB scaffolds, showing adherence of cells to their surface. In particular, the cells covered homogeneously the polymeric coating surface. ESEM results indicate that SAOS-2 cells were confluent and displayed an elongated spindle shape and therefore capable of proliferating and adhering to SB scaffold. At higher magnification (Fig. 3B, C) it was easily visible that cells adhered to the polymeric coating, highlighting the importance of polymer coating to allow cell growth.

The ability of cells to adhere and proliferate was quantitatively assessed by measuring their cellular metabolic activity with Alamar Blue™ assay, as reported in Fig. 3A. Alamar Blue™ assay was used as an indicator of cell proliferation, provided the metabolic activity per cell can be assumed to be relatively constant and not strongly dependent on cell morphology or substrate type. Cell numbers (Fig. 3A) were found to be similar for all the investigated time between SAOS-2 seeded within SB scaffold and control group (CTRL) cultured in classic polystyrene cell culture plates. Similar results were collected also with MG-63 cell line (Fig. 3, E and F).

Fig. 4 shows H&E-stained histological sections of SB scaffolds harvested at 25 days post cell seeding. In Fig. 4A, it can be seen that cells were able to colonize, adhere and spread within the SB scaffold. The H&E stain demonstrated homogeneity in cell distribution and adhesion along the scaffold. The seeded cells proliferated in a multilayer fashion, and there were more cells observed at the surface than in the interior of the scaffold as seen in Fig. 4B. Massive cell proliferation onto the thin polysaccharide and copolymer PLCL coating confirmed its importance as enhancer of cell adhesion. The morphology of cells was well visible, as reported in Fig. 4D, and was in complete accordance with ESEM images (Fig. 3). The use of fluorescent SAOS-2 cells (Fig. 4D) helped us to observe and confirm the colonization of the scaffold, underlining the importance of the reinforcement present in SB scaffolds.

ISO10993 studies

Standard compulsory ISO-10993 investigations on biocompatibility were carried out, under GLP conditions, specifically: Intracutaneous Reactivity Test, Systemic Toxicity Test and Delayed Hypersensitivity Test were performed, all resulting completely negative, thus confirming SB full biocompatibility.

Clinical studies

The implanted SB material used in this study, bone blocks, proved to be elastic and sufficiently robust to be precisely handled and cut to the necessary shape and dimensions in order to best fit (Fig. 5B) the specific patient bone defect (Fig. 5A). The material is not friable, hence it was easily fixed to the receiving bone, previously duly microcanalized, with osteosynthesis screws (Fig. 5B), and the radiography after 2 months post-implantation underlined the good placement of the graft (Fig. 5C): tight and stable contact with the receiving site is essential for bone regeneration. Regenerated ridges healed uneventfully. No post-operative complications

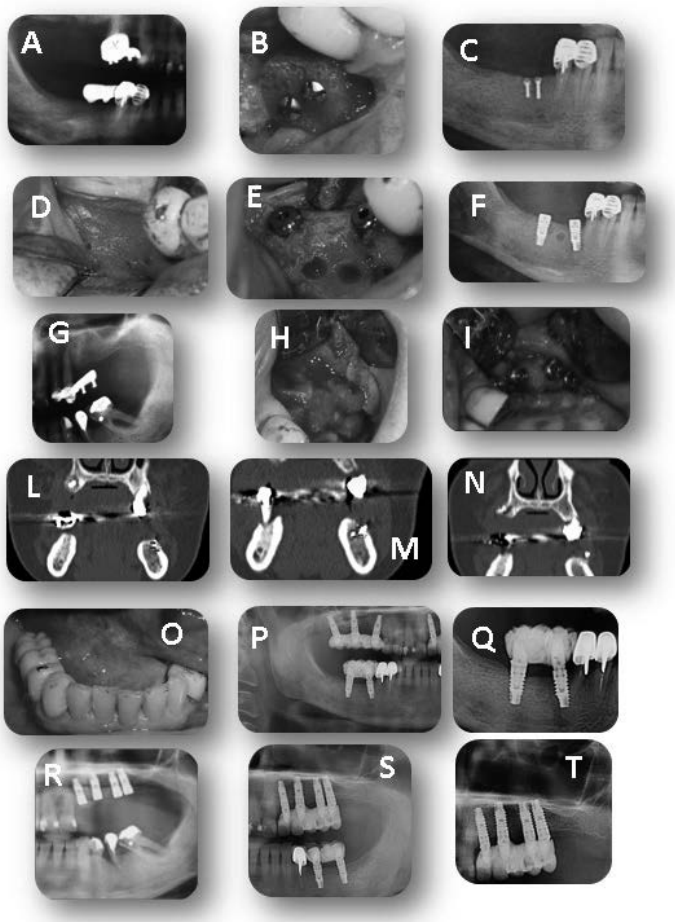

Fig. 5. *Clinical SB studies:* ***A)*** *specific patient bone defect;* ***B)*** *SB bone blocks precisely handled and cut to the necessary shape and dimensions and hence fixed with osteosynthesis miniscrews;* ***C)*** *radiography after 2 months post implantation underlined the good placement of the graft;* ***D)*** *4 months after grafting no evidences of serious adverse local side effects, like inflammation, pain or dehiscence, was observed;* ***E)*** *4 months after grafting implanted material could not be identified in the regenerated sites, being already integrated and capable of sustaining safe implants placement;* ***F)*** *robustness of integration after only 4 months allowed sustaining deep histological sampling;* ***G)*** *same patient, upper surgical site;* ***H)*** *miniscrew fixing and tight mechanical stabilization of SB graft onto bone defect space; I) implant positioning already after 4 months, on a sufficiently strong and dense SB graft; L,M,N) examples of Hounsfield analysis performed on CT scan slices taken 4 months after grafting, showing a well-integrated SB graft, with a good structure and density around mini-screws (i.e. exactly where the graft was) of about an average of 500 HU; O,P,Q) follow-up after 1, 2 and 3 years for lower site and R,S,T) for upper one, respectively, proved robust evidences of good bone formation, x-ray analysis gave high density signals and bone morphology and structure 3 years after grafts appeared comparable with healthy contralateral ones.*

were present after the ridge augmentation and at the time of the implantation surgery. Four months after grafting no evidence of serious adverse effects, such as inflammation, pain or dehiscence, was observed (Fig. 5D), and no implanted material was identified in the regenerated sites (Fig. 5E). From radiography (Fig. 5F) it was visible that newly-formed bone was similar to the surrounding tissue. Moreover, new bone, thanks to its mechanical properties, consented to fix screws for dental implants, as is visible from the radiography (Fig. 5F), and to sustain histological sampling. Similar performances and results were recorded on the upper surgical site (Fig. 5G), where SB mechanical performances allowed both

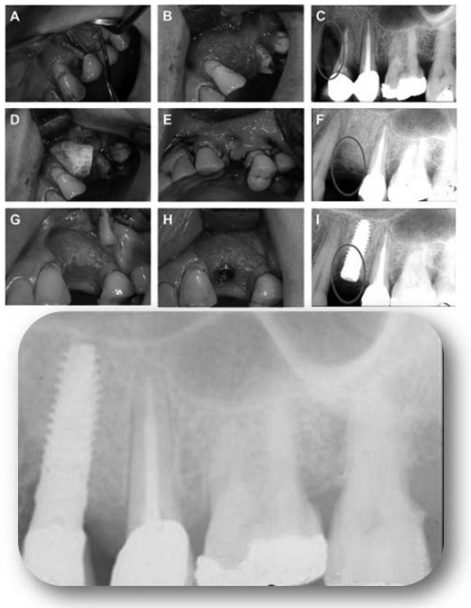

Fig. 6. *A, B, C) Bone defect visions and radiography (C) where bone defect is visible by black color; (D, E) granulated SB grafting; (F) radiography that underlines new bone formation 4 months after grafting procedure; (G) 4 months after implantation good tissue regeneration and osteointegration are observable; (H) screws for dental implants fixation to the new bone 4 months after scaffold implantation; (I) radiography after 8 months underlines bone regrowth and the possibility to fix on it screws for dental implants; (L) radiographic follow-up after 2 years proved robust evidences of good bone formation.*

miniscrew fixing and tight mechanical stabilization onto bone defect space (Fig. 5H). Regenerated bone was tough already after 4 months, sufficiently strong and dense as to easily withstand positioning of implants, as needed (Fig. 5I).

Hounsfield analysis performed on CT scan slices taken 4 months after grafting showed a well integrated SB graft, with a good structure and density: bone density around mini-screws (*i.e.* exactly where the graft was) had an average of 500 HU (Fig. 5. L,M,N). Indeed, the new bone allowed fixing the screw for dental implant (Fig. 5. E-I), and controls showed their good placement and alignment with patient teeth. Follow-up after 1, 2 and 3 years (Fig. 5 O,P,Q for the lower site and Fig 5 R,S,T for the upper site, respectively) proved concrete evidence of good bone formation. X-rays showed high density signals and bone morphology and structure 3 years after grafts which appeared comparable with the healthy contralateral ones. No more graft distinction was possible, nor were discontinuity lines evident from 4 months post-surgery.

Similar results were found also for the second patient: the bone defect was studied and granulated SB were mixed with patient blood and tailor-made to obtain the desired shape once *in situ*. The bone defect was visible (Fig. 6A-B) also in the radiography (Fig. 6C). SB was successfully grafted and covered with a commercial resorbable collage membrane (Fig. 6D). Good osteointegration together with new bone formation were already visible 4 months later (see radiography in Fig. 6F). The new bone allowed fixing screw for dental implant (Fig. 6G, H) and the radiography after 8 months (Fig. 6I) showed their good placement and alignment with the patient's teeth. Similarly to above, follow-up after 2 years proved concrete evidence of good bone formation (Fig. 6L).

In summary, these cases demonstrated successful bone reconstruction with polymer-coated mineral scaffolds implanted *in situ*. Furthermore, the histological analysis of the biopsies demonstrated an intense new formation of bone around the SB graft (bone with empty gaps) and several lines of new bone growth, thus highlighting a good osteoconduction of the biomaterial (Fig. 7 A-F presents slides from case A, lower site, as indicative examples). SB was progressively substituted by new young bone. Inside the new bone matrix, the purple lines (growth-lines) indicated a good osteoinduction (Fig. 7 C-D). This phenomenon is also evidenced by osteoblast presence on the outer surface of the newly formed bone where young woven bone is present. The slices clearly show osteocytes within the gaps and a hint of bone lamellae, therefore the bone is in a maturing process. Indeed, at high magnifications, the images show newly formed, not yet mature bone, as shown by the presence of much larger nuclei within the gaps (not yet quiescent osteoblasts) and a woven bone around them (Fig. 7 E-F).

DISCUSSION

Porosity and pore size of biomaterials play a key role in osteointegration and new bone formation (38). Relatively larger pores favor direct

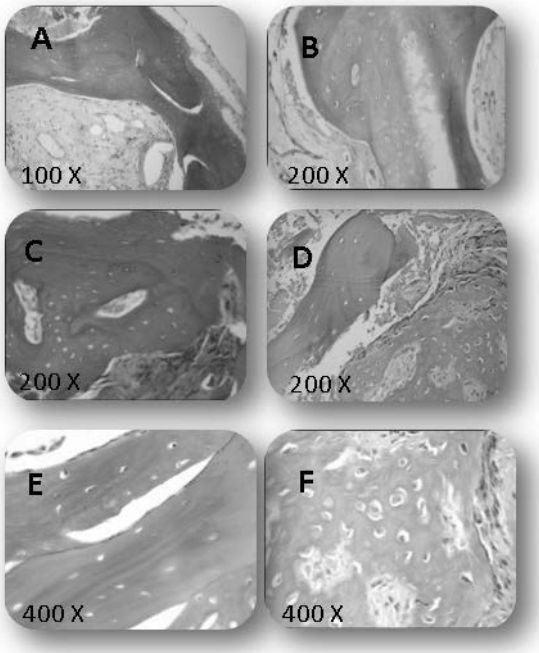

Fig. 7. *Exemplificative histological slides from case A, lower site, respectively: A) showing an intense new formation of bone around the SB graft and several lines of new bone growth; B) indicating SB is progressively substituted by new young bone; C-D) they shown a good osteoinduction; high magnifications images showing newly formed, not yet mature bone, as evidenced by the presence of much larger nuclei within the gaps (not yet quiescent osteoblasts) and a woven bone around them.*

osteogenesis, since they allow vascularization and high oxygenation, while smaller ones result in osteochondral ossification. There is, however, an upper limit in porosity and pore size set by constraints associated with mechanical properties. An increase in the void volume results in a reduction in mechanical strength of the scaffold, which can be critical for regeneration in load-bearing bones. The differences of bone tissues in morphological (pore size and porosity) and mechanical properties set challenges for fabricating biomaterial scaffolds that can meet the requirements set by the specific site of application. Therefore, following these statements, polymer reinforcement seems to be essential to reduce the pore sizes with the aim of mimicking healthy human bone microstructure, presented in Fig. 1B. As known, macroscopic properties of matter are a direct reflection of microscopic ones: here, the presence of the biopolymer film also plays a key role in the mechanical resistance of this new composite bone substitute. As shown in Fig. 2 and Table I, the composition of a mineral matrix, representing a rigid component, with polymers, being the elastic element, allow to obtain a much better performing device which shows resistance and elasticity comparable to target human ones. Moreover, the high and well-known biocompatibility of chosen polymers, together with the thin layering, allows SB to be a cell-supporting scaffold, where cells find the appropriate substrate to adhere to and grow, as shown in Fig. 3. Biocompatibility was among the key criteria to be precisely followed when choosing SB components: all constituents were chosen among those already available on the market of human-approved substances and devices. This choice can be considered a type of "design and development philosophy", where the innovation lies in making a composite out of safe and known components: safety, not only as a result of biocompatibility, is an unavoidable target, which was definitely proven during all mandatory ISO studies. Having straightforwardly and successfully passed all characterization and safety tests.

The key element is RGD-sequence containing proteins, physically entrapped into the thin polymeric layer: proteins that contain the Arg-Gly-Asp (*a.k.a.* RGD) attachment site, together with the integrins that serve as receptors for them, constitute a major recognition system for cell adhesion. Such peptides promote cell adhesion when insolubilized onto a surface (29). Histological analyses performed during human studies confirmed that SB supports the ingrowth of osteoblasts, which then spread and colonize it, hence generating new bone. Furthermore, the ensemble made by SB and the patient's receiving system is osteo-inductive: SB not only serves as a scaffold for currently existing osteoblasts but will also trigger the formation of new osteoblasts, also deriving from stromal stem cells, promoting faster integration of the graft.

In this study, a composite scaffold made of natural mineral matrix (calcium hydroxyapatite) and synthetic polymer coating (PLCL) with the addition of RGD-containing collagen fragments was *ex novo* developed

and investigated. The purpose behind coating mineral scaffold with PLCL and RGD-containing collagen fragments came from the necessity to have higher mechanical properties together with suitable microstructure and to improve hydrophilicity for good cell adhesion and viability, to gain high osteoinductive properties. The fabricated scaffold exhibited a regular microstructure similar to healthy iliac bones (*i.e.* the most commonly harvested autograft) and high ability to allow cell growth using human standard cell lines. The results achieved showed high cell adhesion to the scaffolds and viability values similar to the control groups. SB grafting in human cases was validated in maxillary and mandibular bone defects: in all the specimens presented in this study newly formed bone was visible. No inflammation or foreign body reactions were observed, and these findings confirm animal studies evidence and support the good biocompatibility of SB composite material. The new bone was observed in close contact with the implanted material and neither gaps nor fibrous tissues were observed at the interface. The cellular response to SB graft can be described as a progressive neoformation of healthy bone, which occurs alongside the reabsorbtion of the graft, where both osteoconductive and osteoinductive processes are involved between grafts and receiver bone sites. In summary, all this evidence demonstrates the good suitability of SB grafts for bone regeneration.

ACKNOWLEDGEMENTS

The authors would like to thank the Biocompatibility and Cell Culture (BioCell-Lab, Politecnico di Milano, Italy) Laboratory staff for their cooperation and Dr Mariotti (Università degli Studi di Milano, Italy) for having provided SAOS-2 cell line.

We wish to draw the attention of the Editor to the following facts which may be considered as potential conflicts of interest and to significant financial contributions to this work: two authors, Gianni Pertici and Giuseppe Perale, are affiliated to the Company manufacturing the bone substitute object of this study (as evident from the authors and affiliations).

REFERENCES

1. Senn on the Healing of Aseptic Bone Cavities by Implantation of Antiseptic Decalcified Bone. Ann Surg 1889; 10(5):352-368.
2. Cordonnier T, Sohier J, Rosset P, Layrolle P. Biomimetic materials for bone tissue engineering – state of the art and future trends. Advanced Engineering Materials 2011; 13:135-150.
3. Chen FM, An Y, Zhang R, Zhang M. New insights into and novel applications of release technology for periodontal reconstructive therapies. J Control Release 2011; 149(2):92-110.
4. Mourino V, Boccaccini AR. Bone tissue engineering therapeutics: controlled drug delivery in three-dimensional scaffolds. J R Soc Interface 2010; 7(43):209-227.
5. Zhou M, Peng X, Mao C, Xu F, Hu M, Yu GY. Primate mandibular reconstruction with prefabricated, vascularized tissue-engineered bone flaps and recombinant human bone morphogenetic protein-2 implanted in situ. Biomaterials 2010; 31(18):4935-4943.
6. Gronthos S. Reconstruction of human mandible by tissue engineering. Lancet 2004; 364(9436):735-736.
7. Isikli C, Hasirci V, Hasirci N. Development of porous chitosan-gelatin/hydroxyapatite composite scaffolds for hard tissue-engineering applications. J Tissue Eng Regen Med 2012; 6(2):135-143.
8. Langer R. Perspectives and challenges in tissue engineering and regenerative medicine. Adv Mater 2009; 21(32-33):3235-3236.
9. Hutmacher DW, Schantz JT, Lam CX, Tan KC, Lim TC. State of the art and future directions of scaffold-based bone engineering from a biomaterials perspective. J Tissue Eng Regen Med 2007; 1(4):245-260.
10. Zou D, Zhang Z, He J, et al. Repairing critical-sized calvarial defects with BMSCs modified by a constitutively active form of hypoxia-inducible factor-1alpha and a phosphate cement scaffold. Biomaterials 2011; 32(36):9707-9718.
11. Di Stefano DA, Artese L, Iezzi G, Piattelli A, Pagnutti S, Piccirilli M, Perrotti V. Alveolar ridge regeneration with equine spongy bone: a clinical, histological, and immunohistochemical case series. Clin Implant Dent Relat Res 2009; 11(2):90-100.
12. Gitelis S, Saiz P. What's new in orthopaedic surgery. J Am Coll Surg 2002; 194(6):788-791.

13. Chen M, Le DQ, Baatrup A, Nygaard JV, Hein S, Bjerre L, Kassem M, Zou X, Bunger C. Self-assembled composite matrix in a hierarchical 3-D scaffold for bone tissue engineering. Acta Biomater 2011; 7(5):2244-2255.
14. Duailibi SE, Duailibi MT, Zhang W, Asrican R, Vacanti JP, Yelick PC. Bioengineered dental tissues grown in the rat jaw. J Dent Res 2008; 87(8):745-750.
15. Manferdini C, Guarino V, Zini N, et al. Mineralization behavior with mesenchymal stromal cells in a biomimetic hyaluronic acid-based scaffold. Biomaterials 2010; 31(14):3986-3996.
16. Nolan P, Templeton P, Mollan RA, Wilson DJ. Osteoinductive potential of human demineralised bone and a bioceramic in abdominal musculature of the rat. J Anat 1991; 174:97-102.
17. Shoichet MS. Polymer Scaffolds for Biomaterials Applications. Macromolecules 2010; 43:581–591.
18. Costa-Pinto AR, Reis RL, Neves NM. Scaffolds based bone tissue engineering: the role of chitosan. Tissue Eng Part B Rev 2011; 17(5):331-347.
19. Perale G, Rossi F, Sundstrom E, Bacchiega S, Masi M, Forloni G, Veglianese P. Hydrogels in spinal cord injury repair strategies. ACS Chem Neurosci 2011; 2(7):336-345.
20. Stevens MM. Biomaterials for bone tissue engineering. Materialstoday 2008; 11:18-25.
21. Brey DM, Chung C, Hankenson KD, Garino JP, Burdick JA. Identification of osteoconductive and biodegradable polymers from a combinatorial polymer library. J Biomed Mater Res A 2010; 93(2):807-816.
22. Kim J, Sharma A, Runge B, et al. Osteoblast growth and bone-healing response to three-dimensional poly(epsilon-caprolactone fumarate) scaffolds. J Tissue Eng Regen Med 2012; 6(5):404-413.
23. Arafat MT, Lam CX, Ekaputra AK, Wong SY, Li X, Gibson I. Biomimetic composite coating on rapid prototyped scaffolds for bone tissue engineering. Acta Biomater 2011; 7(2):809-820.
24. Sturm S, Zhou S, Mai YW, Li Q. On stiffness of scaffolds for bone tissue engineering-a numerical study. J Biomech 2010; 43(9):1738-1744.
25. Karande TS, Ong JL, Agrawal CM. Diffusion in musculoskeletal tissue engineering scaffolds: design issues related to porosity, permeability, architecture, and nutrient mixing. Ann Biomed Eng 2004; 32(12):1728-1743.
26. Rose FR, Oreffo RO. Bone tissue engineering: hope vs hype. Biochem Biophys Res Commun 2002; 292(1):1-7.
27. Lin CY, Chang YH, Kao CY, Lu CH, Sung LY, Yen TC, Lin KJ, Hu YC. Augmented healing of critical-size calvarial defects by baculovirus-engineered MSCs that persistently express growth factors. Biomaterials 2012; 33(14):3682-3692.
28. Pertici G, Müller M, Perale G. Bioresorbable bioactive matrix for bone regeneration. Tissue Engineering Part A 2010; 16.
29. Duong LT, Rodan GA. Integrin-mediated signaling in the regulation of osteoclast adhesion and activation. Front Biosci 1998; 3:d757-768.
30. He J, Genetos DC, Leach JK. Osteogenesis and trophic factor secretion are influenced by the composition of hydroxyapatite/poly(lactide-co-glycolide) composite scaffolds. Tissue Eng Part A 2010; 16(1):127-137.
31. Kane RJ, Roeder RK. Effects of hydroxyapatite reinforcement on the architecture and mechanical properties of freeze-dried collagen scaffolds. J Mech Behav Biomed Mater 2012; 7:41-49.
32. Jeong SI, Lee AY, Lee YM, Shin H. Electrospun gelatin/poly(L-lactide-co-epsilon-caprolactone) nanofibers for mechanically functional tissue-engineering scaffolds. J Biomater Sci Polym Ed 2008; 19(3):339-357.
33. Moimas L, Biasotto M, Di Lenarda R, Olivo A, Schmid C. Rabbit pilot study on the resorbability of three-dimensional bioactive glass fibre scaffolds. Acta Biomater 2006; 2(2):191-199.
34. Pertici G, Rossi F, Casalini T, Perale G. Composite polymer-coated mineral grafts for bone regeneration: material characterisation and model study. Annals of Oral & Maxillofacial Surgery 2014; 2.
35. Pertici G, Maccagnan S, Mueller M, Rossi F, Daniele F, Tunesi M, Perale G. Porous biodegradable microtubes-based scaffolds for tissue engineering, part I: production and preliminary in vitro evaluation. J Appl Biomater Biomech 2008; 6(3):186-192.
36. Saino E, Grandi S, Quartarone E, et al. In vitro calcified matrix deposition by human osteoblasts onto a zinc-containing bioactive glass. Eur Cell

Mater 2011; 21:59-72; discussion 72.
37. Leidi M, Dellera F, Mariotti M, Banfi G, Crapanzano C, Albisetti W, Maier JA. Nitric oxide mediates low magnesium inhibition of osteoblast-like cell proliferation. J Nutr Biochem 2012; 23(10):1224-1229.
38. Karageorgiou V, Kaplan D. Porosity of 3D biomaterial scaffolds and osteogenesis. Biomaterials 2005; 26(27):5474-5491.

Positioning of a Contextual Implant Along with a Sinus Lift with Smartbone® Microchips of Composite Heterologous-Synthetic Bone

Ilaria Zollino[1], Giorgio Carusi[2,3], Francesco Carinci[1], Giuseppe Perale[3,4]

Abstract
The present case reports the success rate after 8 months of follow-up in a sinus pneumatization case with maxillary sinus floor cortical bone loss due to 2.5 dental agenesis. Rehabilitation including the opportunity to insert a contextual implant during maxillary sinus lift surgery was planned, using SmartBone® Microchips heterologous bone inserted into the maxillary sinus. The newly developed bone substitute was designed starting from bovine bone derived mineral matrix, reinforced with bioresorbable aliphatic polymers and cell nutrients. SmartBone® Microchips showed a tight contact with the new bone and neither gaps nor fibrous tissues at the interface. No inflammation or foreign body reaction were observed, and these findings support the good biocompatibility of SmartBone® Microchips composite material. Moreover, new bone, thanks to its mechanical properties, consented to fix screw in combination with maxillary sinus floor elevation for a dental implant.

Keywords: Implant; case report; sinus pneumatisation; sinus lift; SmartBone® Microchips.

Introduction

Since the first use of sinus grafting implant placement in the atrophic posterior maxilla, sinus grafting has become a predictable method to increase vertical bone height. The first graft material suggested for the reconstruction of bone defects was autografts bone. Theoretically, autografts bone possesses the pre-requisite properties for the successful incorporation of a grafting material and for bone healing, thanks to it being both osteoconductive and osteoinductive. So, it is considered the gold standard graft for bone reconstruction. The limitations of using autografts bone grafts concern the size of the donor site and risks of morbidity due to demanding surgery. Factors to be taken into account when choosing the donor site are the amount of bone required, the type (cortical vs. cancellous) of bone needed, the recipient site, and the expected biological behaviour (neovascularization and resorption). Donor sites can be extraoral or intraoral. The iliac crest, the calvaria, the ribs and the tibia are the most commonly described extraoral donor sites in the literature. Mandibular symphysis, mandibular ramus, infrazygomatical crest and maxillary tuberosity have been suggested as different intraoral donor sites.[1]

In order to simplify bone reconstruction by avoiding donor site surgery, increased surgical cost, limited amount of material, possible rapid bone resorption, and patient discomfort, the use of bone substitutes is obviously an attractive alternative. Several bone substitutes of biological and synthetic origins are available: biological ones can be allografts, i.e., from other humans or xenografts, i.e., from other species than humans (bovine derived hydroxyapatite). Fresh or untreated allograft are limited in use due to the presence of antigens, which may affect the immune response and trigger a rejection response. As with xenografts, allografts proteins are extracted for reasons of immunological safety. As a consequence, the osteoinductive properties disappear and the graft can only work as an osteoconductive scaffold.[2]

The current focus, thus, is on xenografts vs. synthetic devices: naturally derived materials provide structures extremely similar to living tissues such as stimulating a specific cellular response, which sometimes supersedes the advantages of synthetic polymers. Xenografts may also reduce the stimulation of chronic inflammation or immunological reactions and toxicity, often detected with synthetic polymers and minerals (such as e.g., bioglasses and bioceramics).[3]

On the other side, materials science, in conjunction with bio- and nano-technologies, can satisfy these requirements by developing novel grafting devices. In particular, bioresorbable scaffolds, as key artificial devices widely used in tissue engineering, aim to provide a desirable microenvironment that allows neo-tissue to be generated properly for repairing and replacing damaged tissues or organs. Indeed, synthetic polymers can be tuned in terms of composition, rate of degradation, mechanical and chemical properties.[3,4]

For all these reasons, the goal of the current approach was to combine the biocompatibility and tissue integration of natural materials with the possibility to tune mechanical and physical properties typical of synthetic ones: composite grafts best mimic the real nature of healthy human bone, being rigid and elastic, compact but porous, dense but viable to cells and vessels.

A newly developed bone substitute, named SmartBone® (briefly SB), was design following a new concept of composite approach, starting from bovine bone derived mineral matrix, reinforced with bioresorbable aliphatic polymers and RGD-containing peptide fragments as cell nutrients. In this case report the SmartBone® Microchips, 1-2 mm in diameter, were used to achieve a sinus lift surgery with the placement of a contextual implant screw.

Case report

A 43-year-old male patient (smoker) was referred to private practitioner for implant-supported prosthesis in a sinus

[1]Department of Morphology, Surgery and Experimental Medicine, University of Ferrara, Ferrara, Italy, [2]Private practitioner, Ponsacco, Italy, [3]Industrie Biomediche Insubri SA, Mezzovico-Vira, Switzerland, [4]Department of innovative Technologies, University for Applied Science and Art of Southern Switzerland, Manno, Switzerland. Correspondence: Dr. Francesco Carinci, email: crc@unife.it

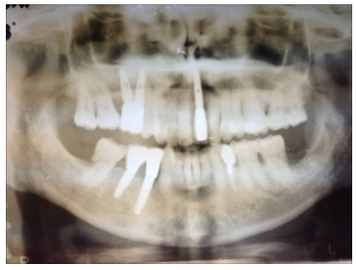

Figure 1: The orthopantomography shows the sinus pneumatization with loss of maxillary sinus floor cortical bone due to 2.5 dental agenesis

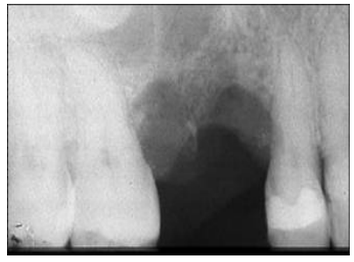

Figure 2: The radiography shows the bone defect

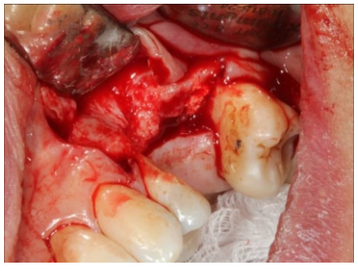

Figure 3: The elevated mucoperiosteal flap exposes the lateral bone aspect of the maxillary sinus

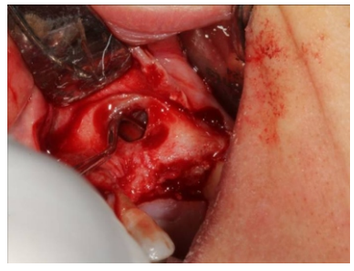

Figure 4: The periosteal elevator in the posterior/superior part of the created cavity prior to its filling with grafting material

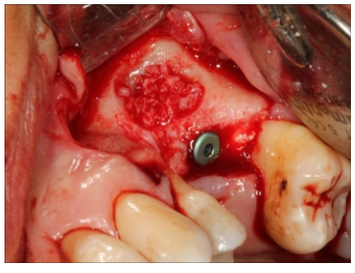

Figure 5: The grafted defect that allowed fixing screw for dental implant

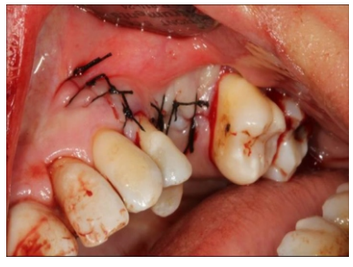

Figure 6: The mucoperiosteal flap replaced in position and sutured to cover the window opening

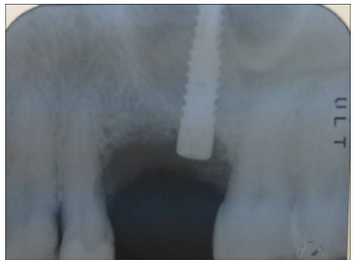

Figure 7: Checkup after surgery

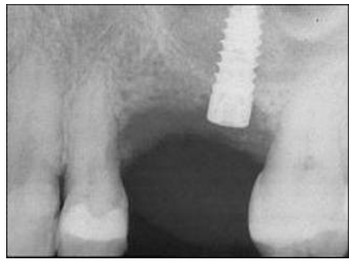

Figure 8: Radiography 4 months later shows good osseointegration together with new bone formation

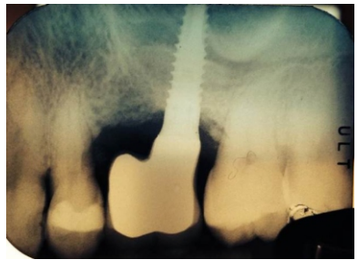

Figure 9: Radiography after 8 months shows good placement of the teeth

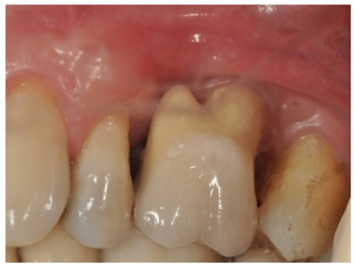

Figure 10: The final prosthetic result

pneumatization with loss of maxillary sinus floor cortical bone due to dental agenesis. Rehabilitation including the opportunity to insert a contextual implant during maxillary sinus lift surgery was planned, using SmartBone® Microchips heterologous bone molded and inserted into the maxillary sinus. The medical history does not note any particular contraindications for surgical therapy. The orthopantomography was performed where there is evidence of sinus pneumatization with loss of maxillary sinus floor cortical bone due to 2.5 dental agenesis (Figure 1).

The bone defect was studied and it is visible in the radiograph (Figure 2). This technique comprised the creation of an access to the maxillary sinus via a window through the lateral bone wall. A mucoperiosteal trapezoidal flap was raised after a midcrestal horizontal incision. The mucoperiosteal flap was elevated so as to expose the lateral bone aspect of the maxillary sinus (Figure 3). The osteotomy in the superior part of the window was carried out with a partial thickness approach so as to make the infraction of the window easier. However, a minimum size has been requested in order to have a comfortable access and for filling with graft material. So, the extent of the bone window to the sinus was marked by drilling with a medium size round bur. Dissection was performed carefully in order to avoid sinus membrane perforation using a periosteal elevator placed to the posterior/superior part of the created cavity prior to its filling with grafting material (Figure 4).

SmartBone® Microchips was mixed with patient blood and tailor modelled to obtain the desired shape once in situ. It was successfully grafted and allowed fixing screw for dental implant (Figure 5) covered with a commercial resorbable collagen membrane. The periosteal elevator was removed and the mucoperiosteal flap was replaced in position and sutured to cover the window opening (Figure 6). Check-up after surgery showed that everything was proceeding well (Figure 7): good osseointegration together with new bone formation were visible 4 months later from radiography (Figure 8) and the radiography after 8 months (Figure 9) showed good placement with patient teeth.

Regenerated ridges healed uneventfully. No post-operative complications were present after the ridge augmentation and at the time of the implantation surgery. Four months after scaffold implantation no evidence of serious adverse local, like inflammation, pain or dehiscence, was observed and no implanted material was identified in the regenerated sites.

From radiography it is visible that newly formed bone is similar to the surrounding tissue (Figure 9). The implanted SmartBone® Microchips used in this study proved precisely handle to the necessary in order to obtain the desired shape for the specific patient bone defect. The success and realisation of the objective gives the patient, within a shorter time frame, the comfort of a rehabilitated set of teeth and the resulting advantages of this (Figure 10).

Discussion

The pneumatization is an important phenomenon that occurs after dental losses or with dental agenesis. If bone density and thickness can be explained, in part, by chewing forces applied, the pneumatisation process is likely an architectural response to the muscles and chewing forces. The positive air pressure occurring during breathing inside the maxillary sinus can have an effect on maxillary sinus floor resorption. So, the presence of a reduced bone height demands an intervention on the maxillary sinus with the purpose to increase the bone amount available to implant insertion.[5]

Different materials are described on the literature to improve the bone volume on this region. These are fundamental important for the prognosis since different materials have different grades of osteogenesis.[1] For this reason, as said, most surgeons prefer to use autologous grafts as theirs first choice for osseous grafting or a mixture of autologous and biomaterial bone grafts for sinus surgeries. However, significant progresses in tissue engineering could yield more favorable outcomes than the current range of approaches used to repair bone defects.[6]

The newly developed bone substitute SmartBone® was designed following a new concept of composite approach, starting from bovine bone derived mineral matrix, reinforced with bioresorbable polymers and cell nutrients. The bovine derived matrix is mineral and mainly made of calcium hydroxyapatite (HA, Ca5(PO4)3(OH)) that presents a chemical structure and a morphology resembling human bone.[7,8] However, its physical properties evidence rigid but not elastic structure which make it too fragile. In addition sterilization processes destroy its porous structure, widening it further then natural limits, and does not consent neither easy graft manufacturing nor cell adhesion. For these reasons bovine structure was reinforced with the addition of an elastic component in terms of polymer coating, loosing thus fragility and reducing porosity to resemble healthy human bones. Finally, the addition of RGD-containing peptide fragments, increases the hydrophilicity of the scaffold with consequent higher cell attachment and thus enhan-

cing biocompatibility and osseointegration.[8]
The insertion of dental implants in combination with maxillary sinus floor elevation represented in this case report a predictable treatment method that showed high implant survival rates and low incidence of surgical complications. The new bone was observed in tight contact with the implanted SmartBone® Microchips material and neither gaps nor fibrous tissues were observed at the interface.
Pjetursson et al., in a systematic review to assess the survival rate of grafts and implants used for sinus floor elevation, reported an estimated annual failure rate of 3.48% translating into a 3-year implant survival rate of 90.1%.[9] So, these authors suggest that this treatment method is safe and predictable in relation to a simultaneous implant insertion.
The difference in osseous formation within the grafted sinuses with mineralized bovine bone associated or not to absorbable or non absorbable membranes placed over the lateral window was studied by Wallace et al.[10] Differences were found in the histomorphometric analyses revealing that the groups with membranes showed a greater newly bone formation of 30% and in the group without membrane 14%. So, in according to these results it is suggested that the placement of membranes (absorbable or non absorbable) should be at the lateral window.

Conclusion

The newly developed bone substitute SmartBone® Microchips showed in a patient with jaw cortical pavement defect a tight contact with the new bone and neither gaps nor fibrous tissues at the interface. No inflammation or foreign body reaction were observed, and these findings support the good biocompatibility of SmartBone® Microchips composite material. Moreover, new bone, thanks to its mechanical properties, consented to fix one screw in combination with maxillary sinus floor elevation for the dental implant. All these statements showed the good suitability of SmartBone® Microchips for alveolar defect repair in sinus lift procedure.

Acknowledgements

This work was partially supported by FAR from the University of Ferrara (FC), Ferrara, Italy.

References

1. Misch CE. Bone-grafting materials in implant dentistry. Implant Dent 1993;2:158-67.
2. Carinci F, Brunelli G, Zollino I, Franco M, Viscioni A, Rigo L, et al. Mandibles grafted with fresh-frozen bone: an evaluation of implant outcome. Implant Dent 2009;18:86-95.
3. Perale G, Rossi F, Sundstrom E, Bacchiega S, Masi M, Forloni G, Veglianese P. Hydrogels in spinal cord injury repair strategies. ACS Chem Neurosci 2011;2:336-45.
4. Arafat MT, Lam CX, Ekaputra AK, Wong SY, Li X, Gibson I. Biomimetic composite coating on rapid prototyped scaffolds for bone tissue engineering. Acta Biomater 2011;7:809-20.
5. Guilherme AS, Zavanelli RA, Fernandes JMA, Castro AT, Barros CA, Souza JEA, Cozac CD, Santos VA. Implantes osseointegráveis em áreas com levantamento do seio maxilare enxertos ósseos. RGO 2009;57:157-63.
6. Chen FM, An Y, Zhang R, Zhang M. New insights into and novel applications of release technology for periodontal reconstructive therapies. J Control Release 2011;149:92-110.
7. He J, Genetos DC, Leach JK. Osteogenesis and trophic factor secretion are influenced by the composition of hydroxyapatite/poly(lactide-co-glycolide) composite scaffolds. Tissue Eng 2010;16:127.
8. Kane RJ, Roeder RK. Effects of hydroxyapatite reinforcement on the architecture and mechanical properties of freeze-dried collagen scaffolds. J Mech Behav Biomed 2012;7:41-49.
9. Pjetursson BE, Tan WC, Zwahlen M, Lang NP. A systematic review of the success of sinus floor elevation and survival of implants inserted in combination with sinus floor elevation. J Clin Periodontol 2008;35:216-40.
10. Wallace SS, Froum SJ, Cho S-C, Elian N, Monteiro D, Kim BS, Tamo DP. Sinus Augmentation Utilizing Anorganic Bovine Bone (Bio-Oss) with Absorbable and Nonabsorbable Membranes Placed over the Lateral Window: Histomorphometric and Clinical Analyses. Int J Perio Restor Dent 2005;25:551-59.

Disclosure : The authors report no conflicts of interest.

POSITIONING OF A CONTEXTUAL IMPLANT ALONG WITH A SINUS LIFT ANCHORED WITH A BLOCK OF HETEROLOGOUS BONE

F. SECONDO[1], C.F. GROTTOLI[2], I. ZOLLINO[3], G. PERALE[2,4], D. LAURITANO[5]

[1] *Private practice, Torino, Italy*
[2] *Industrie Biomediche Insubri SA, Mezzovico-Vira, Switzerland*
[3] *Department of Morphology, Surgery and Experimental Medicine, University of Ferrara, Ferrara, Italy*
[4] *Department of Innovative Technologies, University for Applied Science and Art of Southern Switzerland, Manno, Switzerland*
[5] *Department of Medicine and Surgery, University of Milano "Bicocca", Monza, Italy*

SUMMARY
During a sinus lift procedure the main requirement in order to position an implant is to have a maxillary sinus floor cortical bone thick enough to guarantee a primary stability in the implant inserted. In this way, the healing process is facilitated and osseointegration of the titanium surface may occur simultaneously, thus reducing the waiting time for the engraftment of the implant into the body. Unfortunately, these conditions are not always present. Hence, the need of developing an alternative approach that could simultaneously allow to perform sinus floor elevation along with an implant placement.
Here we present the case of a 62-year-old patient that requires implant-prosthetic rehabilitation from 1.2 to 1.6 at diagnosis. In this study, we reported a novel application derived from the use of a heterologous bone scaffold (SmartBone@) in a sinus lift procedure. We showed the successful implant along with sinus lift with SmartBone@, both at the time of the surgery and after follow-up of the patient at 10 months from the implant. The possibility to perform simultaneously the contextual implant along with sinus lift dramatically reduced the waiting time for the patient of minimum 5-6 months required for osseointegration of the grafted biomaterials, before performing the implant procedure. This surgery represents an advance both in terms of medical technique and as life-benefit for the patient.

Key words: implants, case report, sinus pneumatization, sinus lift, heterologous bone, SmartBone®.

Introduction

Maxillary sinus lift is a surgical procedure that usually requires a period of osseointegration of the grafted biomaterials (1) and an additional recovery period for the correct positioning of the implant, in order to finally achieve a complete engraftment of the prosthetic implant into the body (2, 3, 67).
In case the medical conditions of the patient are permissive, the contextual implant can be positioned during the maxillary sinus lift surgery, in order to promote simultaneously osseointegration of the biomaterials and fixtures, hence reducing the waiting times (4-9, 68).
During a sinus lift, the main requirement in order to efficiently position the implant is to have a proper thickness of maxillary sinus floor cortical bone that might guarantee a primary stability in the inserted implant. Thus, the healing process could be facilitated and osseointegration of the titanium surface around the biomaterials may occur simultaneously, leading to stability and engraftment of the prosthetic implant after a shorter period (10-16).
Unfortunately, these optimal conditions are not always present. Indeed, surgeons often deal with the contraction of the edentulous saddle along with an expansion of the maxillary sinuses,

which determine a rather limited thickness of sinus floor cortical, not suitable for an implant insertion (17-26, 69). In order to overcome the absence of suitable thickness and reduce waiting times, it has been proposed a novel technique that positions the contextual implant at the same time as the sinus lift, by fixing the apical part of the same implant to a block of heterologous bone positioned between the sinus floor and the Schneider membrane. If properly drilled, this functions as a sort of nut to which the apical part of the implant is attached and acts as a screw. The platform for this screw, which rests underneath the same cortical sinus floor, tightens the system at the screwing stage and achieves the stability that is required for osseointegration.

Case description

This case study presents the diagnosis of a 62-years-old patient that requires implant-prosthetic rehabilitation from 1.2 to 1.6, because of a sinus pneumatization associated with loss of jaw cortical pavement bone due to dental agenesis (Figure 1). The medical history does not indicate any particular contraindications for surgical therapy.
The extraction of element 1.6 was performed around eighty days before the CT scan, where there was evidence of posterior maxillary atrophy with low cortical sinus floor thickness. Rehabilitation associated with the opportunity to insert a contextual implant during maxillary sinus lift surgery was planned, using a block of heterologous bone molded and inserted into the maxillary sinus, which acts as a nut for a screw, as previously described.
All clinical investigations were carried out under strict observance of the Declaration of Helsinky, and patient informed consent has been collected and recorded accordingly.

Description of method

In order to fully plan out the work and demonstrate the aim, data from the Cone-Beam radiographic examination were used to make a stereolithographic (3D) model. This solid model was mounted on an articulator and after a diagnostic assembly process the position where the implants should have been inserted was evaluated (Figure 2). The proposal for the distal implant indicated its future position at the level of the first molar and suggested the following point where to situate the block of bone that would serve as a nut. At the time of the sinus lift, this would naturally be immersed in biomaterial granules selected for the purpose.

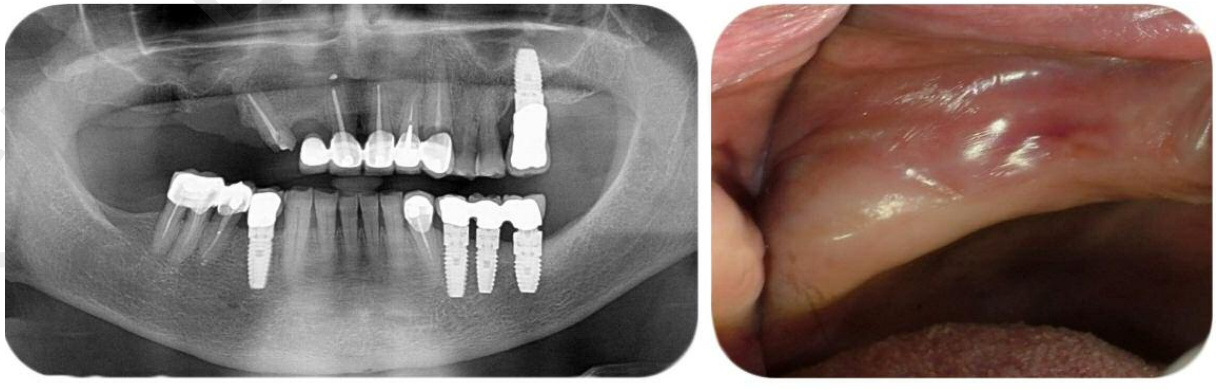

Figure 1
Sinus pneumatization with loss of jaw cortical pavement bone due to edentulism.

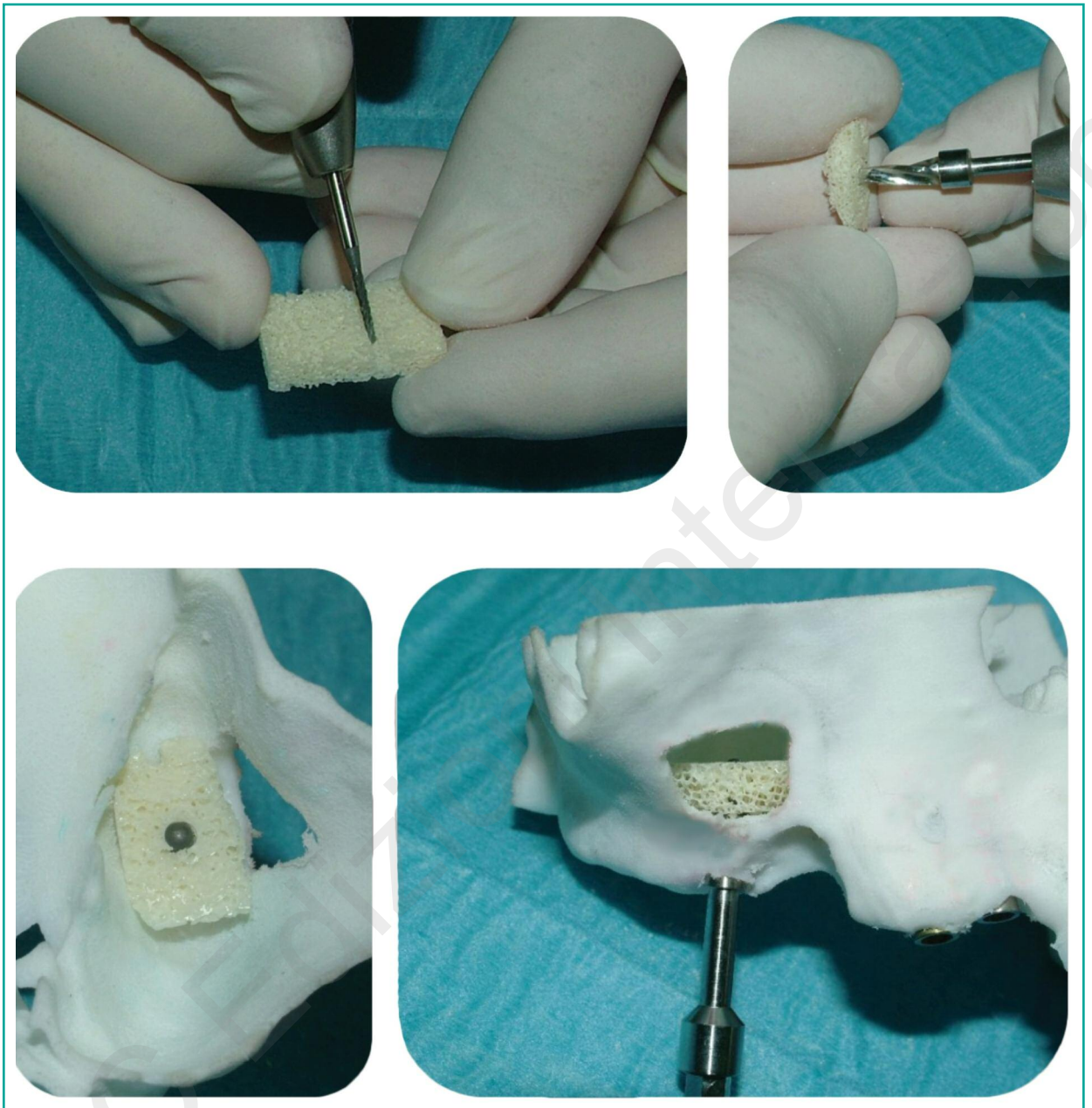

Figure 2
The SmartBone® plate is shaped accordingly with the stereolithographic (3D) model.

Once the length and diameter of the implant were determined the operation was simulated with replicas of the same size, and for this phase, modelling the antrostomy. A SmartBone® (SB@) block, a bovine decellularized bone matrix reinforced with bioresorbable aliphatic polyesters and RGD-containing collagen fragments (obtained by purified gelatin) was taken from a ready-made piece 3 millimeters thick (70-73). SB® was used for this purpose in order to achieve lateral access of restricted size. From these indications, the positions were obtained to build a guide mask with osseous attachment both for the correct insertion of implants and to pre-

cisely place the antrostromy. The geometry of the implant should usually present a coronal portion larger than the body which, in the screwing phase, functions as a halt on the external wall of the cortical bone of the sinus floor, in order to perform an anti-sinking action to which all the components of the system firmly hold in place. Lastly, both the replica implants and the stereolithographic model were packaged and sterilized.

Pre-operative preparation of Bone Block

Before surgery, the adjustment of the piece of bone to the interior of the maxillary sinus was carried out in a sterile field on the model, corresponding to the aforementioned hole for the implant and the antrostomy (Figure 2).
The portion of bone, taken from a piece of bone graft was shorn with bone rongeurs and the contouring completed with cutters. During these procedures, bone granules were produced, kept in small sterile containers and used as filler particles for the sinus.
SB® grafts are obtained by the reinforcement of bovine bone derived matrix with the mixture of PLCL [poly(L-lactic acid) and poly(ε-caprolactone)] and RGD-containing collagen fragments (obtained by purified gelatin) through a proprietary process. The bovine derived matrix is mineral and made of calcium hydroxyapatite (HA, $Ca_5(PO_4)_3(OH)$) that presents a chemical structure and a morphology that resemble the human bone (27, 28, 70-73). The presence of RGD-containing collagen fragments, even if extremely low quantities, increases the hydrophilicity of the scaffold, with consequent higher cell attachment and enhanced biocompatibility and osseointegration (29, 30, 70-73). The resulting composite material is able to mimic human bone microstructure and to ensure macro-scale properties: an adequate-sized open porosity with a combined rigid-elastic behavior, together with surface properties that ensure cell viability and fast tissue integration. SB@ heterologous bone was used for its specific properties of mechanical resistance (31, 70, 71). Once sample was shaped, it had been screwed into this bone; the implant torque was over 60 Newtons with no sign of fracture. This force allows, even at low thickness, the screwing of the implant to the interior bone without risk of cracks, which would cause mobility and prevent osseointegration. Then, the hole for the implant was made with specialist cutters for its size, and thanks to the innate resistance of the bone in question, there was no breakage or loss of stability in the screwing phase.
Moreover, the 3 millimeters' thickness of the bone block allowed the insertion into the sinus of a lateral opening of small size. Once inside the sinus, this reduced size lead to ease movement and accurate positioning for the screwing phase (Figure 3a).
This phase ended with the insertion of the bone and the solid model into sterile packages, which were prepared using double-bagged sterilization.

Surgical phase

After the appropriate anaesthetic procedure, thanks to the correct releasing incision, the flap for an ease of access for the operation was prepared. Beforehand, in this type of procedure, it is common to use a scraper for autologous bone to harvest the patient's own osteoinductive material from the area which contains the largest amount of bone. About a third of the quantity of the material required should be obtained and mixed with two-thirds of SB@ granules before the application.
The canine should be extracted and the previously prepared guide mask should be positioned. Next, the implants should be located in zones 1.2 and 1.3 and the hole prepared for the implant in 1.6, where the heterologous block will be inserted. In this phase, through the appropriate cutters,

the area should also be marked for the antroscopy in the lateral wall bone of the maxillary sinus.

Once the trap door window procedure has been carried out, the Schneider membrane should be lifted and the mix of granules located alongside and below the bone, which can immediately be placed in position. Among the layers of the floor, the walls and the bone block, a small amount of material should be used in a thin layer, not to compress or raise significantly the position of the bone block, which the implant will be screwed into (Figure 3b).

As the site is correctly prepared, while holding the bone block solid with toothed forceps, the implant can be inserted, and before proceeding, the screwing process should be positioned into the hole in the same bone block. While holding the bone in place with forceps, the implant can be screwed loosely into place. When this phase is almost complete, the bone, engaging the implant, will pull on its countersunk coronal part and at the same time it will stabilize firmly onto the base of the maxillary sinus. The whole platform system, countersunk implant, cortical bone floor and the bone block, should be rigidly connected.

At this point we can proceed to fill the empty left spaces surrounding the fixed bone block, attaching a resorbable membrane and replacing the flap. For safety reasons, it is better to use a suture with mattress stitching that finishes with button sutures (Figure 3b).

After six months, a Cone Beam Computed Tomography (CBCT) was requested to check the success of the treatment. This examination showed evidence of successful osseointegration of the implanted surfaces, the bone block and the heterologous bone granules around them (Figure 4b).

Once the results are evaluated, the implants can be crowned and the soft peri-implant tissue management phases begin. Following the healing, there can be fittings and the case can be finalized (Figure 5a, 5b).

Discussion

Sinus floor elevation is a widely-practiced technique for elevation of the maxillary sinus prior to an implant placement. Particularly, in patients with a severely resorbed maxilla, minimally invasive sinus floor elevation with simultaneous implant placement using osteotomes does not appear to be the method of choice. A 2-stage procedure using a lateral window technique (32, 33) or a crestal core approach is preferred (34, 35).

Jensen recommended that the procedure should be performed with simultaneous implant placement when a residual sub-sinus alveolar bone height (RSBH) of at least 5 mm is present. When a smaller RSBH is present, primary implant stability may be compromised (17). Therefore, the implant is inserted simultaneously with a sinus lift procedure, when sufficient primary stabilization can be expected (19, 20). The healing process can be facilitated with a reduced waiting time for the finalization of the prosthetic implant.

Unfortunately, these conditions are not always present and less-than-ideal sites can result in an esthetic and functional compromise because implant placement requires an adequate quantity and quality of bone (36-42). In many cases, this anatomic problem can be solved by replacement or augmentation of autogenous bone grafts, which is considered the most predictable and successful material available (43). Although autografts are the standard procedure for bone grafting, it is sometimes not possible to harvest bone and collect an adequate amount of bone from other donor sites in the same patient (44). Moreover, autologous bone grafts have the drawback of requiring secondary surgery for autograft retrieval, with increased operation time and anesthesia, as well as donor site morbidity. However, many forms of banked bone allograft are available: fresh frozen bone (FFB), freeze-dried bone (FDB) and demineralized fresh dried bone (DFDB). Each one of these grafts carries risks and has unique limitations and handling properties (45, 46).

Figure 3
a) Images for bare explanatory reason: 3 mm bone block thickness inside the sinus allows an accurate positioning for the screwing phase; b) position of the solid bone block and insertion of the implant into the hole in the same bone block during surgery.

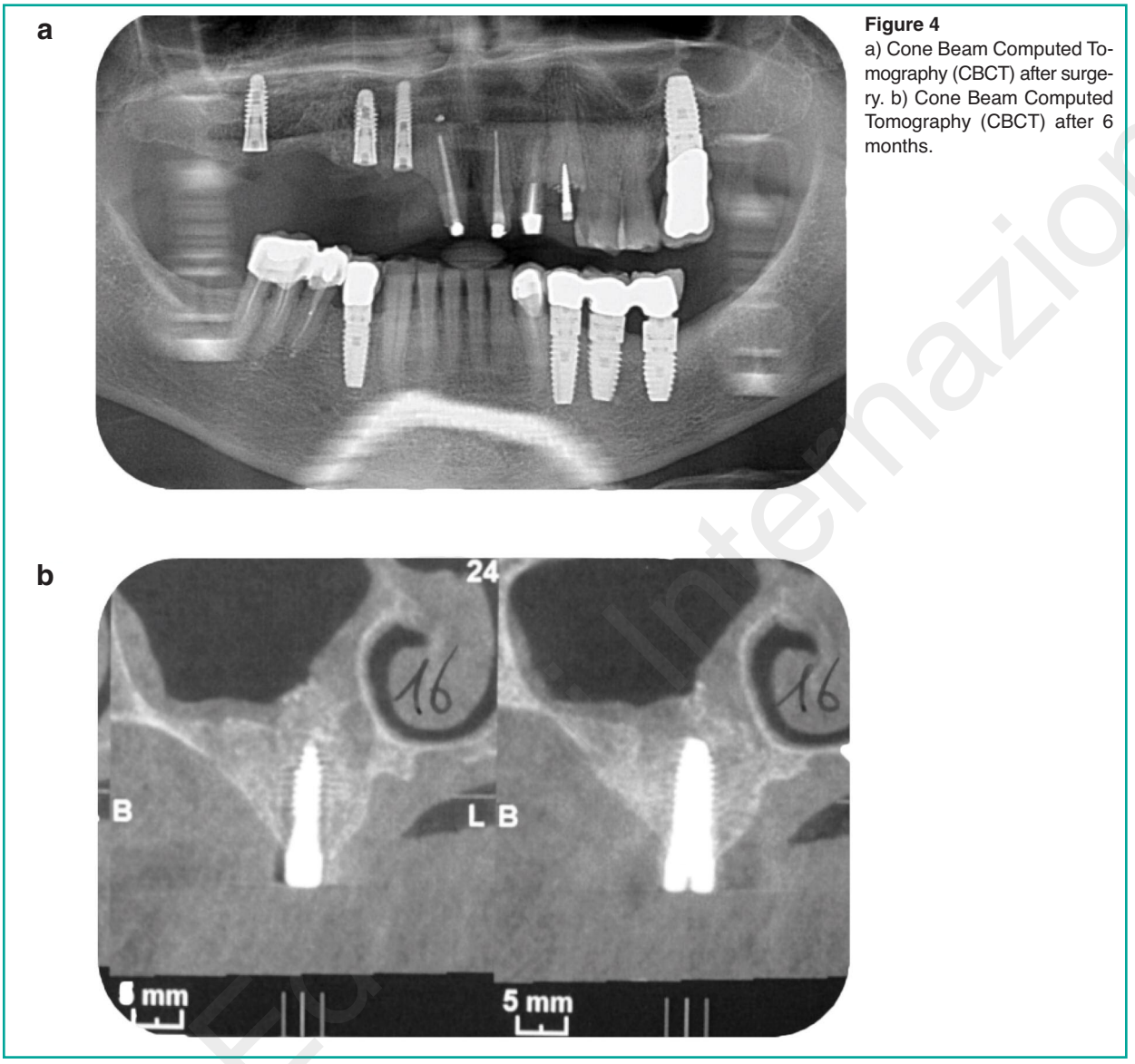

Figure 4
a) Cone Beam Computed Tomography (CBCT) after surgery. b) Cone Beam Computed Tomography (CBCT) after 6 months.

The goal of our approach was to combine the biocompatibility and tissue integration of natural materials with the possibility to tune mechanical and physical properties typical of synthetic ones. Indeed, composite grafts best mimic the real nature of healthy human bone, being rigid and elastic, compact but porous, dense but viable to cells and vessels. Bone regeneration should be performed with adequate material after controlling the periodontal disease since it can have an impact on peri-implantitis onset (47-66).

Custom hand-made SB@ of 3 millimeters was used for this purpose in order to achieve lateral access of restricted size. Data from the CBCT radiographic examination was used to make a stereolithographic (3D) model mounted onto an articulator. The positions were obtained to build a guide mask with osseous attachment both for the correct insertion of implants and to correctly place the antrostomy.

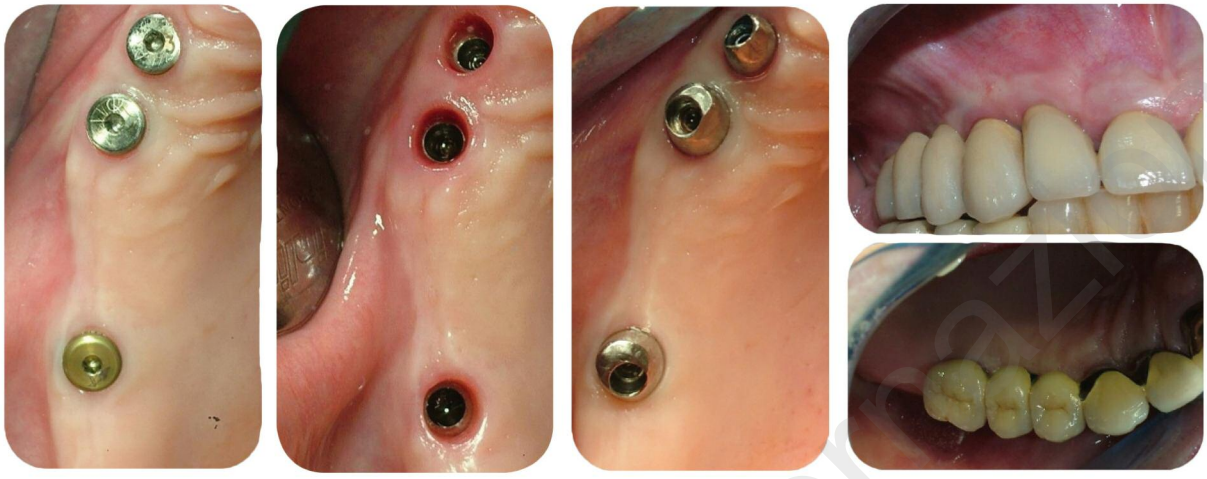

Figure 5
a) Aesthetically good gum contour and good bone augmentation after 9 months. b) Final prosthesis after 10 months.

Conclusions

In this study, we showed that the use of the SmartBone® represents a novel and successful medical application in a maxillary sinus lift procedure, which need to be considered in cases with a limited thickness of the sinus floor cortical.

The quality of life of the patient is strongly improved. The waiting time for the patient is reduced to 5-6 months in order to have a rehabilitated set of teeth, without the necessity to wait for the osseointegration of the grafted biomaterials before performing the implant procedure. Moreover, the simultaneous insertion of the implant with a sinus lift avoid a series of the various inconveniences, which can occur in between the procedure of sinus floor elevation and implant placement, and are due to the absence of dental elements (lack of occlusal function, reduction of masticatory units, aesthetic appearance).

Clinical significance

The successful realization of a contextual implant during maxillary sinus lift surgery allows the 62-year-old patient the comfort of a rehabilitated set of teeth and a consequent improvement of its quality of life, within a shorter time frame of at least 5-6 months.

References

1. de Mel A, Jell G, Stevens MM, Seifalian AM. Biofunctionalization of biomaterials for accelerated in situ endothelialization: a review. Biomacromolecules. 2008; 9(11):2969-79.
2. Chanavaz M. Maxillary sinus: anatomy, physiology, surgery, and bone grafting related to implantology—eleven years of surgical experience (1979-1990). J Oral Implantol. 1990;16(3):199-209.
3. Smiler DG, Johnson PW, Lozada JL, Misch C, Rosenlicht JL, Tatum OH, Jr., Wagner JR. Sinus lift grafts and endosseous implants. Treatment of the atrophic posterior maxilla. Dent Clin North Am. 1992;36(1):151-86; discussion 87-8.

4. Al-Almaie S. Staged osteotome sinus floor elevation for progressive site development and immediate implant placement in severely resorbed alveolar bone: a case report. Case Rep Dent. 2013;2013:310931.
5. Nedir R, Bischof M, Vazquez L, Szmukler-Moncler S, Bernard JP. Osteotome sinus floor elevation without grafting material: a 1-year prospective pilot study with ITI implants. Clin Oral Implants Res. 2006;17(6):679-86.
6. Nedir R, Nurdin N, Szmukler-Moncler S, Bischof M. Osteotome sinus floor elevation technique without grafting material and immediate implant placement in atrophic posterior maxilla: report of 2 cases. J Oral Maxillofac Surg. 2009;67(5):1098-103.
7. Andreasi Bassi M, Andrisani C, Lico S, Ormanier Z, Barlattani A, Ottria L. Endoscopic management of the Schneiderian membrane perforation during transcrestal sinus augmentation: A case report. ORAL and Implantology. 2016;9(4):157-63.
8. Clementini M, Ottria L, Pandolfi C, Bollero P. A Novel Technique to Close Large Perforation of Sinus Membrane. ORAL and Implantology. 2013;6(1):11-14.
9. Bartuli FN, Luciani F, Caddeo F, De Chiara L, Di Dio M, Piva P, Ottria L, Arcuri C. Piezosurgery vs High Speed Rotary Handpiece: a comparison between the two techniques in the impacted third molar surgery. Oral Implantol (Rome). 2013;6:5-10.
10. Slutzkey S, Cohen O, Lauritano D, Moses O, Ormianer Z, Tal H, Kolerman R, Carinci F, Matalon S. Temperature changes of one-piece implants during the setting of acrylic resin temporary crown. The effect of implant diameter. An in vitro study. J Biol Regul Homeost Agents. 2017;31(2 Suppl 1):53-60.
11. Matalon S, Frydman G, Lauritano D, Slutzky H, Shlomo E, Levartovsky S, Carinci F, Ormianer Z. The effect of enriching denture adhesives with chlorhexidine diacetate on the proliferation of Candida albicans: an in vitro analysis. J Biol Regul Homeost Agents. 2017;31(2 Suppl 1):45-52.
12. Lopez MA, Andreasi Bassi M, Confalone L, Carinci F, Ormianer Z, Lauritano D. The use of resorbable cortical lamina and micronized collagenated bone in the regeneration of atrophic crestal ridges: a surgical technique. Case series. J Biol Regul Homeost Agents. 2016;30(2 Suppl 1):81-5.
13. Lopez MA, Manzulli N, Casale M, Ormianer Z, Carinci F. The use of resorbable heterologous cortical lamina as a new sinus lift floor: A technical note. Journal of Biological Regulators and Homeostatic Agents. 2016;30(2):75-79.
14. Conti P, Carinci F, Caraffa A, Ronconi G, Lessiani G, Theoharides TC. Link between mast cells and bacteria: Antimicrobial defense, function and regulation by cytokines. Med Hypotheses. 2017;106:10-14.
15. Ormianer Z, Solodukhin AL, Lauritano D, Segal P, Lavi D, Carinci F, Block J. Bilateral symmetry of anterior maxillary incisors: evaluation of a community-based population. J Biol Regul Homeost Agents. 2017; 31(2 Suppl 1):37-43.
16. Meirowitz A, Nowotny Klein R, Lauritano D, Harel N, Block J, Matalon S, Carinci F, Ormianer Z. Survey results of currently used techniques and materials by dentists for fabrication of complete removable dental prostheses. J Biol Regul Homeost Agents. 2017;31(2 Suppl 1):27-36.
17. ten Bruggenkate CM, van den Bergh JP. Maxillary sinus floor elevation: a valuable pre-prosthetic procedure. Periodontol 2000. 1998;17:176-82.
18. O.T. J. Treatment planning for sinus grafts. In: (eds. Jensen, OT). The Sinus Bone Graf. Carol Stream, Ill, USA: Quintessence Publishing; 1999:49-68.
19. Tatum OH. Maxillary sinus grafting for endosseous implants. In: Annual Meeting of the Alabama Implant Study Group (Birmingham, Alabama, USA, 1977).
20. Tatum H, Jr. Maxillary and sinus implant reconstructions. Dent Clin North Am. 1986;30(2):207-29.
21. Falisi G, Severino M, Rastelli C, Bernardi S, Caruso S, Galli M, Lamazza L, Di Paolo C. The effects of surgical preparation techniques and implant macro-geometry on primary stability: An in vitro study. Medicina Oral, Patologia Oral y Cirugia Bucal. 2017;22(2):e201-e06.
22. Pocaterra A, Caruso S, Bernardi S, Scagnoli L, Continenza MA, Gatto R. Effectiveness of platelet-rich plasma as an adjunctive material to bone graft: a systematic review and meta-analysis of randomized controlled clinical trials. International Journal of Oral and Maxillofacial Surgery. 2016;45(8):1027-34.
23. Marrelli M, Pujia A, Palmieri F, Gatto R, Falisi G, Gargari M, Caruso S, Apicella D, Rastelli C, Nardi GM, Paduano F, Tatullo M. Innovative approach for the in vitro research on biomedical scaffolds designed and customized with CAD-CAM technology. International Journal of Immunopathology and Pharmacology. 2016;29(4):778-83.
24. Giuca MR, Pasini M, Giuca G, Caruso S, Necozione S, Gatto R. Investigation of periodontal status in type 1 diabetic adolescents. European journal of paediatric dentistry: official journal of European Academy of Paediatric Dentistry. 2015;16(4):319-23.
25. Giuca MR, Pasini M, Caruso S, Tecco S, Necozione S, Gatto R. Index of orthodontic treatment need in obese adolescents. International Journal of Dentistry. 2015;2015.
26. Caruso S, Sgolastra F, Gatto R. Dental pulp regeneration in paediatric dentistry: The role of stem cells. European Journal of Paediatric Dentistry. 2014;15(1):90-94.
27. He J, Genetos DC, Leach JK. Osteogenesis and trophic factor secretion are influenced by the composition of hydroxyapatite/poly(lactide-co-glycolide) composite scaffolds. Tissue Eng Part A. 2010;16(1):127-37.
28. Kane RJ, Roeder RK. Effects of hydroxyapatite reinforcement on the architecture and mechanical properties of freeze-dried collagen scaffolds. J Mech Behav Biomed Mater. 2012;7:41-9.

29. Isikli C, Hasirci V, Hasirci N. Development of porous chitosan-gelatin/hydroxyapatite composite scaffolds for hard tissue-engineering applications. J Tissue Eng Regen Med. 2012; 6(2):135-43.
30. Jeong SI, Lee AY, Lee YM, Shin H. Electrospun gelatin/poly(L-lactide-co-epsilon-caprolactone) nanofibers for mechanically functional tissue-engineering scaffolds. J Biomater Sci Polym Ed. 2008;19(3):339-57.
31. Salgado AJ, Coutinho OP, Reis RL. Bone tissue engineering: state of the art and future trends. Macromol Biosci. 2004;4(8):743-65.
32. Fugazzotto PA. Maxillary sinus grafting with and without simultaneous implant placement: technical considerations and case reports. Int J Periodontics Restorative Dent. 1994;14(6):544-51.
33. Wheeler SL, Holmes RE, Calhoun CJ. Six-year clinical and histologic study of sinus-lift grafts. Int J Oral Maxillofac Implants. 1996;11(1):26-34.
34. Fugazzotto PA. The modified trephine/osteotome sinus augmentation technique: technical considerations and discussion of indications. Implant Dent. 2001;10(4): 259-64.
35. Toffler M. Staged sinus augmentation using a crestal core elevation procedure and modified osteotomes to minimize membrane perforation. Pract Proced Aesthet Dent. 2002;14(9):767-74; quiz 76.
36. Baj A, Trapella G, Lauritano D, Candotto V, Mancini GE, Gianni AB. An overview on bone reconstruction of atrophic maxilla: success parameters and critical issues. J Biol Regul Homeost Agents. 2016;30(2 Suppl 1):209-15.
37. Grecchi F, Perale G, Candotto V, Busato A, Pascali M, Carinci F. Reconstruction of the zygomatic bone with smartbone®: Case report. Journal of Biological Regulators and Homeostatic Agents. 2015;29(3):42-47.
38. Lauritano D, Avantaggiato A, Candotto V, Cura F, Gaudio RM, Martinelli M, Palmieri A. Insulin activity on dental pulp stem cell differentiation: An in vitro study. Journal of Biological Regulators and Homeostatic Agents. 2015;29(3):48-53.
39. Tettamanti L, Andreasi Bassi M, Trapella G, Candotto V, Tagliabue A. Applications of biomaterials for bone augmentation of jaws: Clinical outcomes and in vitro studies. ORAL and Implantology. 2017;10(1):37-44.
40. Baj A, Sollazzo V, Lauritano D, Candotto V, Mancini GE, Gianni AB. Lights and shadows of bone augumentation in severe resorbed mandible in combination with implant dentistry. Journal of Biological Regulators and Homeostatic Agents. 2016;30(2):177-82.
41. Lauritano D, Avantaggiato A, Candotto V, Cura F, Gaudio RM, Scapoli L, Palmieri A. Effect of somatostatin on dental pulp stem cells. Journal of Biological Regulators and Homeostatic Agents. 2015;29(3):54-58.
42. Baj A, Muzio LL, Lauritano D, Candotto V, Mancini GE, Gianni AB. Success of immediate versus standard loaded implants: A short literature review. Journal of Biological Regulators and Homeostatic Agents. 2016; 30(2):183-88.
43. Carinci F, Farina A, Zanetti U, Vinci R, Negrini S, Calura G, Laino G, Piattelli A. Alveolar ridge augmentation: a comparative longitudinal study between calvaria and iliac crest bone grafrs. J Oral Implantol. 2005;31(1):39-45.
44. Carinci F, Guidi R, Franco M, Viscioni A, Rigo L, De Santis B, Tropina E. Implants inserted in fresh-frozen bone: a retrospective analysis of 88 implants loaded 4 months after insertion. Quintessence Int. 2009;40(5): 413-9.
45. Viscioni A, Franco M, Rigo L, Guidi R, Brunelli G, Carinci F. Implants inserted into homografts bearing fixed restorations. Int J Prosthodont. 2009;22(2):148-54.
46. Gajiwala K, Lobo Gajiwala A. Use of banked tissue in plastic surgery. Cell Tissue Bank. 2003;4(2-4):141-6.
47. Lauritano D, Martinelli M, Mucchi D, Palmieri A, Muzio LL, Carinci F. Bacterial load of periodontal pathogens among Italian patients with chronic periodontitis: A comparative study of three different areas. Journal of Biological Regulators and Homeostatic Agents. 2016;30(2):149-54.
48. Lauritano D, Scapoli L, Mucchi D, Cura F, Muzio LLO, Carinci F. Infectogenomics: Lack of association between vdr, il6, il10 polymorphisms and "red Complex" bacterial load in a group of Italian adults with chronic periodontal disease. Journal of Biological Regulators and Homeostatic Agents. 2016;30(2):155-60.
49. Checchi L, Gatto MR, Checchi V, Carinci F. Bacteria prevalence in a large Italian population sample: A clinical and microbiological study. Journal of Biological Regulators and Homeostatic Agents. 2016;30(2):199-208.
50. Meynardi F, Pasqualini ME, Rossi F, Dal Carlo L, Biancotti P, Carinci F. Correlation between dysfunctional occlusion and periodontal bacterial profile. Journal of Biological Regulators and Homeostatic Agents. 2016;30(2):115-21.
51. Lombardo L, Carinci F, Martini M, Gemmati D, Nardone M, Siciliani G. Quantitive evaluation of dentin sialoprotein (DSP) using microbeads - A potential early marker of root resorption. ORAL and Implantology. 2016;9(3):132-42.
52. Lauritano D, Cura F, Candotto V, Gaudio RM, Mucchi D, Carinci F. Evaluation of the Efficacy of Titanium Dioxide with Monovalent Silver Ions Covalently Linked (Tiab) as an Adjunct to Scaling and Root Planing in the Management of Chronic Periodontitis Using Pcr Analysis: A Microbiological Study. J Biol Regul Homeost Agents. 2015;29(3 Suppl 1):127-30.
53. Scapoli L, Girardi A, Palmieri A, Martinelli M, Cura F, Lauritano D, Carinci F. Quantitative Analysis of Periodontal Pathogens in Periodontitis and Gingivitis. J Biol Regul Homeost Agents. 2015;29(3 Suppl 1):101-10.
54. Lauritano D, Cura F, Candotto V, Gaudio RM, Mucchi D, Carinci F. Periodontal Pockets as a Reservoir of He-

licobacter Pylori Causing Relapse of Gastric Ulcer: A Review of the Literature. J Biol Regul Homeost Agents. 2015;29(3 Suppl 1):123-6.
55. Scapoli L, Girardi A, Palmieri A, Martinelli M, Cura F, Lauritano D, Pezzetti F, Carinci F. Interleukin-6 Gene Polymorphism Modulates the Risk of Periodontal Diseases. J Biol Regul Homeost Agents. 2015;29(3 Suppl 1):111-6.
56. Roncati M, Lauritano D, Cura F, Carinci F. Evaluation of light-emitting diode (led-835 nm) application over human gingival fibroblast: An in vitro study. Journal of Biological Regulators and Homeostatic Agents. 2016;30(2):161-67.
57. Andreasi Bassi M, Andreasi Bassi S, Andrisani C, Lico S, Baggi L, Lauritano D. Light diffusion through composite restorations added with spherical glass mega fillers. ORAL and Implantology. 2016;9(80-89.
58. Carinci F, Palmieri A, Girardi A, Cura F, Lauritano D. Aquolab ® ozone-therapy is an efficient adjuvant in the treatment of chronic periodontitis: A case-control study. Journal of Orofacial Sciences. 2015;7(1):27-32.
59. Lauritano D, Cura F, Gaudio RM, Pezzetti F, Andreasi Bassi M, Carinci F. Polymerase Chain Reaction to Evaluate the Efficacy of Silica Dioxide Colloidal Solutions in the Treatment of Chronic Periodontitis: A Case Control Study. J Biol Regul Homeost Agents. 2015;29(3 Suppl 1):131-5.
60. Di Girolamo M, Arullani CA, Calcaterra R, Manzi J, Arcuri C, Baggi L. Preservation of extraction socket in immediate implant placement: A clinical study. ORAL and Implantology. 2016;9(4):222-32.
61. Calcaterra R, Di Girolamo M, Mirisola C, Baggi L. Effects of Repeated Screw Tightening on Implant Abutment Interfaces in Terms of Bacterial and Yeast Leakage in Vitro: One-Time Abutment Versus the Multiscrewing Technique. Int J Periodontics Restorative Dent. 2016;36(2):275-80.
62. Calcaterra R, Di Girolamo M, Mirisola C, Baggi L. Expression of Pattern Recognition Receptors in Epithelial Cells Around Clinically Healthy Implants and Healthy Teeth. Implant Dent. 2016;25(3):348-52.
63. Calcaterra R, Pasquantonio G, Vitali LA, Nicoletti M, Di Girolamo M, Mirisola C, Prenna M, Condo R, Baggi L. Occurrence of Candida species colonization in a population of denture-wearing immigrants. Int J Immunopathol Pharmacol. 2013;26(1):239-46.
64. Moretto D, Gargari M, Nordsjo E, Gloria F, Ottria L. Immediate loading: a new implant technique with immediate loading and aesthetics: Nobel Active. Oral Implantol (Rome). 2008;1(2):50-5.
65. Scarano A, Sinjari B, Di Orio D, Murmura G, Carinci F, Lauritano D. Surface analysis of failed oral titanium implants after irradiated with ErCr:ysgg 2780 laser. European Journal of Inflammation. 2012;10(1 S2):49-54.
66. Fanali S, Carinci F, Zolliiqo I, Brugnati C, Lauritano D. One-piece implants installed in restored mandible: A retrospective study. European Journal of Inflammation. 2012;10(1):37-41.
67. Stevens MM. Biomaterials for bone tissue engineering. Mater Today. 2008;11(5):18-25.
68. Ferrigno N, Laureti M, Fanali S. Dental implants placement in conjunction with osteotome sinus floor elevation: a 12-year life-table analysis from a prospective study on 588 ITI implants. Clinical Oral Implants Research. 2006;17(2):194-205.
69. Ten Bruggenkate CM, Van den Bergh JPA. Maxillary sinus floor elevation: a valuable pre-prosthetic procedure. Periodontology 2000. 1998;17(1):176-82.
70. Pertici G, Rossi F, Casalini T, Perale G. Composite polymer-coated mineral grafts for bone regeneration: material characterisation and model study, Annals of Oral & Maxillofacial Surgery. 2014;2(1):4.
71. Pertici G, Carinci F, Carusi G, Epistatus D, Villa T, Crivelli F, et al. Composite Polymer-Coated Mineral Scaffolds for Bone Regeneration: From Material Characterization to Human Studies. J Biol Regul Homeost Agents. 2015;29:136-48.
72. Rossi F, Santoro M, Perale G. Polymeric scaffolds as stem cell carriers in bone repair, J Tissue Eng Regen Med. 2015;9:1093-119.
73. D'Alessandro D, Perale G, Milazzo M, Moscato S, Stefanini C, Pertici G et al. Bovine bone matrix/poly(l-lactic-co-epsilon-caprolactone)/gelatin hybrid scaffold (SmartBone(R)) for maxillary sinus augmentation: A histologic study on bone regeneration. Int J Pharm. 2017;523:534-544.

Correspondence to:
Dorina Lauritano
Department of Medicine and Surgery
University of Milano "Bicocca"
Via Cadore 48
20052 Monza, Italy
Phone: +39.0392332301
Fax: +39. 03923329892
E-mail: dorina.lauritano@unimib.it

Current Pharmaceutical Biotechnology, 2018, *19*, 1005-1013

RESEARCH ARTICLE

Improving Bovine Bone Mechanical Characteristics for the Development of Xenohybrid Bone Grafts

Alberto Cingolani[1,2], Carlo Francesco Grottoli[2], Raffaella Esposito[3], Tomaso Villa[3], Filippo Rossi[4] and Giuseppe Perale[2,5,6*]

[1]*Department of Chemistry and Applied Bioscience ETH Zurich, Institute for Chemical and Bioengineering, Vladimir-Prelog-Weg 1-5/10, 8093 Zürich, Switzerland;* [2]*Industrie Biomediche Insubri SA (IBI), Via Cantonale 67, 6805 Mezzovico-Vira, Switzerland;* [3]*Laboratory of Biological Structure Mechanics, Department of Chemistry, Materials and Chemical Engineering "G. Natta", Politecnico di Milano, 20133 Milan, Italy;* [4]*Laboratory of Applied Physical Chemistry, Department of Chemistry, Materials and Chemical Engineering "G. Natta", Politecnico di Milano, 20133 Milan, Italy;* [5]*Biomaterials Laboratory, Institute for Mechanical Engineering and Materials Technology, SUPSI – University of Applied Sciences and Arts of Southern Switzerland. Via Cantonale 2C, Galleria 2, 6928 Manno, Switzerland;* [6]*Department of Surgical Sciences, Orthopaedic Clinic-IRCCS A.O.U. San Martino, 16132 Genova, Italy*

Abstract: ***Background***: The further functionalization of natural existing biomaterials is a very efficient method to introduce additional advanced characteristics on a unique structural composition and architecture.

Objective: As an example, different animal sources, if properly treated, can be used to develop bone xenograft active in hard tissues regeneration. In this sense, it is also important to consider that the selected process has to take into consideration the intrinsic variability of the base material itself and possibly being able to compensate for it.

Methods: In this work we characterize cancellous bovine bone treated by deposition of polymer and collagen and we show that the added components not only lead to a more resistant and more hydrophilic material, but also reduce the conventional correlation between apparent density and elastic modulus, which, in general, is a major source of uncertainty and risk in xenografts usage.

Results: Moreover, though intrinsically reinforcing the material, the deposition process leaves the specific open-porous structure, that allows cells proliferation and vessels ingrowth, basically unaltered.

Conclusion: The final material combines in a single piece and at the same time, mechanical resistance, homogeneous mechanical response and proper structural characteristics that allow further integration within the patient autochthonous tissues.

ARTICLE HISTORY

Received: June 19, 2018
Revised: September 03, 2018
Accepted: November 25, 2018

DOI:
10.2174/1389201020666181129115839

Keywords: Hard tissues regeneration, xenografts, tissue engineering, biomaterials, bovine bone, biopolymers.

1. INTRODUCTION

As recent studies and characterization at nano and micro-scale of biological complex systems enabled to enlighten and understand the mechanism of action of many of them [1], novel and elaborated multi-functional materials, mimicking [2, 3] or taking inspiration [4] from their natural counterparts started to be properly developed and implied in diverse engineering strategic fields, from surface [5] and structure design [6] to tissue regeneration [7-10]. In most biological materials the advanced peculiarities are provided by the unique structural composition, both in terms of chemistry as well as physical arrangement, which is, in general, obtained following a naturally occurring bottom-up approach [11]. A very good example, in this sense, is represented by the biomineralization processes leading to complex hierarchical structures [12]. It appears evident that replicating or externally guiding the development of such a refined solid framework in three dimensions, is all but trivial and, most of the time, highly

*Address correspondence to this author at Biomaterials Laboratory, Institute for Mechanical Engineering and Materials Technology, SUPSI – Universityof Applied Sciences and Arts of Southern Switzerland. *Via* Cantonale 2C, Galleria 2, 6928 Manno, Switzerland; Tel: +41919306640;
Fax: +41912207200; E-mail: giuseppe.perale@supsi.ch

1873-4316/18 $58.00+.00

complicated strategic paths and methodologies need to be properly devised [3, 13, 14]. Moreover, most biological materials do not have only one functionality, but rather a combination of different ones and need to be treated as composites. Indeed, *e.g.* in biomaterials intended for bone grafting and substitution, a mineral or ceramic component is needed to provide strength and stiffness whereas other biopolymer constituents are needed to provide the viscoelastic damping and toughness while also offering enhanced cell viability [1, 15].

Another possibility that allows the overcoming of the aforementioned difficulties in synthetic strategies, is represented by the utilization of already naturally existing biomaterials, either directly or after a post-treatment providing additional advanced functionalities [16, 17]. Certainly, bone-grafts obtained from animal-derived cancellous bone, and implied as substitutes and filler in hard tissue regeneration, represent a major category in this sense, also being routinely used in clinical practice ever since many decades [18, 19]. Indeed, autografts (when the bone comes from the patient itself) as well as allografts (when the bone comes from another human donor, either living or cadaver) and xenografts (when the bone comes from an animal) have been all successfully applied in bone repair, in a wide spectrum of reconstructive surgical specialties [20]. It is acknowledged that bovine-derived cancellous bone grafts are the closest xenograft to human bone to be regenerated, second self-evidently only to autografts [21-23]. These biomaterials clearly present a major advantage over their synthetic competitors (*e.g.* hydroxyapatite, beta-TriCalciumPhospate, *etc.*), since they have much higher osteogenic and osteoconductive performances [16, 20, 24]. Indeed, the hierarchical porous structure [25], naturally present in cancellous bone, acts as a scaffold for cells favoring their colonization and proliferation [20]. This way, the implanted device gets completely integrated into the body and over long periods completely replaced by the patient autochthonous tissues [16]. However, necessary cleaning and sterilization processes of starting raw materials of animal origin result in a decay of both mechanical and biological performances. Moreover, when dealing with naturally produced biomaterials, it is always necessary to keep in mind that they arise from processes which preserve an intrinsic biological variability in the final product [1]. This concept is both valid for materials coming from equivalent part, but different individual systems (*i.e.* the bone of the same part of two bovines of the same species) as well as for distinct section within the same one (the bone between the different segments of the same animal). Focusing on bovine-derived bone xenografts, it is well known that the density of cancellous bone varies along trabecular trajectories with a major consequence on its mechanical properties [23, 26]. Therefore, in the frame of using it as a base material for the development of implantable devices, which need to meet both requirements of tissue regeneration and structural support, this represents a huge limitation. As a matter of fact, the lack of possibility of predicting a priori, the mechanical response to the applied load once placed inside the patient body generates a high risk that should be mitigated, also according to new regulatory framework requirements [27]. Consequently, in order to make animal-derived cancellous bone, a desirable material for bone grafts, a technique not only improving but also homogenizing the mechanical properties, making them independent on the raw, untreated material characteristics, is required [23]. Last but not the least, the actual porous structure needs to be left open, interconnected and very poorly altered to preserve the osteogenic and osteoconductive performances [23]. Indeed, similar to what has been commonly seen for synthetic biomaterials [23], the application of composite technologies to bovine xenografts is becoming an interesting trend, not only in research [28, 29] but also in industrial and clinical practices [17, 30]: the addition of resorbable polymeric components improves mechanical and biological performances [10] and can also be used to locally carry active molecules, or drugs to be delivered locally, to increase cell colonization, promote osteoinduction and finally promote osteogenesis [16, 24]. Overall, increased performance of bone graft is still the major focus in orthobiologics [23].

Within this framework, we here present the characterization of a material developed upon treatment of cancellous decellularized, deproteinized and defatted bovine bone with additional biopolymer and collagen fragments [17] in order to track the effect of the post-modification on the final product. It was found that the treatment not only improves considerably the mechanical properties and hydrophilicity of the initial bovine-derived matrix, but rather makes them more independent of the intrinsic porous structure, overcoming the difficulties of using a nonuniform base material.

Single 15x30x60mm^^{3} pieces of cancellous bovine bone, biggest harvestable from adult bull femur head, have been subdivided in the different subsections which have been individually analyzed before and after the treatment. If the mechanical properties, as expected, were highly dependent on the density of the raw material, a considerable homogenization of them is instead recorded after modification, together with an overall increased mechanical resistance. In addition, the conventional porous structure is not modified, and very similar density and porosity values are recorded before and after the treatment. The combination of these two concepts is of utmost importance: on the one hand, the homogenous mechanical response is ensured; on the other hand, cells proliferation and vascular ingrowth are not hindered by changes in the porous structure, being even further enhanced by the presence of collagen fragments [24]. As a matter of fact, the characteristics of the final product support it in being a proper xenograft, able to be not only effectively implanted but also fully substituted by patient living healthy bone [16, 30].

2. MATERIALS AND METHODS

2.1. Materials

Among modified xenografts, a scaffold composed of processed bovine bone matrix, mainly mineral constituted, reinforced with biopolymers, namely block copolymer of poly(L-lactic acid) and poly(ε-caprolactone), with selected physical properties to allow proper withstanding of treatment and sterilization [31], and arginylglycylaspartic acid (RGD) containing collagen fragments (mainly type I), obtained from animal-derived gelatin [32], has recently been proposed as a bone substitute for reconstructive surgeries, available as a

class III medical device (commercially named SmartBone®, by Industrie Biomediche Insubri SA, Switzerland) [16, 17, 24, 30]. Bovine-derived decellularized, defatted and deproteinized cancellous bone is sourced certified for human use and of BSE/TSE (Bovine Spongiform Encephalopathy/ Transmissible Spongiform Encephalopathies) free origin (currently "Negligible BSE risk Countries", former "OIE1 Countries").

2.2. Cutting of the Bone and Reinforcement Process

Raw bovine bone blocks used in this study present a nominal size of 15x30x60mm^3. Before applying reinforcement with biopolymers and collagen, each block was subdivided into smaller identical cubes of nominal dimension of 7x7x7mm^3 by properly cutting the initial shape with a diamond-edged automatic saw. The reason for which the sum of the length of the individual cubes is smaller than the total one of the initial block resides in the thickness of the blade that indeed consumes roughly 1.5 mm when cutting. During this phase, the bone was wet with water and ethanol in order to minimize temperature increase, due to friction, and dust generation. Proper sizing of the samples was measured with a digital calibrated caliber with a resolution of 0.05 mm (Adolf Würth GmbH & Co. KG, Germany).

Once oven dried (in vacuum at 37°C for 18 h), the obtained cubes (56 per each starting block, see also scheme depicted in Fig. **3**) had been treated with the proprietary reinforcement process that allowed deposition, over the bone surfaces, of biopolymers embedding animal-derived gelatin that allows RGD-containing collagen fragments [17, 33, 34]. This process involves: a) preparation of a solution of reinforcing mixture containing a dissolved polymer and gelatin b) immersion of the base matrix and c) drying in a vacuum oven at 37°C for 24 h for removing possible solvents residues.

2.3. Physical-chemical Characterization

Each individual sample has been weighted and measured using an electronic calibrated balance Mark 8055 (Bel Engineering, Monza, Italy) and digital caliber with a resolution of 0.05 mm (Adolf Würth GmbH & Co. KG, Germany) before and after the treatment. Apparent density has been determined by the classical definition of mass over volume. The volume was computed using the conventional geometrical formulas for parallelepiped solids (L1xL2xL3). For the measurement of the contact angle and wetting properties, pictures of the drops were taken using a digital microscope AM4115T from Dino-lite (AnMo Electronics corporations, Taiwan). The actual values have been computed using Image J software [35, 36]. The reported values are averaged over five independent measurements. Environmental scanning electron microscopy (ESEM) and energy dispersive analysis (EDS) were performed at 10 kV with 50 EP Instrumentation (Zeiss, Jena, Germany), according to previously published methodology [34], to assess the correct presence of the polymeric domains. FTIR analysis has been performed as follows: samples were laminated with potassium bromide and then recorded using a Thermo Nexus 6700 spectrometer coupled to a Thermo Nicolet Continuum microscope equipped with a ×15 Reflachromat Cassegrain objective.

2.4. Mechanical Tests and Analysis of the Data

According to previously published methodology [34], compression tests were run on MTS 858 MiniBionix testing machine (S/N 1015457, MTS, Minneapolis, MN, USA) driven by a digital controller Test Star II. The machine was equipped with a hydraulic axial actuator with a load capacity of 25 kN and an LVDT displacement transducer with a working range of 100 mm. The compression tests were run after placing the specimen in the lower center of the two rigid parallel steel plates, connected to the load cell of the testing machine: the upper plate, connected to the actuator of the same machine, was then moved downward at 1 mm/min speed under displacement control. The test was stopped when the maximum load peak was reached. During the test, force and displacement data were collected at 10 Hz frequency: the data were then elaborated to obtain the stress σ on a generical section S computed as $\sigma = F / S$, where F is the actual force measured by the load cell. Moreover, the strain of the specimen was calculated as $\varepsilon = \Delta L / L_0$, where L_0 is the initial height of the sample in the direction of the test and ΔL is the measured value of the actuator displacement equivalent to the shortening of the specimen during the test. These data were used to build, for each individual sample, the stress-strain plot, from which the elastic modulus E was obtained as the initial linear slope of the curve. Experimental data were analyzed using Analysis of Variance (ANOVA); statistical significance was set to P value < 0.05. Results are presented as mean $\pm$ standard deviation.

3. RESULTS AND DISCUSSION

3.1. Intrinsic Variability in Untreated Pristine Cancellous Bone Tissues

As generally known and already discussed by Langton *et al*. [25] and Skedros *et al*. [26], cancellous bone has a non-uniform porous structure, whose internal arrangement depends indeed on many factors, including position within the body, functions and applied loads [37]. Moreover, bone experiences continuous re-shaping also during an individual's life and changes its structure continuously depending on the external stimuli, which include diet, diseases, traumas and lifestyle [38, 39]. Fig. (**1**) shows the top view of a decellularized cancellous bovine block as purchased to manufacture SmartBone®. Clearly, different trajectories can be identified within the constituting trabeculae and, already by visual inspection, major differences in porosity are visible over the whole volume of the block itself. This reflects also in high apparent density gradient along the block body with a consequential contiguous variation of the mechanical characteristics as well. Although a correlation between these two aforementioned parameters exists and is well established [40], one has to be very careful in using it. Indeed, as shown in Fig. (**1** and **2**), over a huge volume of bone (in this case 15x30x60mm3, being the biggest harvestable cancellous bone block from an adult femur head) some areas might be considerably denser than the others with the consequence of having regions which have different resistance. Therefore, the overall apparent density might be not really representative of the distribution of mechanical properties within the block. This previous statement becomes even more im-

portant when considering that, in general, the block would not be used as such but rather properly cut or milled to reach complex geometries to be adapted to fit into real bone defects. As a matter of fact, hardly it is possible to find a contiguous way through the bone presenting homogeneous structure and eventually also the finished piece will have inevitably a substantial inhomogeneity in its final properties, even different from the ones of the initial block itself, as depicted in Fig. (**2**). This represents a huge limitation for an implantable device, especially considering that it is often very difficult to know in advance where exactly and in which conditions, the piece will be placed into the patient body and which loads it will have to withstand over a long period of time. In order to properly rationalize what previously discussed, we decided to investigate and identify the actual density gradient of the bone blocks and establish in which way it affects the distribution of mechanical properties in the untreated, pristine bovine bone. Apart from the already introduced intrinsic variability of the bone itself, related to its animal origin, it is also true that visually all blocks present a similar trabecular pattern, with defined orientation of the trabecular paths, being related to harvesting made when extracting raw materials from adult male cattle. Indeed, coming from a bovine femur's head, they present a trajectorial structure, which enables to roughly identify the orientation of the block within the initial femur's matrix, following Wolff trajectory hypothesis [41]. The obtained value is 40° over the plane tangential to the femur's head. Moreover, it is important to state that there are not too many lines over which the cut can be applied in order to obtain such a huge volume of bone in a single shape, with the best possible homogeneity. This statement is also confirmed by the supplier, who ensure identical shaping conditions and cutting orientation for all his products, being a medical device manufacturing process. The initial blocks, therefore, have been first split into two halves, the top one named ***v*** and the bottom named ***o***. Subsequently, both of them have been also parted into four smaller sections along the longer side, named A, B, C and D. In order to obtain representative values, these four sections have also been subdivided into seven pieces each, obtaining cubes of 7x7x7mm^3, as previously described and shown in Fig. (**3**). Each of these pieces has been characterized individually in terms of density and mechanical properties and average values for each of the four sections obtained. In this sense, only variation in average density of at least 0.01 g/cm^3 has been considered relevant in the frame of an accurate quantification of the difference before and after the treatment. Moreover, since in general bone is anisotropic [25], it was decided to apply a vertical load to the pieces coming from section ***v*** and a horizontal one to those coming from ***o***, in order to obtain a more complete and more statistically robust characterization [42].

3.1.1. Apparent Density

As mentioned before, there is a substantial difference in measuring the apparent density of the block as a whole and of its diverse sections. The results are reported in Fig. (**4**) and it can be seen that density increases moving from section A to D over the whole block volume in both sections ***v*** and ***o***. Moreover, though the trend is the same, some difference is observed also between the top and the bottom of the block itself. Therefore, it can be stated that the density, and therefore the porosity, of the block varies both in the horizontal as well as vertical axis of the block. On the other hand, though the recorded values are not homogeneous, they all ensure the right porosity and arrangement for cell colonization of the support, being a matching result with the orthobiologics' main paradigm.

Fig. (1). Top view of the prisitne cancellous bovine bone (scale bar = 10 mm), showing the trabecular arrangement and the consequent porous structure.

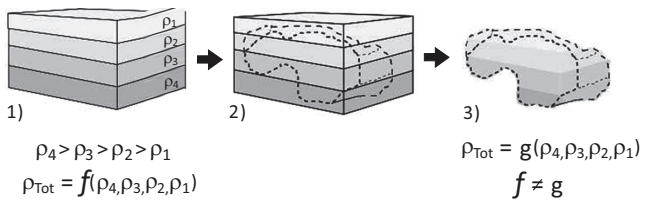

Fig. (2). General scheme of the usage of the block for the preparation of derived products. 1) An initial block of bone presents a gradient of density along its volume. Each different sector, with his own density contribute to overall density of the block. When the block is milled and shaped in complex geometries 2), it is often hard to be able to work only within a section with homogenous density, with the result 3) that the final piece might have a different density distribution along its volume.

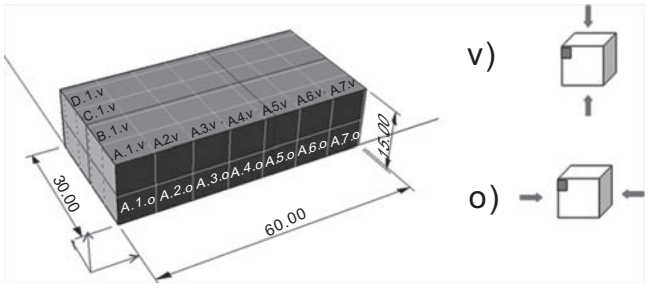

Fig. (3). Subdivision of the block into smaller sections and individual pieces. On the top section v the load has been applied vertically whereas on the bottom one o, horizontally.

3.1.2. Mechanical Properties

The analysis of mechanical properties reveals a substantial, yet expected, dependence of the elastic modulus E on the apparent density of the tested cubic sample, as reported

in Fig. (**5**). Moreover, moving from section A to D, in both part ***v*** and ***o***, a clear gradient in the value of E can be noticed. In general, the higher is the density, the higher the mechanical resistance, independently of the direction over which the load is applied. In particular, the value of E moves from 258.07 ± 72.8 MPa to 518.2 ± 76.4 MPa in the case of applied horizontal load and from 182.94 ± 70.5 MPa to 410.45 ± 64 MPa for the vertical one. As a matter of fact, it can be easily observed that the huge variability of the apparent density within the different section, reflects in a similar variability on the mechanical properties of the untreated material. For the sake of completeness, it is important to remind that the apparent density is not the only parameter affecting the elastic modulus value, but also many others, such as the trabeculae orientation and the actual position of the bone within the body might have an impact. In our specific case, the obtained values find good accordance with those reported by Töyräs *et al.* [43] who measured an elastic modulus of 278 ± 154 MPa for a femur's head and 495 ± 245 MPa for a bovine tibia.

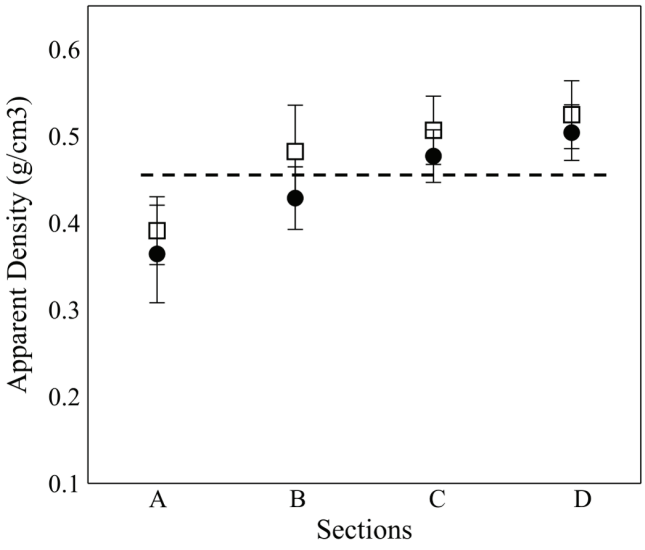

Fig. (4). Apparent density within the different block sections (A,B,C,D) for the pristine bone block, both in the v part (●) as well as o one (□). In addition, also the overall apparent density of the block is plotted (dashed line).

3.2. Effect of the Reinforcement Treatment

In this section, the effect of the treatment on the previously investigated physical and structural characteristics of the initial matrix is evaluated. As mentioned before, the process basically involves the deposition of polymer (PLA-PCL) and gelatin on the pristine cancellous bovine-derived bone. The first component provides elasticity and toughness and limits the otherwise fragile behavior of the bone. The second one improves hydrophilicity and ensures good cell adhesion and viability [34]. The block has been first subdivided in sections and pieces following the same procedure as before. Afterward those samples have been treated and characterized in the same way as the untreated ones. As already highlighted, because of equivalent cutting angle and procedure directly out of the femur's head, good correspondence is found within the orientation of the trabecular frame among the two used starting blocks. This visual check makes the obtained results, despite very little intrinsic variability, properly and reasonably comparable.

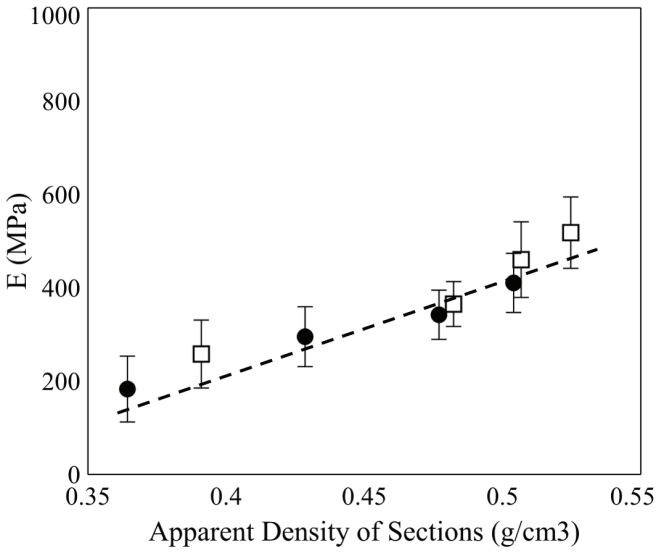

Fig. (5). Elastic modulus vs density of the prisitne bone block, for the vertical applied load (●) and the horizontal one (□). For the apparent density, average values have been reported. The dashed line is plotted for trend evidencing only.

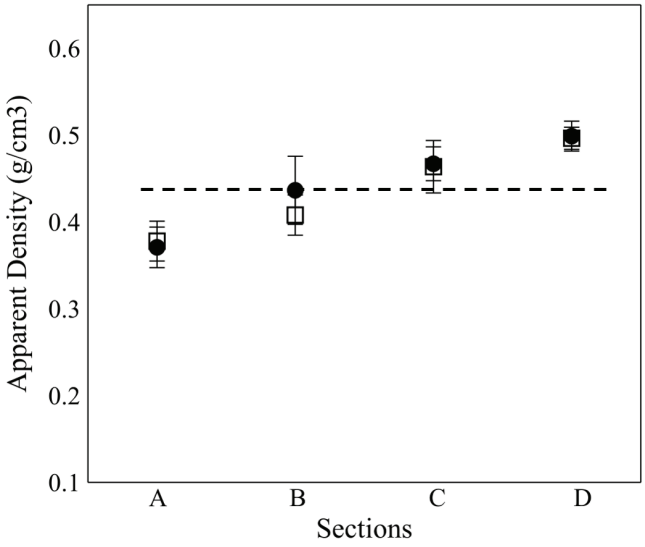

Fig. (6). Apparent density within the different block sections (A,B, C,D) for the treated bone block, both in the v part (●) as well as o one (□). In addition, also the overall apparent density of the block is reported (dashed line).

3.2.1. Apparent Density

As it can be seen from Fig. (**6**), after the reinforcement treatment, a trend very similar, with even properly similar density values, is observed for the case of the treated block with respect to untreated ones. Therefore, the intrinsic variability of untreated bone among the different sections is preserved. In light of these results, indeed, to make sure that

polymer and gelatin are actually present on the treated bone surfaces, two additional measurements have been run. In Fig. (**7**), an example of two contact angle measurements of water in the air over the surface of the untreated (left) and treated (right) bone are reported. Though hydroxyapatite is in general hydrophilich [44] due to the porosity of the surface (Cassie-Baxter mode [45-47]) an apparent hydrophobic behavior is recorded before the treatment, with apparent contact angle of 100° ± 4°, whereas, after it, a rather hydrophilic one with contact angle of 69° ± 15° after 6 seconds. Moreover, it is important to mention that, if no changes in drop displacement were observed for the untreated samples, often a full water penetration within the bone porous domain was recorded over longer times for the treated ones. Gelatin is well known and used in drug formulation [48] for its water absorption and swelling ability. It is therefore not surprising that its presence, even in small amount, on the bone surface, leads to enhanced hydrophilicity and water absorption capacity. This makes the xenograft also more accessible from the patient's blood upon implantation, favoring cells colonization and vascular ingrowth [16].

In addition, the ESEM pictures in Fig. (**8.a** and **8.b**) show the presence of deposited material (darker part) within the internal surface of the pores, while the energy dispersive analysis (Fig. **8.c** and **8.d**) reveals difference within the relative abundance of atomic species in different sections of the treated bone. Specifically, in the darker area, a much higher presence of carbon atoms, due to the polymer composition, is detected. These results have also been confirmed *via* FTIR analysis (Fig. **S1**), in which clearly peaks corresponding to -OH (3450 cm^{-1}), -CH_3 (2960 cm^{-1}), carbonyl (1640 cm^{-1}) and C-O-C (1100 cm^{-1}) bonds are detectable after treatment, whereas before only the ones corresponding to the mineral nature of the samples are present (1050 and 600 cm^{-1}). Therefore, it is confirmed that polymer and gelatin are effectively deposited over the starting bone matrix. Though the involved quantities are not enough to affect the apparent

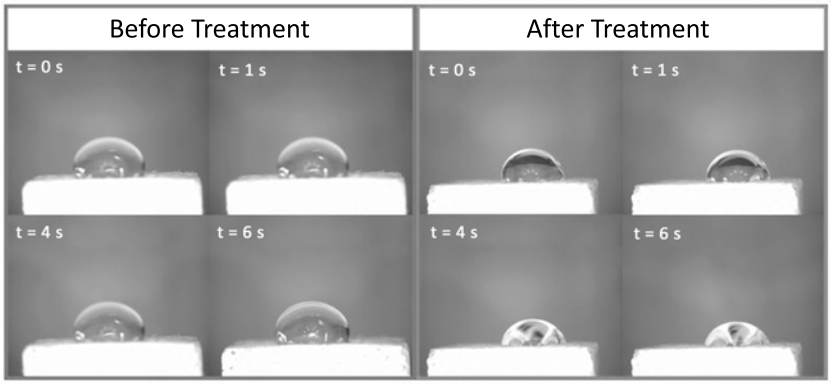

Fig. (7). Displacement of a water droplet at different instants on the surface of the prisitne bone (left) and after the treatment (right). Actual values of contact angle have been measured for both cases on the picture in the last square (t = 6 s), as afterwards no further changing in the displacement of the drop over the surface was recorded. Specifically, for the shown case of the pictures before the tratement (left) the recorded angle is 103° ± 6° and afterwards (right) 73° ± 4°.

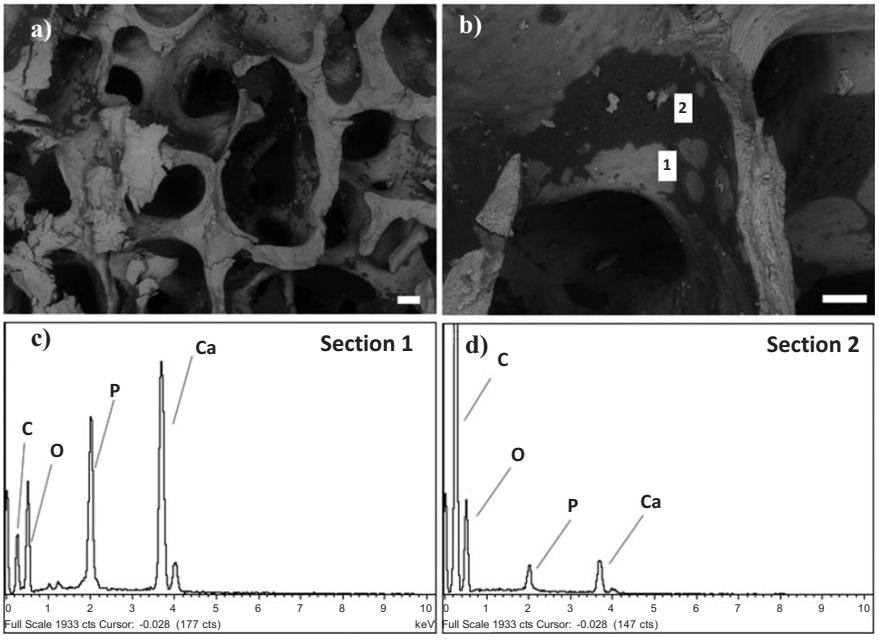

Fig. (8). ESEM pictures of the bone after the treatment, at different magnifications. For a, scale bar = 200 μm and for b with scale bar = 100 μm. c) and d) are the energy dispersive analysis of the two different sections, c of the lighter (1) and d for the darker one (2) in b.

density of the samples they are, on the contrary, enough to modify some other physical properties and to relevantly influence biological behavior and hence clinical performances [24, 30].

3.2.2. Mechanical Properties

As one can see from Fig. (**9**) the effect produced by the deposited materials on the pristine bone matrix can be subdivided in two major points. First, it increases the mechanical resistance of the actual sample, moving the values of E towards considerably higher ones, specifically from an average value of 384.46 ± 124.8 MPa to one of 461.49 ± 66.5 MPa for section ***v*** and from 485.17 ± 63.66 MPa to 531.5 ± 82.3 MPa for section ***o***. This represents an improvement of roughly 27% over the initial material in the ***v*** section and of 25% in the ***o*** one. As the polymer and gelatin properly stick on the bone support, certainly there is a contribution of adhesion forces to the observed structural reinforcement. Moreover, the presence of a polymer phase, even in very low amounts, significantly stabilizes crack propagation within the mineral matrix. With dependence on the polymer characteristics, toughening (if the polymer is soft) and increased mechanical strength (if the polymer is stiff) can be provided. Additionally, the toughness of the polymer phase itself also contributes to the enhanced mechanical response of the composite material.

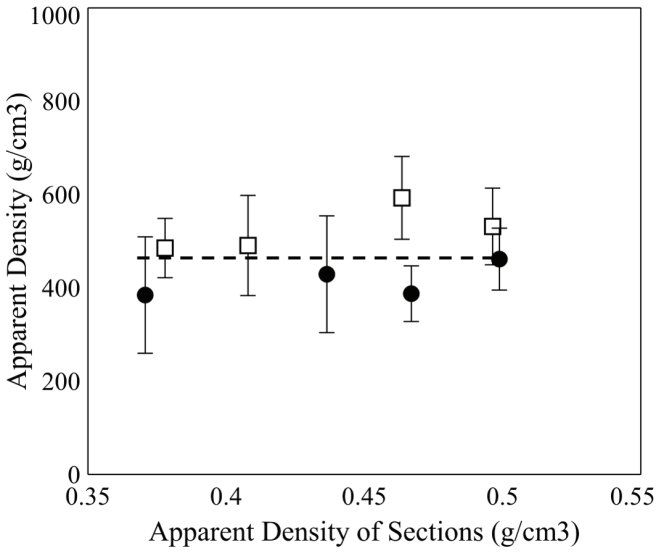

Fig. (9). Elastic modulus vs the apparent density of the different sections of the treated bone block, for the vertical applied load (●) and the horizontal one (□). For the apparent density, average values have been reported. The dashed line is plotted for trend evidencing only.

Considering the characteristics of our polymer, which at room temperature is a very though, rubbery-like solid (T_g = 16°C; E = 200 MPa, tensile strength = 240 N/mm^2; strain at failure = 160%), such an improvement is expected when even only traces are deposited on the pristine bone, as already observed for similar systems, like nacre-like materials[6]. Moreover, as already discussed by Chen [40], protein and mineral constituents of the bone at micro and nanoscales may interpenetrate, thus enhancing the mechanical properties by interlocking [49]. Indeed, in general, as soon as natural bone is deproteinized its mechanical properties fall considerably and it presents a rather fragile and brittle behavior [40]. Secondly, the treatment considerably homogenates the actual mechanical response over the different sections of the block, once again independently on the direction of the applied load, lowering substantially the dependence of the elastic modulus on the apparent density. This, again, can be explained by the effect of the polymer presence within the trabeculae of the original matrix, generating a more homogeneous stress distribution, limiting stress concentration at the mineral bridges [6, 50].

Mechanical properties hence become much more distributed over the body of the block and/or any other complex volume therefrom extracted, limiting consistently the intrinsic variability of such a peculiar base material. Notably, as in most composite materials, even a small amount of polymer and gelatin incorporation is enough to provide proper additional strength. Moreover, being the deposition process controlled by the affinity of polymer and gelatin for the bone support itself, it can be expected that on samples with higher porosity, and therefore, more surface area a higher quantity of material is deposited with a more relevant effect on the reinforcement. Remarkably, as already shown before, the apparent density of all samples is only minimally affected by the process and the peculiar structure ensuring cell colonization is preserved [51].

CONCLUSION

In this work, we have characterized deproteinized and decellularized cancellous bovine bone before and after the deposition of polymer and gelatin. This way, we have shown that its mechanical properties can be improved and homogenized. Specifically, the added components not only lead to a more resistant material, but also, they allow the overcoming of an intrinsic, naturally occurring limitation in pure bovine cancellous bone characteristics. Indeed, the conventional correlation between apparent density and elastic modulus, the major source of uncertainty and risk of poor outcomes in the possible usage of pure xenografts in bone tissue engineering, is considerably reduced on the samples that underwent the treatment. Combined with the enhanced hydrophilicity provided by the gelatin, the presented biohybrid composite stands as one of the best candidates for hard tissue integration and regeneration practice. Indeed, though intrinsically reinforcing the material, the deposition process leaves the specific porous structure, that allows cells proliferation, basically unaltered. As a matter of fact, the final material presents many advantages as it combines and address in a single piece and at the same time mechanical resistance, homogeneous mechanical response and proper structural characteristics[51] that allow full integration within the patient receiving site tissues and complete tissue remodeling [16].

ETHICS APPROVAL AND CONSENT TO PARTICIPATE

Not applicable.

HUMAN AND ANIMAL RIGHTS

No Animals/Humans were used for studies that are the basis of this research.

CONSENT FOR PUBLICATION

Not applicable.

CONFLICT OF INTEREST

Prof. Dr. Giuseppe Perale is one of the owners of the proprietary process involved in the preparation of the samples, executive vice president and a co-founder of the company IBI SA using that technology. Dr. Alberto Cingolani and Ing. Carlo Grottoli also work for the same company.

ACKNOWLEDGEMENTS

The authors are very thankful to Arnaldo Varesti for his kind help with the preparation of the samples and the usage of the microscope. Moreover, they would like to express their gratitude to Dario Picenoni for the ESEM measurements. Many thanks also to Marco Binelli for the FTIR measurements.

SUPPLEMENTARY MATERIAL

Supplementary material is available on the publisher's website along with the published article.

REFERENCES

[1] Chen, P.Y.; McKittrick, J.; Meyers, M.A. Biological materials: Functional adaptations and bioinspired designs. *Prog. Mater. Sci.,* **2012**, *57*(8), 1492-1704.

[2] Espinosa, H.D.; Juster, A.L.; Latourte, F.J.; Loh, O.Y.; Gregoire, D.; Zavattieri, P.D. Tablet-level origin of toughening in abalone shells and translation to synthetic composite materials. *Nat. Commun.,* **2011**, *2*(1), 173-179.

[3] Yeom, B.; Sain, T.; Lacevic, N.; Bukharina, D.; Cha, S.H.; Waas, A.M.; Arruda, E.M.; Kotov, N.A. Abiotic tooth enamel. *Nature,* **2017**, *543*(7643), 95-98.

[4] Launey, M.E.; Munch, E.; Alsem, D.H.; Barth, H.B.; Saiz, E.; Tomsia, A.P.; Ritchie, R.O. Designing highly toughened hybrid composites through nature-inspired hierarchical complexity. *Acta Mater.,* **2009**, *57*(10), 2919-2932.

[5] Yang, H.; Liang, F.; Chen, Y.; Wang, Q.; Qu, X.; Yang, Z. Lotus leaf inspired robust superhydrophobic coating from strawberry-like janus particles. *NPG Asia Mater.* **2015**, *7*(4), e176.

[6] Niebel, T.P.; Bouville, F.; Kokkinis, D.; Studart, A.R. Role of the polymer phase in the mechanics of nacre-like composites. *J. Mech. Phys. Solids,* **2016**, *96*, 133-146.

[7] Santoro, M.; Perale, G. Using synthetic bioresorbable polymers for orthopedic tissue regeneration. *Durab. Reliab. Med. Polym.,* **2012**, 119-139.

[8] Sheikh, Z.; Najeeb, S.; Khurshid, Z.; Verma, V.; Rashid, H.; Glogauer, M. Biodegradable materials for bone repair and tissue engineering applications. *Materials (Basel),* **2015**, *8*(9), 5744-5794.

[9] Stevens, B.; Yang, Y.; Mohandas, A.; Stucker, B.; Nguyen, K.T. A review of materials, fabrication methods, and strategies used to enhance bone regeneration in engineered bone tissues. *J. Biomed. Mater. Res. - Part B Appl. Biomater.,* **2008**, *85*(2), 573-582.

[10] Rossi, F.; Santoro, M.; Perale, G. Polymeric scaffolds as stem cell carriers in bone repair. *J. Tissue Eng. Regen. Med.,* **2015**, *9*, 1093-1119.

[11] Meyers, M.A.; Chen, P.Y.; Lopez, M.I.; Seki, Y.; Lin, A.Y.M. Biological materials: A materials science approach. *J. Mech. Behav. Biomed. Mater.,* **2011**, *4*(5), 626-657.

[12] Currey, J.D. Hierarchies in Biomineral Structures. *Science (80-).* **2005**, *309*(5732), 253-254.

[13] Bose, S.; Vahabzadeh, S.; Bandyopadhyay, A. Bone tissue engineering using 3D printing. *Mater. Today,* **2013**, *16*(12), 496-504.

[14] Minas, C.; Carnelli, D.; Tervoort, E.; Studart, A.R. 3D printing of emulsions and foams into hierarchical porous ceramics. *Adv. Mater.,* **2016**, *28*(45), 9993-9999.

[15] Wegst, U.G.K.; Ashby, M.F. The mechanical efficiency of natural materials. *Philos. Mag.,* **2004**, *84*(21), 2167-2181.

[16] D'Alessandro, D.; Perale, G.; Milazzo, M.; Moscato, S.; Stefanini, C.; Pertici, G.; Danti, S. Bovine bone matrix/poly(l-lactic-co-ε-caprolactone)/gelatin hybrid scaffold (SmartBone®) for maxillary sinus augmentation: A histologic study on bone regeneration. *Int. J. Pharm.,* **2017**, *523*(2), 534-544.

[17] Pertici, G.; Rossi, F.; Casalini, T.; Perale, G. Composite polymer-coated mineral grafts for bone regeneration: Material characterisation and model study. *Ann. oral Maxilofac. Surg.,* **2014**, *2*(1), 1-7.

[18] Campana, V.; Milano, G.; Pagano, E.; Barba, M.; Cicione, C.; Salonna, G.; Lattanzi, W.; Logroscino, G. Bone substitutes in orthopaedic surgery: From basic science to clinical practice. *J. Mater. Sci. Mater. Med.,* **2014**, *25*(10), 2445-2461.

[19] Knöfler, W.; Barth, T.; Graul, R.; Krampe, D. Retrospective analysis of 10,000 implants from insertion up to 20 years-analysis of implantations using augmentative procedures. *Int. J. Implant Dent.,* **2016**, *2*(1), 25.

[20] Sarkar, S.K.; Lee, B.T. Hard tissue regeneration using bone substitutes: An update on innovations in materials. *Kor. J. Intern. Med.,* **2015**, *30*, 279-293.

[21] Athanasiou, V.T.; Papachristou, D.J.; Panagopoulos, A.; Saridis, A.; Scopa, C.D.; Megas, P. Histological comparison of autograft, allograft-dbm, xenograft, and synthetic grafts in a trabecular bone defect: An experimental study in rabbits. *Med. Sci. Monit.,* **2010**, *16*(1), BR24-R31.

[22] Datta, A.; Gheduzzi, S.; Miles, A.W. A comparison of the viscoelastic properties of bone grafts. *Clin. Biomech.,* **2006**, *21*(7), 761-766.

[23] Planell, J.A. *Bone Repair Biomaterials*; Woodhead Publishing Limited, 2009.

[24] Roato, I.; Belisario, D.C.; Compagno, M.; Verderio, L.; Sighinolfi, A.; Mussano, F.; Genova, T.; Veneziano, F.; Pertici, G.; Perale, G.; Ferracini, R. Adipose-derived stromal vascular fraction/xenohybrid bone scaffold: An alternative source for bone regeneration. *Stem Cells Int.,* **2018**, *2018*.

[25] Langton, C.M.; Njeh, C.F. *The Physical Measurement of Bone*; Institute of Physics Publishing Bristol and Philadelphia, 2003.

[26] Skedros, J.G.; Baucom, S.L. Mathematical analysis of trabecular "trajectories" in apparent trajectorial structures: The unfortunate historical emphasis on the human proximal femur. *J. Theor. Biol.,* **2007**, *244*(1), 15-45.

[27] Zioupos, P.; Cook, R.B.; Hutchinson, J.R. Some basic relationships between density values in cancellous and cortical bone. *J. Biomech.,* **2008**, *41*(9), 1961-1968.

[28] Ceccarelli, G.; Presta, R.; Benedetti, L.; Cusella De Angelis, M.G.; Lupi, S.M.; Rodriguez, Y.; Baena, R. Emerging perspectives in scaffold for tissue engineering in oral surgery. *Stem Cells Int.,* **2017**, *2017*.

[29] Colaço, H.B.; Shah, Z.; Back, D.; Davies, A.; Ajuied, A. Xenograft in orthopaedics. *Orthop. Trauma,* **2015**, *29*(4), 253-260.

[30] Stacchi, C.; Lombardi, T.; Ottonelli, R.; Berton, F.; Perinetti, G.; Traini, T. New bone formation after transcrestal sinus floor elevation was influenced by sinus cavity dimensions: A prospective histologic and histomorphometric study. *Clin. Oral Implants Res.,* **2018**, 465-479.

[31] Cingolani, A.; Casalini, T.; Caimi, S.; Klaue, A.; Sponchioni, M.; Rossi, F.; Perale, G. A methodologic approach for the selection of bio-resorbable polymers in the development of medical devices: The case of poly(l-lactide-co-ε-caprolactone). *Polymers (Basel).* **2018**, *10*(8), 851.

[32] Schrieber, R.; Herbert, G. *Gelatine Handbook: Theory and Industrial Practice*; Wiley, Ed.; UK, 2007.

[33] Pertici, G. Bone implant matrix and method of preparing the same. WO2010070416A1, 2010.

[34] Pertici, G.; Carinci, F.; Carusi, G.; Epistatus, D.; Villa, T.; Crivelli, F.; Rossi, F.; Perale, G. Composite polymer-coated mineral scaffolds for bone regeneration: From material characterization To

Human Studies. *J. Biol. Regul. Homeost. Agents,* **2015**, *29*(3 Suppl 1), 136-148.

[35] Eliceiri, K.; Schneider, C.A.; Rasband, W.S.; Eliceiri, K.W. NIH image to image J: 25 years of image analysis historical commentary nih image to imageJ: 25 Years of image analysis. *Nat. Methods,* **2012**, *9*(7), 671-675.

[36] Schindelin, J.; Rueden, C.T.; Hiner, M.C.; Eliceiri, K.W. The imageJ ecosystem: An open platform for biomedical image analysis. *Mol. Reprod. Dev.,* **2015**, *82*, 518-529.

[37] Reznikov, N.; Chase, H.; Brumfeld, V.; Shahar, R.; Weiner, S. The 3D structure of the collagen fibril network in human trabecular bone: Relation to trabecular organization. *Bone,* **2015**, *71*, 189-195.

[38] Florencio-Silva, R.; Sasso, G.R.D.S.; Sasso-Cerri, E.; Simões, M.J.; Cerri, P.S. Biology of bone tissue: structure, function, and factors that influence bone cells. *Biomed. Res. Int.,* **2015**, *2015*.

[39] Alghadir, A.H.; Gabr, S.A.; Al-Eisa, E. Physical activity and lifestyle effects on bone mineral density among young adults: Sociodemographic and biochemical analysis. *J. Phys. Ther. Sci.,* **2015**, *27*(7), 2261-2270.

[40] Chen, P.Y.; McKittrick, J. Compressive mechanical properties of demineralized and deproteinized cancellous bone. *J. Mech. Behav. Biomed. Mater.* **2011**, *4*(7), 961-973.

[41] Wolff, J. *Uber Die Innere Architektur Der Knochen Und Ihre Bedeutung Fuer Die Frage Vom Knochenwachstum*; Berlin : Druck und Verlag von Georg Reimer, 1870.

[42] Bonfield, W.; Grynpas, M.D. Anisotropy of the Yound's Modulus of Bone. *Nature,* **1977**, *270*, 453-454.

[43] Töyräs, J.; Kröger, H.; Jurvelin, J.S. Bone properties as estimated by mineral density, ultrasound attenuation, and velocity. *Bone,* **1999**, *25*(6), 725-731.

[44] Joschek, S.; Nies, B.; Krotz, R.; Göpferich, A. Chemical and physicochemical characterization of porous hydroxyapatite ceramics made of natural bone. *Biomaterials,* **2000**, *21*(16), 1645-1658.

[45] Milne, A. J. B.; Amirfazli, A. The cassie equation: How it is meant to be used. *Adv. Colloid Interface Sci.,* **2012**, *170*(1-2), 48-55.

[46] Cassie, B.D.; Baxter, S. Wettability of porous surfaces. *Trans. Faraday Soc.,* **1944**, *40*(5), 546-551.

[47] Bormashenko, E. Progress in understanding wetting transitions on rough surfaces. *Adv. Colloid Interface Sci.,* **2015**, *222*, 92-103.

[48] Laguta, I.V; Stavinskaya, O.N.; Kuzema, P.A.; Kazakova, O.A.; Nasedkin, D.B. Hybrid materials on the basis of gelatin and hydrophilic-hydrophobic silica. *Prot. Met. Phys. Chem. Surfaces,* **2017**, *53*(5), 807-811.

[49] Launey, M.E.; Buehler, M.J.; Ritchie, R.O. On the mechanistic origins of toughness in bone. *Annu. Rev. Mater. Res.,* **2010**, *40*(1), 25-53.

[50] Mirkhalaf, M.; Khayer Dastjerdi, A.; Barthelat, F. Overcoming the brittleness of glass though bioinspiration and micro-architecture. *Nat. Commun.,* **2014**, *5*, 3166.

[51] Hannink, G.; Arts, J.J.C. Bioresorbability, porosity and mechanical strength of bone substitutes: What is optimal for bone regeneration? *Injury,* **2011**, *42*(Suppl. 2), S22-S25.

smartbone®

THE NEXT FRONTIER OF BONE REGENERATION

where Technology meets Nature

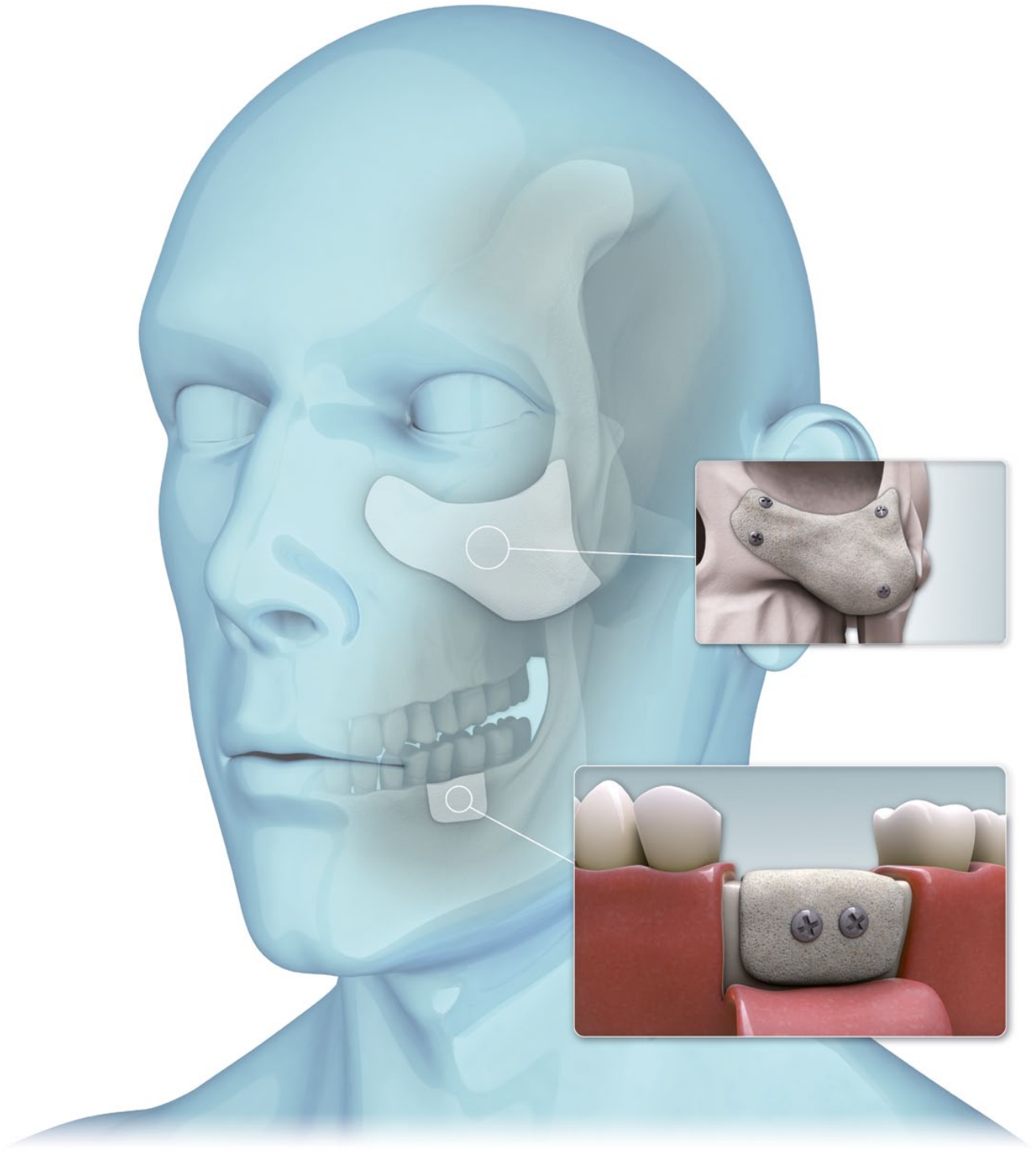

swiss made

smartbone®

SmartBone is a new **hybrid bioactive** bone substitute specifically developed for **bone regeneration** in **reconstructive surgery**.
SmartBone is produced by combining a bovine mineral bone matrix with bioactive resorbable polymers and cell nutrients. This new concept of composite biomaterial promotes a quick growth of the patient's cells into SmartBone while its biopolymers degrade, providing perfect **integration** and **osteogenesis**.

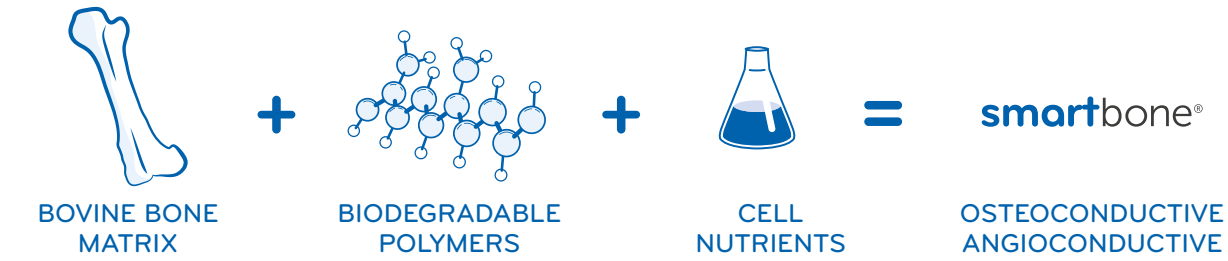

BIODEGRADABLE POLYMERS

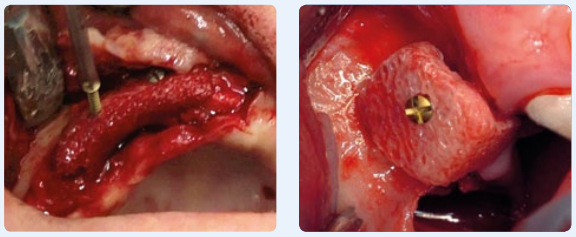

Give SmartBone:

- high loading resistance
- high volumetric stability (>95%); the polymers protect the bone from early resorption
- high tenacity to screws fixation

CELL NUTRIENTS

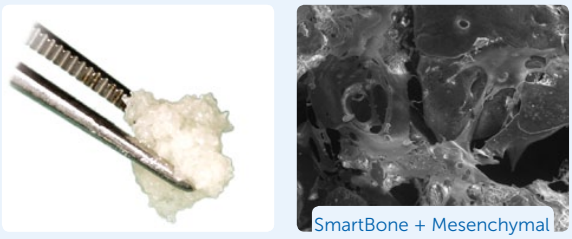

SmartBone + Mesenchymal Stem Cells

Help SmartBone to:

- promote blood cell adhesion and colonization
- guarantee a high hydrophilicity thus enhancing the chemical cascade of signals that promotes the osteogenic process

smartbone® PROMOTES

OSTEOINTEGRATION and VASCULARIZATION

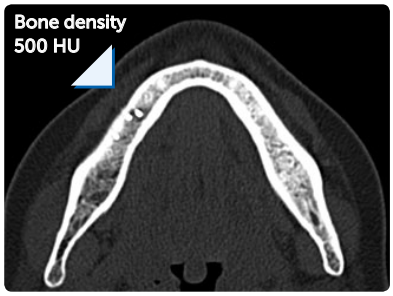

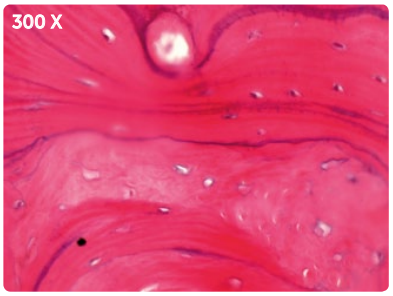

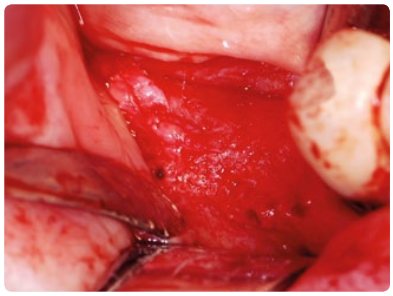

Clinical case: 4 months after surgery

SmartBone is completely resorbed and replaced by the patient's own bone within 1-2 years: this excellent outcome grants a vital, functional bone-implant integration.
SmartBone is extremely biocompatible and is fully compliant with **ISO 10993-1** requirements.

PERFECT FOR:

- Sinus lift procedures
- Intrabony defects
- Peri-implant defects
- Socket preservation
- Vertical and horizontal bone augmentations
- Craniofacial and maxillofacial applications
- Custom-made applications

FROM CHIPS TO CUSTOM-MADE GRAFTS

ADVANTAGES OF SMARTBONE BLOCKS:

- Easy dust free shaping with any type of surgical tool (bone cutter, drill, piezo)
- Resistant to extreme loads and to heavy surgical maneuvering
- Far better stability of the augmented bone graft vs the loose granules
- Strongly osteogenic
- Bigger defects do not need autologous bone, thus reducing the patient's morbidity
- No resorption: the polymeric coating protects the graft during the first healing/osteointegration period
- Readly absorb blood



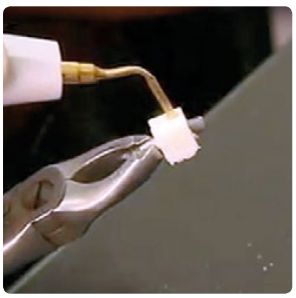


smartbone® IN ACTION

Filling of a bone gap after extraction and vertical increase using SmartBone Block

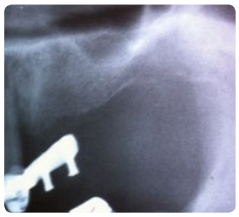

Patient's initial conditions

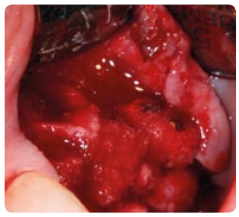

Insertion of a cone shaped SmartBone in 23 and placement of Microchips (1 - 2 mm) in position 22

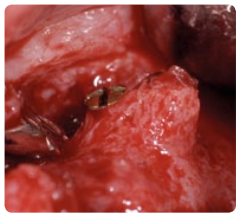

4 months:
the graft has maintained the volume and an excellent bone formation permits the placement of four implants

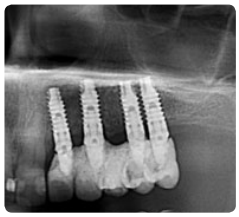

2 years:
a complete bone maturation is achieved

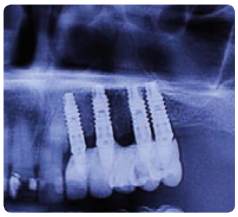

3 years:
the bone surrounding the implants has a very good quality and density

Lateral augmentation in 45-46 using SmartBone Block

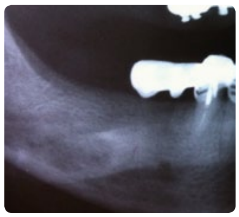

Patient's initial conditions

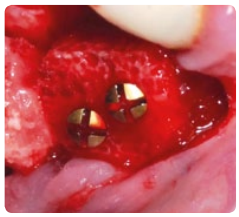

Due to its high fixation tenacity, the block is fixed with two osteosynthesis screws to obtain a perfect primary stability

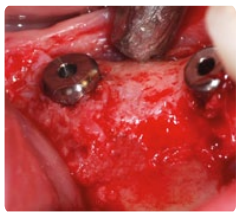

4 months:
perfect three-dimensional bone reconstruction accompanied by an adequate bone density for the placement of two implants

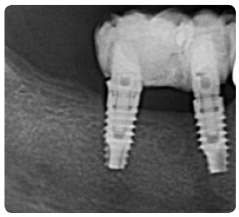

2 years:
a good osteointegration is achieved

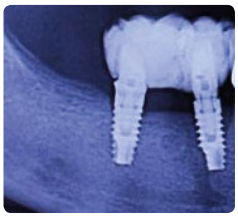

3 years:
the implants are surrounded by excellent bone quality

Large bone loss due to fracture treated using SmartBone Granules (2-4 mm)

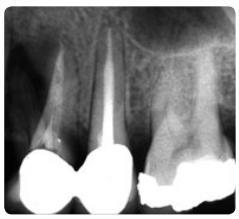

Patient's initial conditions

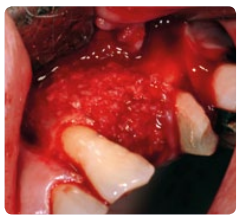

Filling of the defect with SmartBone Granules for bone augmentation and fast blood absorption

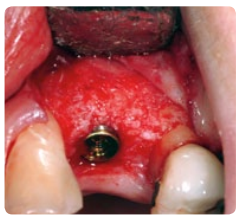

5 months:
good bone regeneration for implant placement

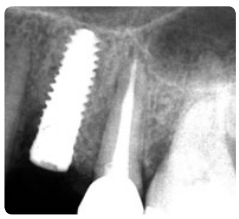

8 months:
good osteointegration around the implant

2 years:
perfect bone maturation and stable bone volume

Sinus lift and vertical bone augmentation using SmartBone Microchips (1-2 mm)

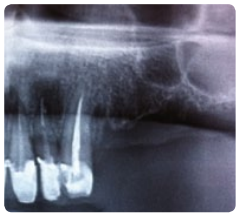

Patient's initial conditions

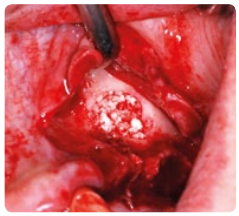

SmartBone Microchips application both for sinus lift and vertical bone augmentation

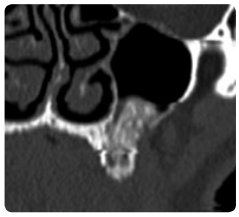

5 months:
average bone density 500 HU, adequate for the placement of three implants

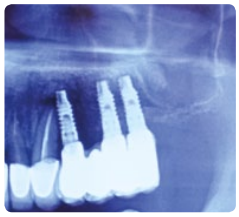

2 years:
complete osteointegration and maturation of soft and hard-tissues

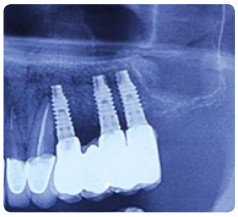

3 years:
a very good bone quality around the implants ensures a perfect stability

KEY FEATURES

OPEN POROSITY AND MICROSTRUCTURE

The microstructure of SmartBone's composite matrix strongly resembles the human bone in terms of open and mid-sized 27% porosity.

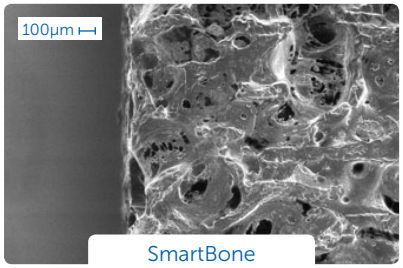

SmartBone

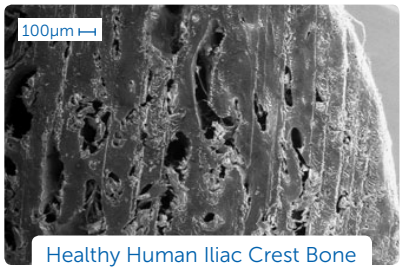

Healthy Human Iliac Crest Bone

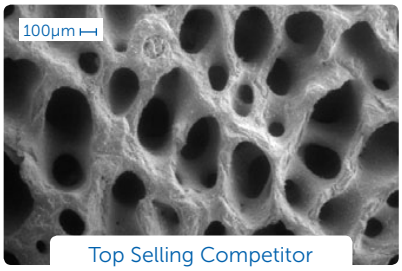

Top Selling Competitor

HIGH MECHANICAL PERFORMANCES

SmartBone has a rigid pseudoelastic behaviour. It bears 3 times the competitor's maximum load and is 4 times more rigid.

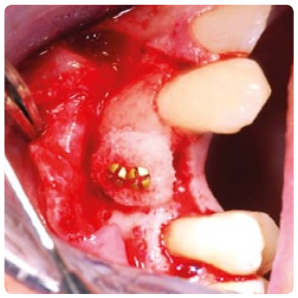

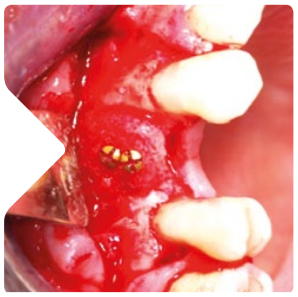

HIGH HYDROPHILICITY

Thanks to its microcomposition, SmartBone quickly reaches an av. 38% w/w blood swelling, thereby allowing a robust osteointegration.

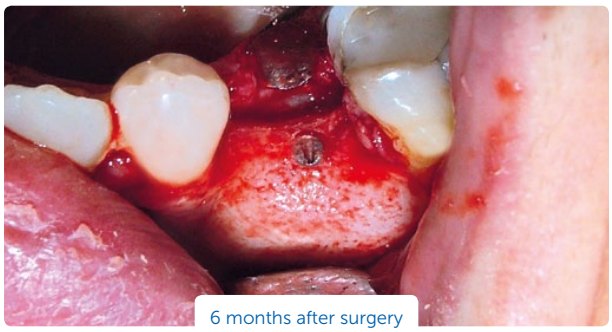
6 months after surgery

HIGH TISSUE INTEGRATION

SmartBone's microstructure and composition favour cell colonization.
The electronic microscopy analysis of in vitro cell colonization tests evidenced the presence of wide and well-structured cell formations inside SmartBone.

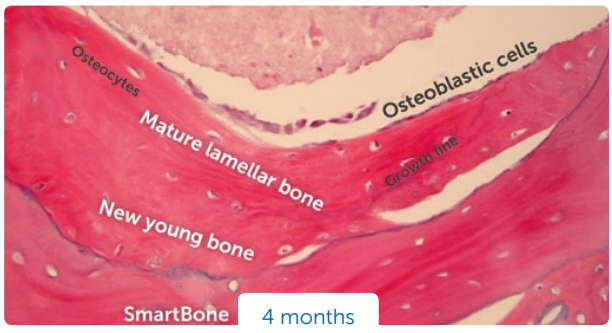

4 months

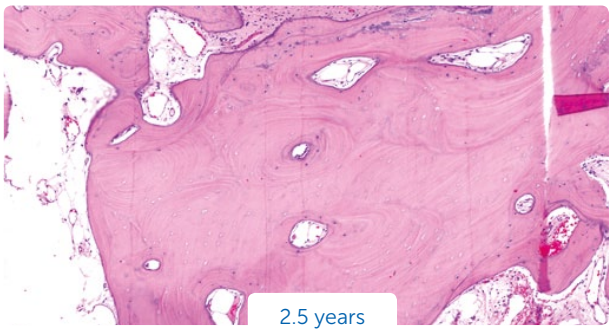
2.5 years

SmartBone is progressively replaced by new young bone: osteoblasts are visible both in the active and in the quiescent state, when, after having formed mature lamellar bone, they become osteocytes, as evidenced inside the lacunae. After 2.5 years the graft has been completely replaced and the osteogenesis has formed a lamellar bone with cement lines; there is evidence of a great amount of osteocytes inside the lacunae and of a good angiogenesis.
SmartBone combined with the native bone forms an osteoinductive system.

smartbone® on demand™

Custom made grafts for oral and maxillofacial reconstructive surgery are only four steps away

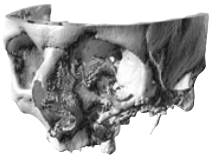

1. DIAGNOSIS PRESCRIPTION

The doctor sends the patient's CT Scan with a brief clinical description

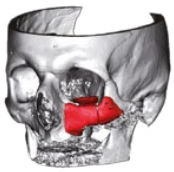

2. DIGITAL PLANNING

IBI designs the graft in accordance with the doctor's prescriptions

3. CUSTOM MADE BONE GRAFT

IBI produces the custom made graft based on the stl file

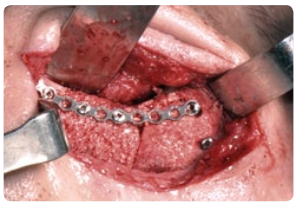

4. SURGERY

The doctor receives the graft and is ready for surgery

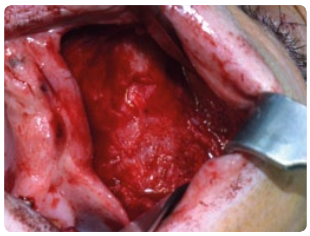

2.5 YEARS AFTER SURGERY

the graft has been completely replaced and a **mature lamellar bone** has formed

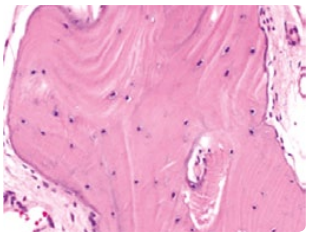

SMARTBONE ON DEMAND GUARANTEES YOUR SUCCESS:

- custom-made to the specific needs of each of your patients
- ensures a perfect contact between the graft and the recipient site for improved integration
- ensures a precise creation of the desired shape
- helps you to resolve complex situations
- saves your time during surgery
- reduces your patient's risks
- helps you to reduce surgical costs

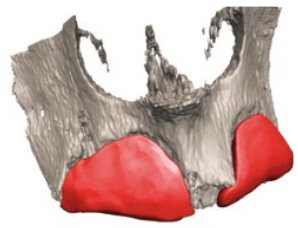

Digital planning

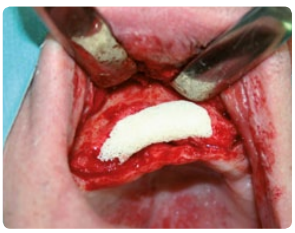

Surgery

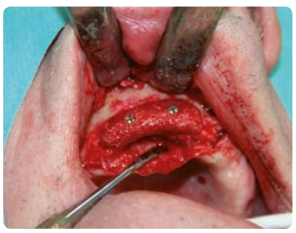

Surgery

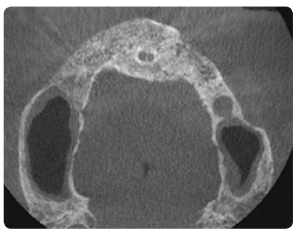

CT scan
8 months

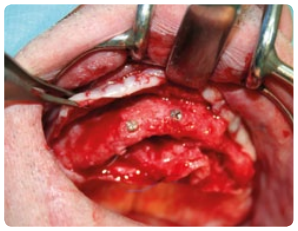

Post-op
8 months

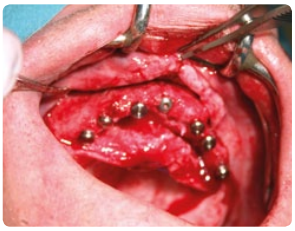

Implant placement
8 months

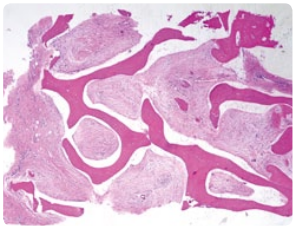

Histological analysis
8 months

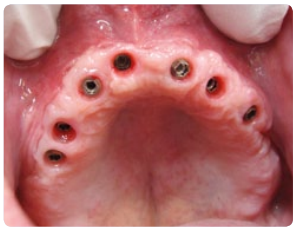

Follow up
1 year

smartbone® CATALOGUE

SmartBone Microchips	0.25 - 1 mm | 0.5 cc (~0.3 g)	SMC010050
	0.25 - 1 mm | 1 cc (~0.6 g)	SMC010100
	0.25 - 1 mm | 2 cc (~1.2 g)	SMC010110
	0.25 - 1 mm | 5 cc (~3 g)	SMC010190
	1 - 2 mm | 1 cc (~0.38 g)	SMC010221
	1 - 2 mm | 2 cc (~0.75 g)	SMC010200
	1 - 2 mm | 4 cc (~1.5g)	SMC010201
SmartBone Granules	2 - 4 mm | 5 cc (~1.6g)	SMC010300
SmartBone Block	7 x 7 x 7 mm	SMB011005
	10 x 10 x 10 mm	SMB011010
	10 x 10 x 20 mm	SMB011020
	10 x 20 x 20 mm	SMB011030
	14 x 12 x 6 mm	SMB011110
	14 x 12 x 7 mm	SMB011120
	14 x 12 x 8 mm	SMB011130
	14 x 12 x 9 mm	SMB011140
	14 x 12 x 10 mm	SMB011150
	16 x 14 x 6 mm	SMB011310
	14 x 12 x 12 mm	SMB011160
	14 x 12 x 16 mm	SMB011170
	14 x 12 x 20 mm	SMB011180
	14 x 12 x 24 mm	SMB011190
	14 x 12 x 24mm	SMB011210
	15 x 30 x 20 mm	SMB011220
	15 x 30 x 30 mm	SMB011230
	15 x 30 x 40 mm	SMB011240
	15 x 30 x 50 mm	SMB011250
	16 x 14 x 7 mm	SMB011320
	16 x 14 x 8 mm	SMB011330
	16 x 14 x 9 mm	SMB011340
SmartBone Plate	3 x 25 x 15 mm	SMP013010
	3 x 10 x 10 mm	SMP013030
	4 x 10 x 10 mm	SMP013040
SmartBone Wedge	35 x 22 x 5 mm	SMW014010
	35 x 22 x 8 mm	SMW014020
	35 x 25 x 10 mm	SMW014030
	35 x 25 x 12 mm	SMW014040
	40 x 25 x 12 mm	SMW014050
	40 x 25 x 14 mm	SMW014060
SmartBone Cylinder	Ø 11 x h. 20 mm	SMC012010
	Ø 12 x h 20 mm	SMC012020
	Ø 14 x h 20 mm	SMC012030
	Ø 11 x h 10 mm	SMC012050
	Ø 14 x h 14 mm	SMC012060
SmartBone Rod	35 x 4 x 3 mm	SMR015010
SmartBone Special U Shape	15 x 6 x 4 mm	SMS016010
	15 x 7 x 3.5 mm	SMR016020
SmartBone Special L Shape	15 x 7 x 6 mm	SMS016210
SmartBone Special C Shape	Ø 8 x h 12 mm	SMS016110

All products in this page are CE 0434 marked

The codes in blue are available immediately.
The codes in black are available upon request.

IBI'S PRODUCTS

smartbone®

SmartBone is a CE 0434 marked class III medical device

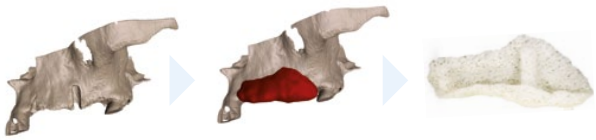

smartbone® on demand™

smartscrews™

SmartScrews are CE 0434 marked class IIb medical devices

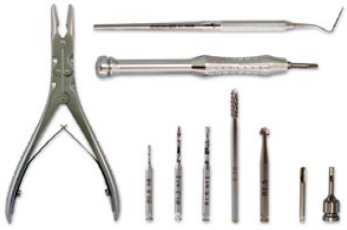

smarttools™

SmartTools Drills are CE 0434 marked class IIa medical devices

smartkit™

ibi SA industrie biomediche insubri

THE NEXT FRONTIER OF OSTEOGENIC BIOMATERIALS

IBI is an innovative hi-tech Swiss biomedical company focused on research, development and on the production of medical devices for tissue engineering and regenerative medicine: substitutes, grafts, 3D matrixes and 2D scaffolds. IBI believes that regenerative medicine and tissue engineering represent the future in healthcare. IBI has advanced competencies and core skills in processing materials for biomedical applications, which are used to develop proprietary technologies to build new and innovative products. IBI commits to safety and quality management: IBI Qualitiy System is ISO 13485 and ISO 9001 compliant.

QUALITY SYSTEM CERTIFICATION DNV·GL ISO 13485

QUALITY SYSTEM CERTIFICATION DNV·GL ISO 9001

Industrie Biomediche Insubri SA
Via Cantonale, 67
Mezzovico-Vira
CH-6805
Switzerland
Ph. +41 91 93 06 640

www.ibi-sa.com
info@ibi-sa.com
www.smartbone.ch

CAUTION: The law restricts the sales of these devices made by, or on the order of, a dentist or physician.
Warning: Possible complications which may occur with any surgery include swelling at the surgical site, flap sloughing, bleeding, local inflammation, bone loss, infection or pain. Since SmartBone contains collagen, cases of allergic reactions may occur in very rare circumstances.
Instructions for Use at: www.ibi-sa.com/products/smartbone/download/

IBI-SBD002UK rev6

applied sciences

MDPI

Technical Note

Xeno-Hybrid Composite Scaffold Manufactured with CAD/CAM Technology for Horizontal Bone-Augmentation in Edentulous Atrophic Maxilla: A Short Communication

Maria Paola Cristalli [1], Gerardo La Monaca [2], Nicola Pranno [2,*], Susanna Annibali [2], Giovanna Iezzi [3] and Iole Vozza [2]

[1] Department of Biotechnologies and Medical Surgical Sciences, Sapienza, University of Rome, 00161 Rome, Italy; mariapaola.cristalli@uniroma1.it
[2] Department of Oral and Maxillo-Facial Sciences, Sapienza, University of Rome, 00161 Rome, Italy; gerardo.lamonaca@uniroma1.it (G.L.M.); susanna.annibali@uniroma1.it (S.A.); iole.vozza@uniroma1.it (I.V.)
[3] Department of Medical, Oral and Biotechnological Sciences, University of Chieti-Pescara, 66100 Chieti, Italy; giovanna.iezzi@unich.it
* Correspondence: nicola.pranno@uniroma1.it; Tel.: +39-06-49976651; Fax: +39-06-44230811

Received: 9 March 2020; Accepted: 10 April 2020; Published: 12 April 2020

Abstract: The present short communication described a new procedure for the reconstruction of the horizontal severely resorbed edentulous maxilla with custom-made deproteinized bovine bone block, fabricated using three-dimensional imaging of the patient and computer-aided design/computer-aided manufacturing (CAD/CAM) technology. The protocol consisted of three phases. In the diagnosis and treatment planning, cone-beam computed tomographic scans of the patient were saved in DICOM (digital imaging and communication in medicine) format, anatomic and prosthetic data were imported into a dedicated diagnostic and medical imaging software, the prosthetic-driven position of the implants, and the graft blocks perfectly adapted to the residual bone structure were virtually planned. In the manufacturing of customized graft blocks, the CAD-CAM technology and the bovine-derived xenohybrid composite bone (SmartBone® on Demand - IBI SA - Industrie Biomediche Insubri SA Switzerland) were used to fabricate the grafts in the exact shape of the 3D planning virtual model. In the surgical and prosthetic procedure, the maxillary ridge augmentation with custom-made blocks and implant-supported full-arch screw-retained rehabilitation were performed. The described protocol offered some advantages when compared to conventional augmentation techniques. The use of deproteinized bovine bone did not require additional surgery for bone harvesting, avoided the risk of donor site morbidity, and provided unlimited biomaterial availability. The customization of the graft blocks reduced the surgical invasiveness, shorting operating times because the manual shaping of the blocks and its adaptation at recipient sites are not necessary and less dependent on the clinician's skill and experience.

Keywords: bone tissue regeneration; xenografts; bone substitutes; computer-aided design/computer-aided manufacturing; deproteinized bovine bone

1. Introduction

Fixed implant-supported prostheses are considered a successful and predictable treatment for the rehabilitation of edentulous patients in the presence of an adequate volume of available bone. In edentulous atrophic jaws, bone deficiencies can prevent implants placement in the ideal prosthetic position with impairment of function and aesthetics. To overcome these limitations,

augmentation procedures for improving bone dimensions are needed. To date, bony reconstruction approaches of advanced maxillary horizontal atrophy involve the use of guided bone regeneration, "split" ridge osteotomy, and block grafts with different types of materials [1–3].

Guided bone regeneration (GBR) is a well-documented surgical procedure that uses particulate autogenous bone or bone substitutes in conjunction with occlusive membranes to prevent undesirable competing migration of non-osteogenic cells into the bony defect. The stability of the graft and barrier membrane and the tension-free flap closure are essential to secure successful outcomes [4]. There is strong evidence for the effectiveness and predictability of GBR in promoting lateral bone augmentation for limited to moderate bony deficiencies [5]. Nevertheless, to achieve ridge augmentations in severe and extensive defects, the technique, requiring non-resorbable membranes or titanium mesh and a long-term healing period, is more prone to soft tissue dehiscence, with subsequent infection and possible failure of regeneration procedure [6–9].

The ridge splitting/expansion procedure consists of a sagittal osteotomy and a controlled greenstick out-fracture of the buccal cortical plate, labially displaced to create the space that is filled with an interpositional particulate graft and covered with a membrane [3,10]. This technique has proved to be a predictable and effective to correct alveolar width deficiencies of limited edentulous areas with high implant survival rate, gain in horizontal alveolar ridge width, and few biological and technical complications [11]. In severe and extensive bony deficiencies, with the horizontal width less than 3 mm, treatment outcomes could be jeopardized since the alveolar ridge expansion predisposes to fractures of the buccal or palatal cortical plate and hampers a sufficient blood supply during the healing phase [3,10,11].

Autogenous bone block grafting is the best scientifically documented technique for the treatment of advanced horizontal atrophy in edentulous jaws [1,2]. However, this is a complex intervention and requires the need for general anesthesia, operation theater, and hospitalization because, in extensive and severe bone resorptions, block grafts are often harvested from the iliac crest or calvaria. Furthermore, the procedure is an operator-sensitive technique, which requires surgical skills in trimming and adapting blocks to the native bone, in achieving grafts immobilization, filling residual gaps, covering the grafted area with resorbable membranes, and suturing the flap tension-free [2]. The main drawbacks for the patients are the increased surgery invasiveness, longer surgical times, and more severe postoperative morbidity, mainly due to the extraoral donor sites.

In the augmentation procedures, a variety of bone restorative materials with different characteristics may be used, including autogenous bone, allografts, xenografts, and alloplasts, as well as different barrier membranes or osteosynthesis materials [12–15].

Autogenous bone, harvested from intra- or extraoral donor sites, is still considered the gold standard among the different biomaterials for bone thickness reconstruction due to its osteogenic, osteoinductive, and osteoconductive properties. Further advantages are a physical and chemical structure identical to that of the host site, a better vascularization potential, and the absence of immunogenicity and disease transmission capacity. Nevertheless, the use of autogenous bone presents some drawbacks, such as two different surgical sites, morbidity and complications of the donor site, lengthy surgical procedure, and unpredictable resorption [14].

Homologous, heterologous, or alloplastic grafts, instead, are only osteoconductive, promoting the proliferation of new vessels and guiding the growth and proliferation of osteoblasts onto their surface. Bone substitute materials provide biological support during healing, and their low and gradual replacement with the newly formed bone maintains the augmented volume and prevents soft tissue collapse. Furthermore, when compared to autogenous bone, they have the advantage of unlimited availability and less biologic costs to patients since the additional surgery for harvesting is not required [12,14].

The choice between different augmentation techniques and different grafting materials is related to the bony defect location and extension, morphological features of the site, hard and soft tissue characteristics, patient's individual needs and expectations, and, lastly, the surgeon's preferences/skill.

New possibilities in the reconstruct maxillary bony structures have been introduced over the past decade, with recent advancements in three-dimensional (3D) imaging acquisition with computed tomography (CT) and in computer-aided design/computer-aided manufacturing (CAD/CAM) technologies, which made it possible to directly produce customized biocompatible scaffold based on individual patient-specific anatomical data [16–18].

The present short communication reported a new therapeutic approach for the reconstruction of the horizontal severely resorbed edentulous maxilla with custom-made bovine-derived xeno-hybrid composite bone blocks, fabricated using CT and CAD/CAM technology.

2. Materials and Methods

No Ethical Committee approval was required as, according to the Italian national legislation and ordinance of the local inspection authority, it is not needed for short communications reporting the description of a surgical protocol. Nevertheless, the patient's informed consent related to the therapeutic plan and associated risks and the use of the images was obtained.

The protocol for horizontal bone-augmentation in the edentulous atrophic maxilla with the deproteinized bovine-bone composite scaffold, custom-made using CAD/CAM technologies, is indicated for patients requiring full-arch fixed prosthesis. In the horizontal severely resorbed edentulous maxilla (class IV according to the Cawood and Howell classification), the knife-edge edentulous ridge, sufficient in height but very deficient in thickness, prevents the placement of implants in the ideal prosthetic position for supporting a full-arch fixed rehabilitation [19].

2.1. Diagnosis and Treatment Planning

All patients were subjected to a complete examination of the oral hard and soft tissues and radiographic assessment by cone-beam computed tomography (CBCT). The pre-existing removable prosthesis was evaluated. If this denture was not adequate, a new provisional diagnostic denture with teeth in the ideal position to satisfy functional, phonetic, and aesthetic requisites was fabricated. The pre-existing or new denture was used both as a radiographic template, to transfer prosthetic information during the radiographic exam for a correct treatment planning, and as a temporary prosthesis during the healing phase.

Cone-beam computed tomography (CBCT) of the patient, wearing the radiographic template and a bite index with an extra-oral volume transfer element, was carried out (Evobite, 3DIEMME, Cantù, Italy, 2014). The CT scans were saved in digital imaging and communication in medicine (DICOM) format, and anatomic and prosthetic data were imported into a dedicated diagnostic and medical imaging software (3Diagnosys 4.2, 3DIEMME). The software, superimposing the digital model of the denture on the three-dimensional computer images, allowed to virtually plan the prosthetic-driven position of the implants, and the consequent ridge augmentation with graft blocks perfectly adapted to the residual bone structure (Figure 1).

2.2. Manufacturing of Customized Graft Blocks

The 3D planning virtual models were saved in a stereolithographic (STL) file and mailed to the IBI SA - Industrie Biomediche Insubri SA (Switzerland). The customized blocks in the exact 3D model shape were manufactured using the 5axes CAD-CAM process to machine-mill the bovine-derived mineral matrix (SmartBone® on Demand graft. IBI S.A. Industrie Biomediche Insubri S.A. via Cantonale 67, Switzerland). After the physical-chemical reinforcement process with biodegradable aliphatic polymers and bioactive agents, the customized blocks were packaged, sterilized, and sent to the surgeon, ready for clinical use.

2.3. Surgical and Prosthetic Procedure

The surgical procedure was performed by the same experienced surgeon (G.L.M.) in the outpatient setting and aseptic conditions. Immediately prior to surgery, patients rinsed with a 0.2% chlorhexidine

digluconate solution (Corsodyl, GlaxoSmithKline Consumer Healthcare, Genval, Belgium) for 2 min. The intervention was carried out under oral sedation with diazepam 0.25 mg/kg (Valium-2, Roche S.p.A., Italy) and local anesthesia with 2% mepivacaine and 1:100,000 epinephrine (Carbocaine, AstraZeneca, Milan, Italy).

A midcrestal incision from the maxillary tuberosity on one side to the opposite one was performed, and a mucoperiosteal flap was raised to obtain the full exposition of the maxillary bone (Figure 2a).

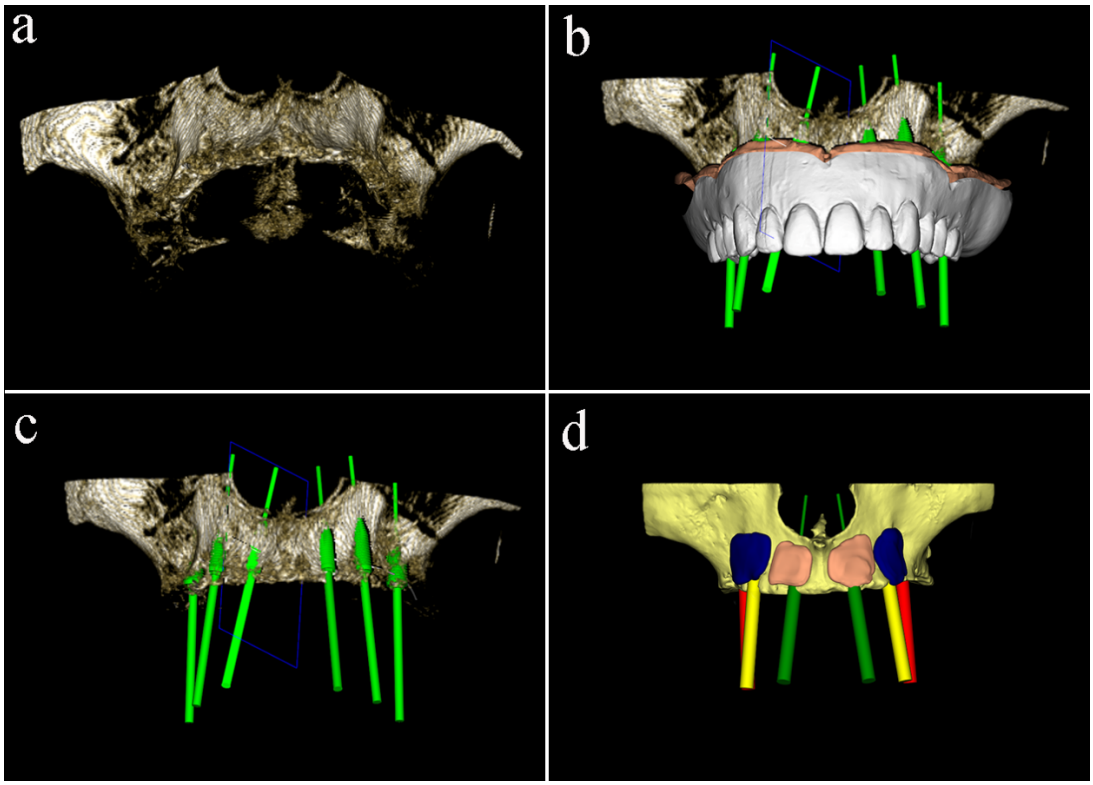

Figure 1. Diagnosis and treatment planning: (**a**) pre-operative cone-beam computed tomography (CBCT); (**b**) virtually planned prosthetic-driven position of the implants; (**c**) bone defects at planned implant sites; (**d**) virtual model of the graft blocks.

After the flap elevation, the cortical plate was perforated with a small round bur to expose the marrow spaces for increasing the migration of osteogenic cells and accelerating revascularization of the graft. The custom-made blocks were placed into planned positions on the maxillary buccal surface and rigidly fixed with titanium screws with caution to not break the grafts. Six immediate provisional implants were inserted to support the temporary denture during the healing period (Figure 2b). Two resorbable porcine collagen membranes (Creos ™ Matricel GmbH, Herzogenrath, Germany) were fixed on the palatal plate using titanium screws to avoid connective tissue ingrowth, which might compromise the integration of the grafts. Blocks and remaining spaces of the recipient site were filled with a mix of particulate deproteinized bovine bone mineral (Creos ™ Matricel GmbH, Herzogenrath, Germany) and autogenous bone chips, previously collected with bone-scraper (Figure 2c). Membranes were stabilized over the augmented area with additional buccal titanium self-tapping screws, to protect and prevent the partial resorption of grafted materials. The flap was coronally advanced through periosteal releasing incisions, adapted, and sutured to achieve tension-free primary closure (Figure 2d). At last, the temporary denture was delivered, fittingly modified, for avoiding any harmful compression on the grafted area, which might jeopardize the integration process.

Medication protocol included administering 875 mg of amoxicillin plus 125 mg of clavulanic acid (Augmentin, GlaxoSmithKline, London, UK) twice daily for 7 days, starting 1 h before surgery. Analgesia was achieved with 400 mg of ketoprofen (Ibifen, Aprilia, Latina, Italy) for a maximum of

three times daily according to individual needs. During the first month postoperatively, patients were instructed to gently clean the surgical area with a soft toothbrush and rinse with 0.12% chlorhexidine digluconate (Corsodyl, GlaxoSmithKline Consumer Healthcare S.p.A., Baranzate (MI), Italy) three times daily.

After six months of uneventful healing, a CBCT was carried out to assess the integration of the grafts, and the second intervention was scheduled for removing titanium screws and positioning implants. In addition, a stereolithographic surgical template was produced.

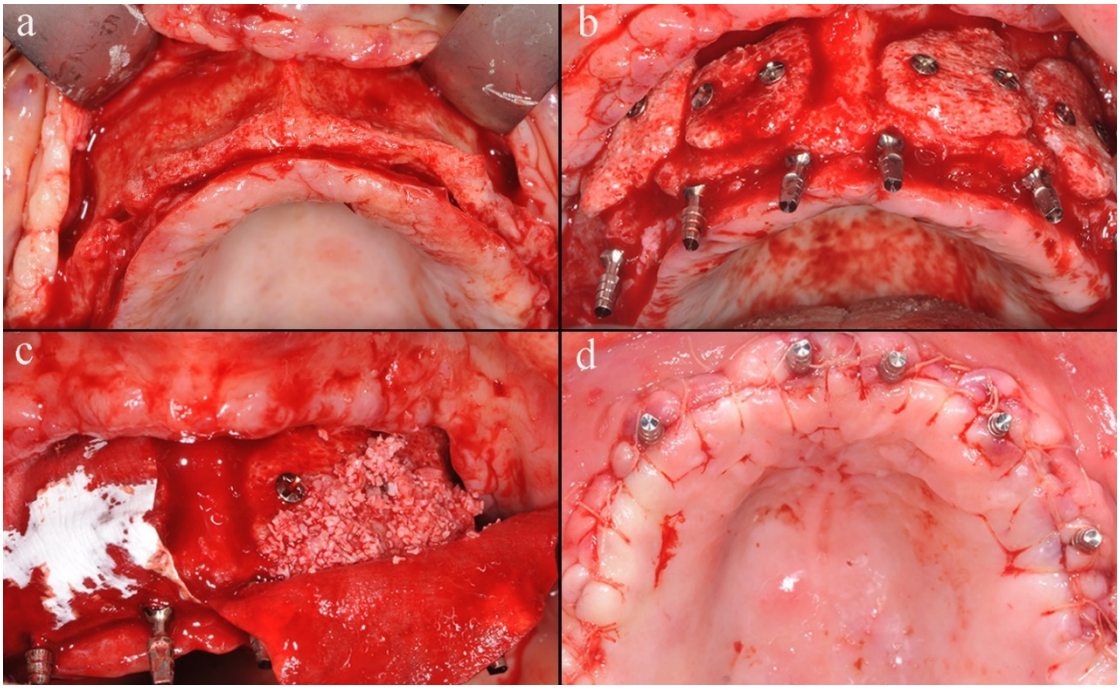

Figure 2. Reconstructive surgery: (**a**) exposition of the maxillary buccal surface after the elevation of the mucoperiosteal trapezoidal flap; (**b**) custom-made blocks fixed into planned positions and six provisional implants insertion; (**c**) grafted blocks and remaining spaces of the recipient site filled with a mix of biomaterial and autogenous bone chips and covered by resorbable membranes; (**d**) suture of the coronally advanced flap.

A full-thickness flap was performed along the same incisions of the reconstructive surgery, the fixation screws were removed (Figure 3a), and bone biopsies were harvested at grafted sites with a trephine bur used from the buccal to palatal aspect.

Six implants were placed at planning sites with the surgical template, and good primary stability was achieved, the healing abutments were connected, for avoiding the uncovering intervention, and the flap was repositioned and sutured (Figure 3b–d). During the osseointegration phase, before implants loading, the patient wore the temporary denture supported by immediate provisional implants.

After 6–8 months, the six immediate provisional implants were removed, and a new full-arch screw-retained temporary prosthesis was delivered. After soft tissue maturation, the definitive prosthetic rehabilitation was performed (Figure 4).

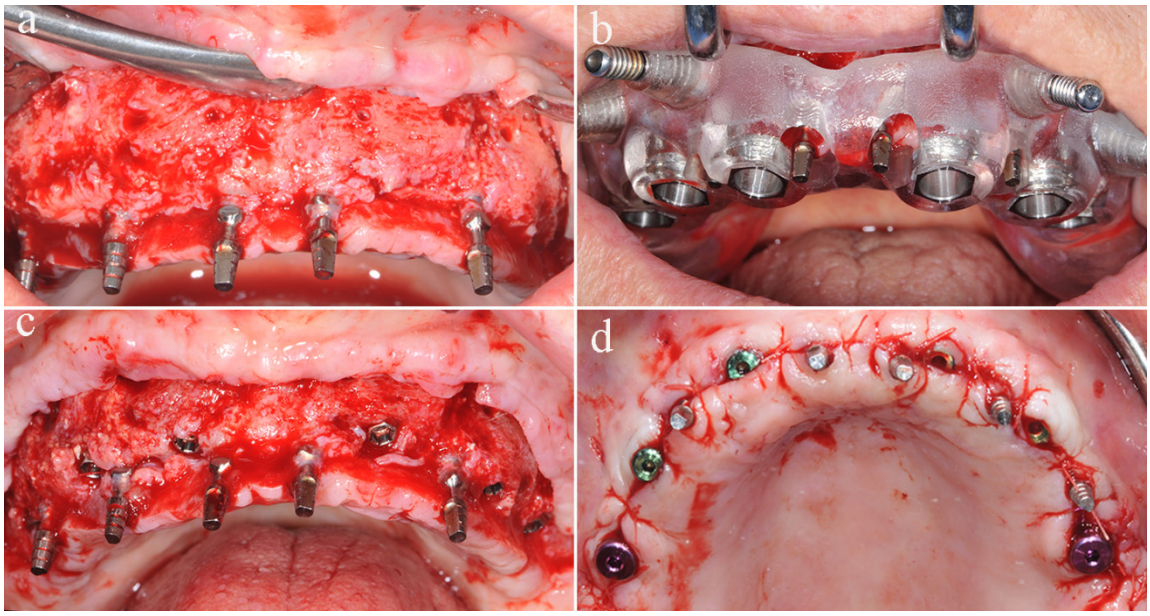

Figure 3. Implants insertion: (**a**) exposition of the grafted maxillary buccal surface after the mucoperiosteal flap elevation and screws removal; (**b**) stereolithographic surgical template in place; (**c**) six implants positioned at planning sites; (**d**) the flap repositioned and sutured around healing abutments.

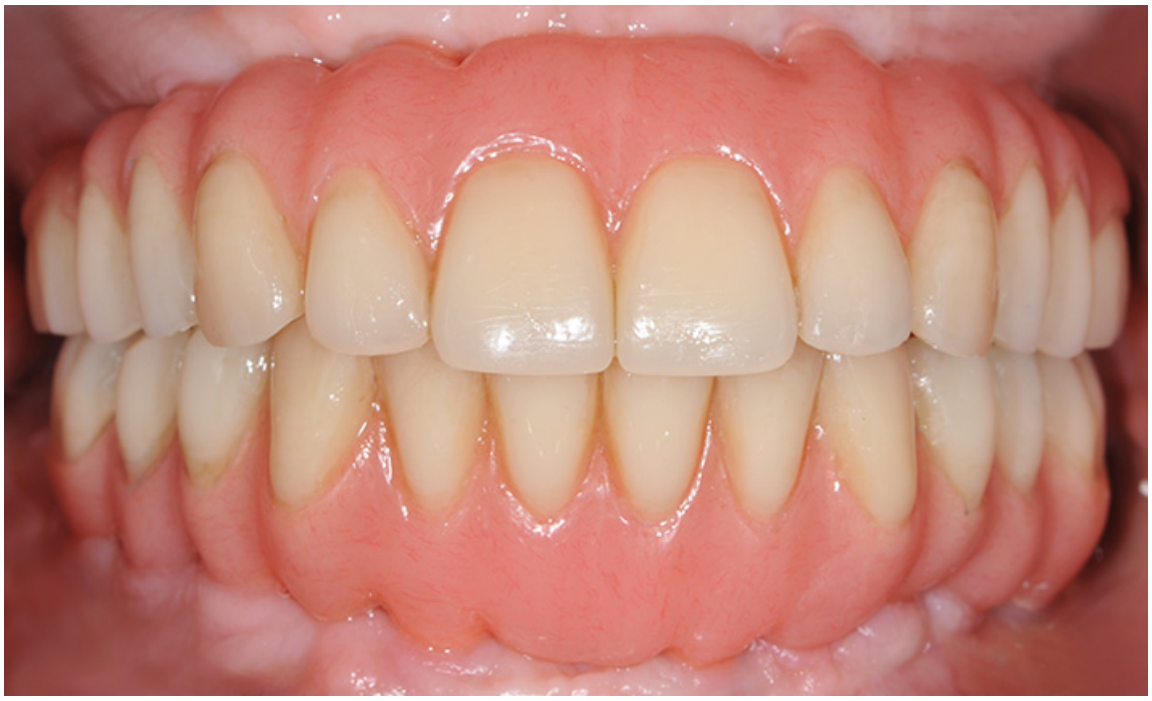

Figure 4. Definitive prosthetic rehabilitation.

3. Results

The CBCT performed at six months after the first intervention of the bone reconstruction showed the integration between the graft and the recipient site and a three-dimensional volume of the alveolar ridge adequate for the placement of the implants (Figure 5).

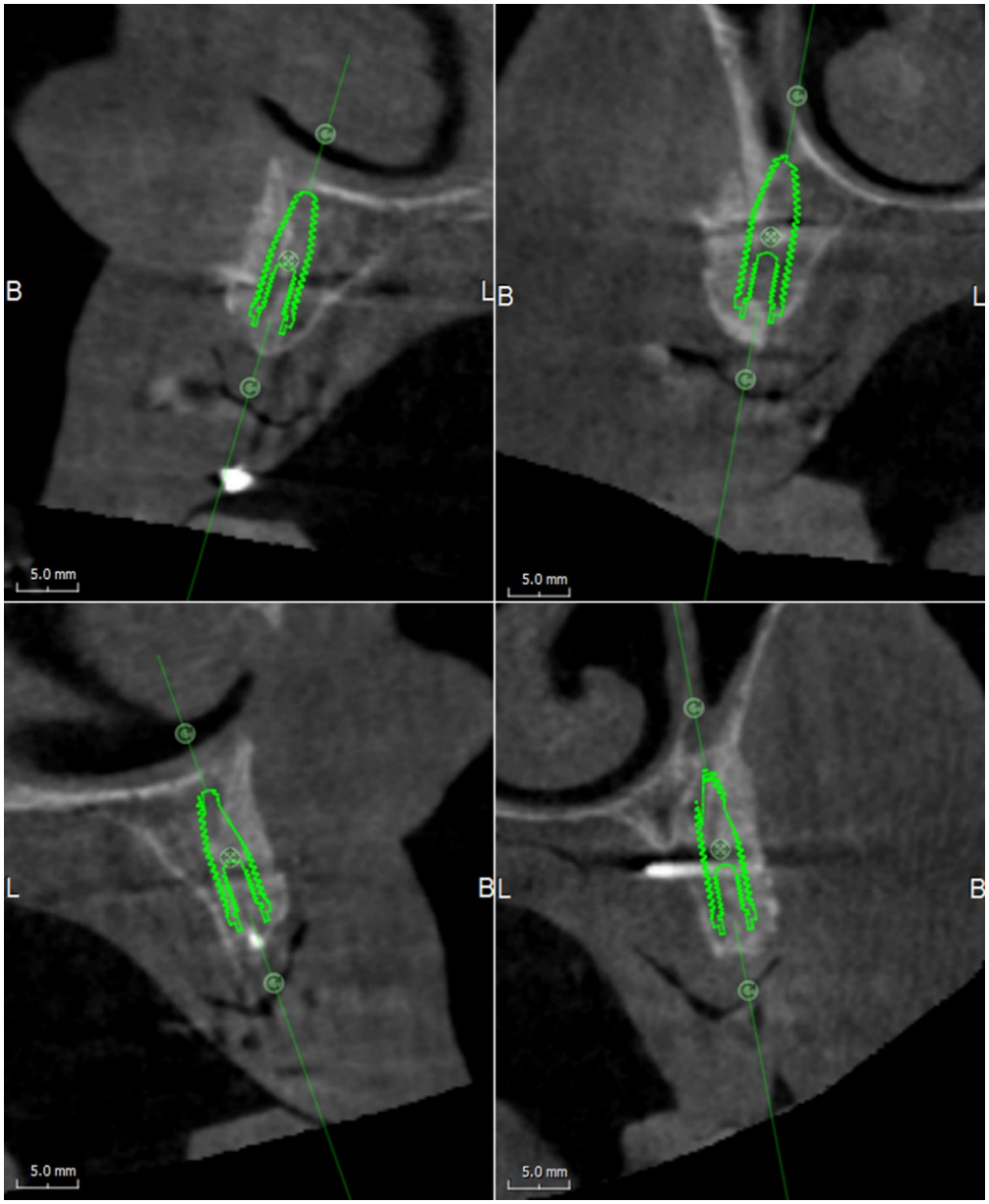

Figure 5. CBCT, performed at six months after reconstructive surgery, shows the integration of grafted blocks at planned implant sites.

At low magnification, the histological analysis showed the specimens consisting of biomaterial block, recognizable by the shape and the regular arrangement of the trabeculae with large marrow spaces representing about 25% of the bone structure. In the marginal portion of the biopsies, only a newly formed bone was detected (Figure 6).

In many fields, biomaterial trabeculae were lined by newly formed bone, showing large osteocytes lacunae embedded into the newly formed bone, which was close to the biomaterial surface (Figure 7a).

The newly formed bone also had a high affinity for dyes and was positive for acid fuchsin. Moreover, in some fields, the biomaterial interface showed a similar affinity when it was close to the newly formed bone (Figure 7b). In these areas, the osteocyte lacunae of biomaterials were colonized by cells (Figure 8a). Close to the biomaterial, osteoblasts depositing osteoid matrix, newly formed bone, and blood vessels were present (Figure 8b). In some portions, the connective tissue, close to the biomaterial, appeared dense with many fibroblasts and without an inflammatory

infiltrate. Resorption or remodeling of the scaffold seemed not related to the presence of osteoclasts or multinucleated cells.

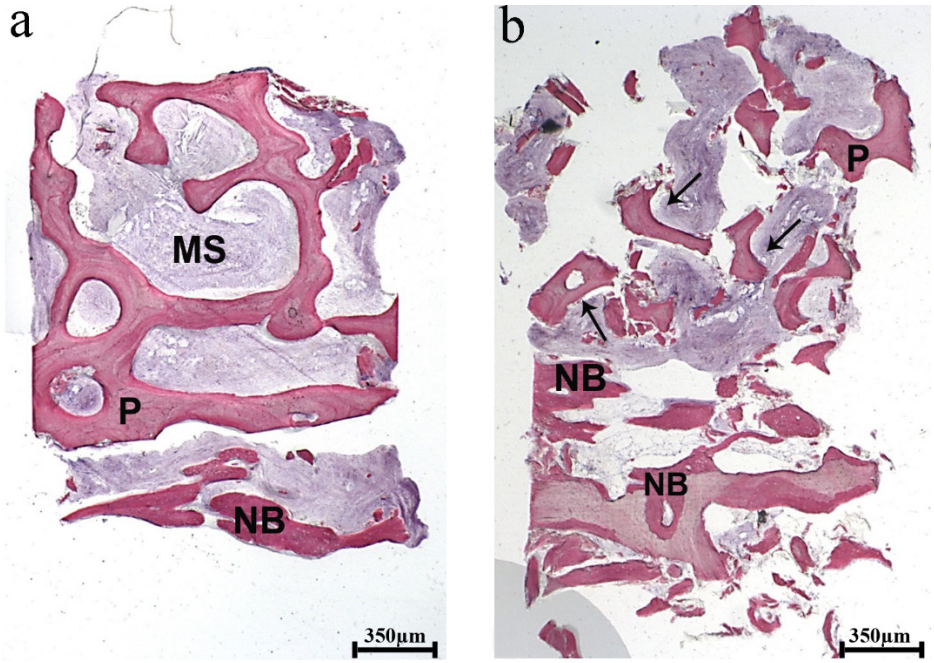

Figure 6. Histologic views: (**a**) light microscopic ground section of the specimen shows the biomaterial block (P), with a regular arrangement of the intact trabeculae. Large marrow spaces (MS) are present. In the marginal portion of the biopsy, only newly formed bone (NB) is observed; (**b**) this sample was damaged during the removal from the trephine bur, and, therefore, a portion of the biomaterial block was fractured (black arrows). The biomaterial (P) appears surrounded by soft tissues. In the marginal portion of the specimen, newly formed bone (NB) is observed. (Acid fuchsin-Toluidine blue 12 X).

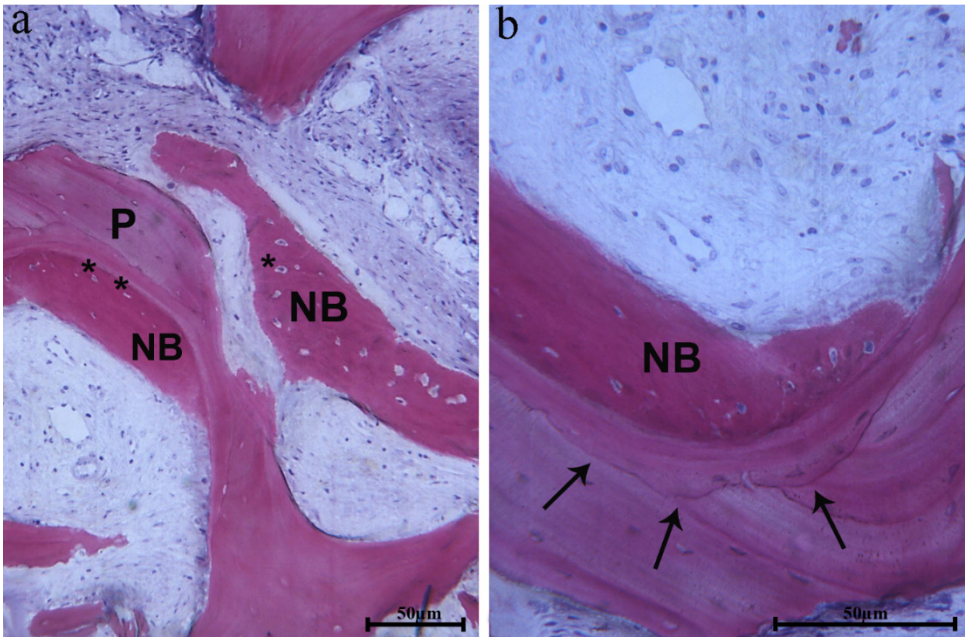

Figure 7. Histologic views: (**a**) newly formed bone (NB), with the presence of large osteocytes lacunae (*) close to the biomaterial particles (P) is observed; (**b**) newly formed bone (NB) and biomaterial interface (black arrows) show a similar affinity for dyes. (Acid fuchsin-Toluidine blue 100 and 200X).

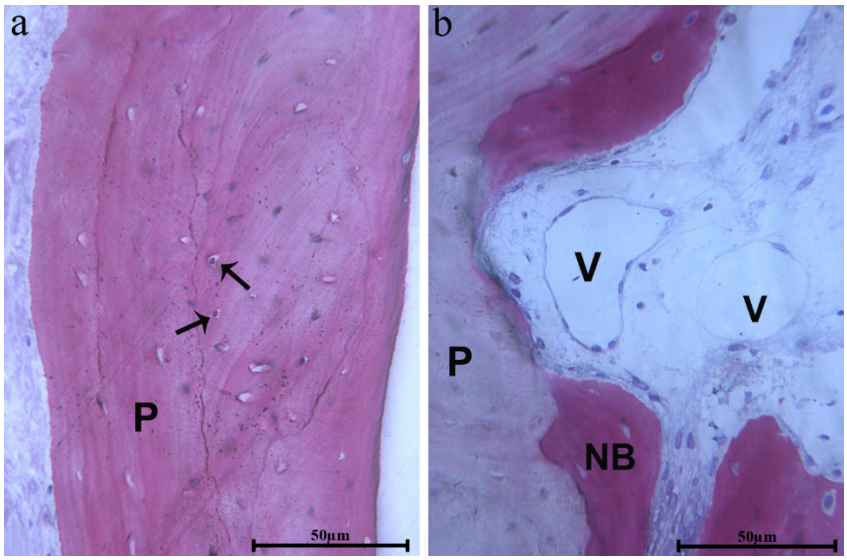

Figure 8. Histologic views: (**a**) some osteocytic lacunae of biomaterial block (P) appear to be filled by cells (black arrows); (**b**) close to the newly formed bone (NB) and biomaterial block (P), many blood vessels (V) are present. (Acid fuchsin-Toluidine blue 200X).

At 2-year control CBCT, no signs of inflammation and bone resorption were observed at the grafted sites and around implants (Figure 9).

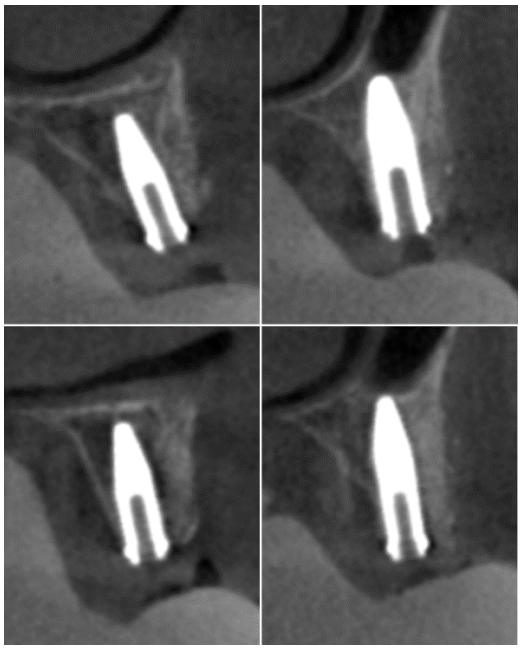

Figure 9. CBCT, performed at a 2-year follow-up, shows no signs of inflammation and bone resorption at the grafted sites and around implants.

4. Discussion

Given the constant updating of surgical bone grafting-techniques, the approach described in this short communication for the reconstruction of horizontal atrophic edentulous maxillae aimed to offer a potential alternative.

In the recent years, the use of bone substitutes in the augmentation procedures has gained attention to overcome the drawbacks of the autogenous bone, including the additional surgery for harvesting,

the risk of donor site morbidity, the limited availability, the possible need of general anesthesia and hospitalization, and the unpredictable graft resorption [20].

An organic bovine bone substitute is one of the best-documented biomaterials, being commercially available in a wide range of products, and its osteoconductive properties and high biocompatibility have been tested in many clinical trials [21,22].

The bovine-derived xenohybrid composite bone has proven to have effective integration and bone regeneration when it is used in oral and orthopedic fields [23]. Its composite structure is based on a deproteinized bovine-derived bone matrix reinforced with biodegradable aliphatic polymers and bioactive agents. The bovine-derived matrix, made of calcium hydroxyapatite (HA, Ca5(PO4)3(OH)), maintains an adequate 3D structure for strength. The biopolymers (poly(L-lactic acid) and poly(e-caprolactone) enhance mechanical properties. The bioactive agents (RGD-containing collagen fragments, obtained by purified gelatin) promote cell adhesion, proliferation, and high hydrophilicity. Furthermore, morphological analysis has shown a well-diffused open-porosity and microstructure comparable in terms of size and cell seeding spaces to human cortical bone.

Furthermore, the possibility to custom-make scaffolds using CAD/CAM technologies speeds up the surgical procedure and limits any potential biological and technical complications. Indeed, the manual cutting and shaping of the blocks and the adaptation at recipient sites during surgery increase the risk of intraoral and extraoral contamination and result in a procedure that is time-consuming and highly dependent on the clinician's skill and experience. Additionally, the size and shape of the conventional bone grafts often are imprecise, and the difficulty of achieving a stable position on the native bone might jeopardize the integration process. Manufacturing of customized block grafts offers some advantages also compared to the grafts manually shaped on the 3D stereolithographic model of patients' jaws. The manual adjustment of the prefabricated block leads to less precise fitting, needs a greater quantity of material, and exposes to a risk of graft infection due to the prolonged contact to possible sources of contamination, such as the gloves of the surgeon, oral fluids of the patient, burs, and other environmental factors [24].

The therapeutic approach using bovine-derived bone blocks combined with 3D-CT and CAD/CAM technologies seems to be promising to overcome the above-mentioned limits of conventional bock grafting procedures.

The use of deproteinized bovine bone, not requiring additional surgery for bone harvesting, avoids the risk of donor sites, reduces postoperative morbidity, and provides an unlimited biomaterial availability.

3D-CT and the surgical planning software allow virtually to analyze the patient's anatomical and prosthetic parameters, to plan the exact implant position and direction, to verify bone defects at implant sites, and to design the graft blocks.

CAD/CAM technologies manufacture on the exact 3D virtual planning models saved in STL files the prefabricated blocks of the xenogenic material, decreasing the amount of graft material required for conventional bone regeneration. Cutting bone substitute blocks into the most appropriate 3D shape facilitates graft adaptation, improves scaffold fitting and stability, and minimizes dead spaces, promoting regeneration [25]. Furthermore, the customization of the graft blocks is less dependent on the clinician's skill and experience and reduces the surgical invasiveness and operating times because the manual shaping of the blocks and its adaptation at recipient sites are not necessary.

The decrease in postoperative morbidity, complications and discomfort at the donor site, the lack of need for general anesthesia and hospitalization, and the shortened treatment period increase patient's acceptance and satisfaction.

Nevertheless, the procedure presents some limitations, such as computer and digital skills, added costs of the biomaterial, and the CAD/CAM manufacturing, and, finally, the preoperative virtual modeling session is time-consuming.

Besides, caution must be used to interpret these results due to the lack of controlled trials and the long-term follow-up to investigate the efficacy of the procedure.

5. Conclusions

The ridge augmentation protocol with custom-made deproteinized bovine bone scaffolds, fabricated using 3D-TC and CAD/CAM technologies, represents a promising alternative for the horizontal atrophic edentulous maxilla reconstruction. Nonetheless, scientific evidence supporting the use of prefabricated xenogeneic block grafts remains minimal, and additional studies with long-term follow-ups of the grafted areas and implants and controlled clinical trials are necessary to validate the procedure.

Author Contributions: I.V. and S.A. contributed to the conception and design of the study and critically revised the manuscript; G.L.M. and M.P.C. contributed to data acquisition, analysis, and interpretation and drafted the manuscript; N.P. contributed to manuscript preparation and to review and editing the manuscript; G.I. contributed to the histological evaluation. All authors gave final approval and agreed to be accountable for all aspects of the work. All authors have read and agreed to the published version of the manuscript.

Funding: This research received no external funding

Conflicts of Interest: The authors declare no conflict of interest.

References

1. Milinkovic, I.; Cordaro, L. Are there specific indications for the different alveolar bone augmentation procedures for implant placement? A systematic review. *Int. J. Oral Maxillofac. Surg.* **2014**, *43*, 606–625. [CrossRef] [PubMed]
2. Chiapasco, M.; Casentini, P. Horizontal bone-augmentation procedures in implant dentistry: Prosthetically guided regeneration. *Periodontology 2000* **2018**, *77*, 213–240. [CrossRef] [PubMed]
3. Tolstunov, L.; Hamrick, J.F.E.; Broumand, V.; Shilo, D.; Rachmiel, A. Bone Augmentation Techniques for Horizontal and Vertical Alveolar Ridge Deficiency in Oral Implantology. *Oral Maxillofac. Surg. Clin. N. Am.* **2019**, *31*, 163–191. [CrossRef] [PubMed]
4. Urban, I.A.; Monje, A. Guided Bone Regeneration in Alveolar Bone Reconstruction Oral Maxillofacial. *Surg. Clin. N. Am.* **2019**, *31*, 331–338.
5. Wessing, B.; Lettner, S.; Zechner, W. Guided Bone Regeneration with Collagen Membranes and Particulate Graft Materials: A Systematic Review and Meta-Analysis. *Int. J. Oral Maxillofac. Implant.* **2018**, *33*, 87–100. [CrossRef] [PubMed]
6. Benic, G.I.; Hämmerle, C.H.F. Horizontal bone augmentation by means of guided bone regeneration. *Periodontology 2000* **2014**, *66*, 13–40. [CrossRef] [PubMed]
7. Lim, G.; Monje, A.; Lin, G.; Chan, H.; Wang, H.-L. Wound Healing Complications Following Guided Bone Regeneration for Ridge Augmentation: A Systematic Review and Meta-Analysis. *Int. J. Oral Maxillofac. Implant.* **2018**, *33*, 50–51. [CrossRef]
8. Garcia, J.; Dodge, A.; Luepke, P.; Wang, H.-L.; Kapila, Y.; Lin, G. Effect of membrane exposure on guided bone regeneration: A systematic review and meta-analysis. *Clin. Oral Implant. Res.* **2018**, *29*, 328–338. [CrossRef]
9. Urban, I.A.; Monje, A.; Lozada, J.L.; Wang, H. Long-term Evaluation of Peri-implant Bone Level after Reconstruction of Severely Atrophic Edentulous Maxilla via Vertical and Horizontal Guided Bone Regeneration in Combination with Sinus Augmentation: A Case Series with 1 to 15 Years of Loading. *Clin. Implant. Dent. Relat. Res.* **2016**, *19*, 46–55. [CrossRef]
10. Annibali, S.; Bignozzi, I.; Sammartino, G.; La Monaca, G.; Cristalli, M.P. Horizontal and Vertical Ridge Augmentation in Localized Alveolar Deficient Sites. *Implant. Dent.* **2012**, *21*, 175–185. [CrossRef]
11. Starch-Jensen, T.; Becktor, J.P. Maxillary Alveolar Ridge Expansion with Split-Crest Technique Compared with Lateral Ridge Augmentation with Autogenous Bone Block Graft: A Systematic Review. *J. Oral Maxillofac. Res.* **2019**, *10*, e2. [CrossRef] [PubMed]
12. Zizzari, V.L.; Zara, S.; Tetè, G.; Vinci, R.; Gherlone, E.; Cataldi, A. Biologic and clinical aspects of integration of different bone substitutes in oral surgery: A literature review. *Oral Surg. Oral Med. Oral Pathol. Oral Radiol.* **2016**, *122*, 392–402. [CrossRef] [PubMed]
13. La Monaca, G.; Iezzi, G.; Cristalli, M.P.; Pranno, N.; Sfasciotti, G.L.; Vozza, I. Comparative Histological and Histomorphometric Results of Six Biomaterials Used in Two-Stage Maxillary Sinus Augmentation Model after 6-Month Healing. *BioMed Res. Int.* **2018**, *2018*, 1–11. [CrossRef] [PubMed]

14. Titsinides, S.; Agrogiannis, G.; Karatzas, T. Bone grafting materials in dentoalveolar reconstruction: A comprehensive review. *Jpn. Dent. Sci. Rev.* **2019**, *55*, 26–32. [CrossRef]
15. Haugen, H.J.; Lyngstadaas, S.; Rossi, F.; Perale, G. Bone grafts: Which is the ideal biomaterial? *J. Clin. Periodontol.* **2019**, *46*, 92–102. [CrossRef]
16. Mangano, F.; Macchi, A.; Shibli, J.A.; Luongo, G.; Iezzi, G.; Piattelli, A.; Caprioglio, A.; Mangano, C. Maxillary Ridge Augmentation with Custom-Made CAD/CAM Scaffolds. A 1-Year Prospective Study on 10 Patients. *J. Oral Implant.* **2014**, *40*, 561–569. [CrossRef]
17. Garagiola, U.; Grigolato, R.; Soldo, R.; Bacchini, M.; Bassi, G.; Roncucci, R.; De Nardi, S. Computer-aided design/computer-aided manufacturing of hydroxyapatite scaffolds for bone reconstruction in jawbone atrophy: A systematic review and case report. *Maxillofac. Plast. Reconstr. Surg.* **2016**, *38*, 2. [CrossRef]
18. Yu, N.; Nguyen, T.; Cho, Y.D.; Kavanagh, N.M.; Ghassib, I.; Giannobile, W. Personalized scaffolding technologies for alveolar bone regenerative medicine. *Orthod. Craniofacial Res.* **2019**, *22*, 69–75. [CrossRef]
19. Cawood, J.I.; Howell, R.A. A classification of the edentulous jaws. *Int. J. Oral Maxillofac. Surg.* **1988**, *17*, 232–236. [CrossRef]
20. Papageorgiou, S.N.; Papageorgiou, P.; Deschner, J.; Götz, W. Comparative effectiveness of natural and synthetic bone grafts in oral and maxillofacial surgery prior to insertion of dental implants: Systematic review and network meta-analysis of parallel and cluster randomized controlled trials. *J. Dent.* **2016**, *48*, 1–8. [CrossRef]
21. Monje, A.; Wang, H. Biological and physical properties of bone block grafting biomaterials for alveolar ridge augmentation. *J. Oral Sci. Rehab.* **2017**, *3*, 18–30.
22. Jo, S.H.; Kim, Y.-K.; Choi, Y. Histological Evaluation of the Healing Process of Various Bone Graft Materials after Engraftment into the Human Body. *Materials* **2018**, *11*, 714. [CrossRef] [PubMed]
23. Grottoli, C.; Ferracini, R.; Compagno, M.; Tombolesi, A.; Rampado, O.; Pilone, L.; Bistolfi, A.; Borrè, A.; Cingolani, A.; Perale, G. A Radiological Approach to Evaluate Bone Graft Integration in Reconstructive Surgeries. *Appl. Sci.* **2019**, *9*, 1469. [CrossRef]
24. Jacotti, M.; Wang, H.-L.; Fu, J.-H.; Zamboni, G.; Bernardello, F. Ridge Augmentation with Mineralized Block Allografts. *Implant. Dent.* **2012**, *21*, 444–448. [CrossRef] [PubMed]
25. Gialain, I.O.; Pinhata-Baptista, O.H.; Cavalcanti, M.G.P.; Cortes, A.R.G. Computer-Aided Design/Computer-Aided Manufacturing Milling of Allogeneic Blocks Following Three-Dimensional Maxillofacial Graft Planning. *J. Craniofacial Surg.* **2019**, *30*, e413–e415. [CrossRef] [PubMed]

smartbone®

integration

Notes from a human histologic study

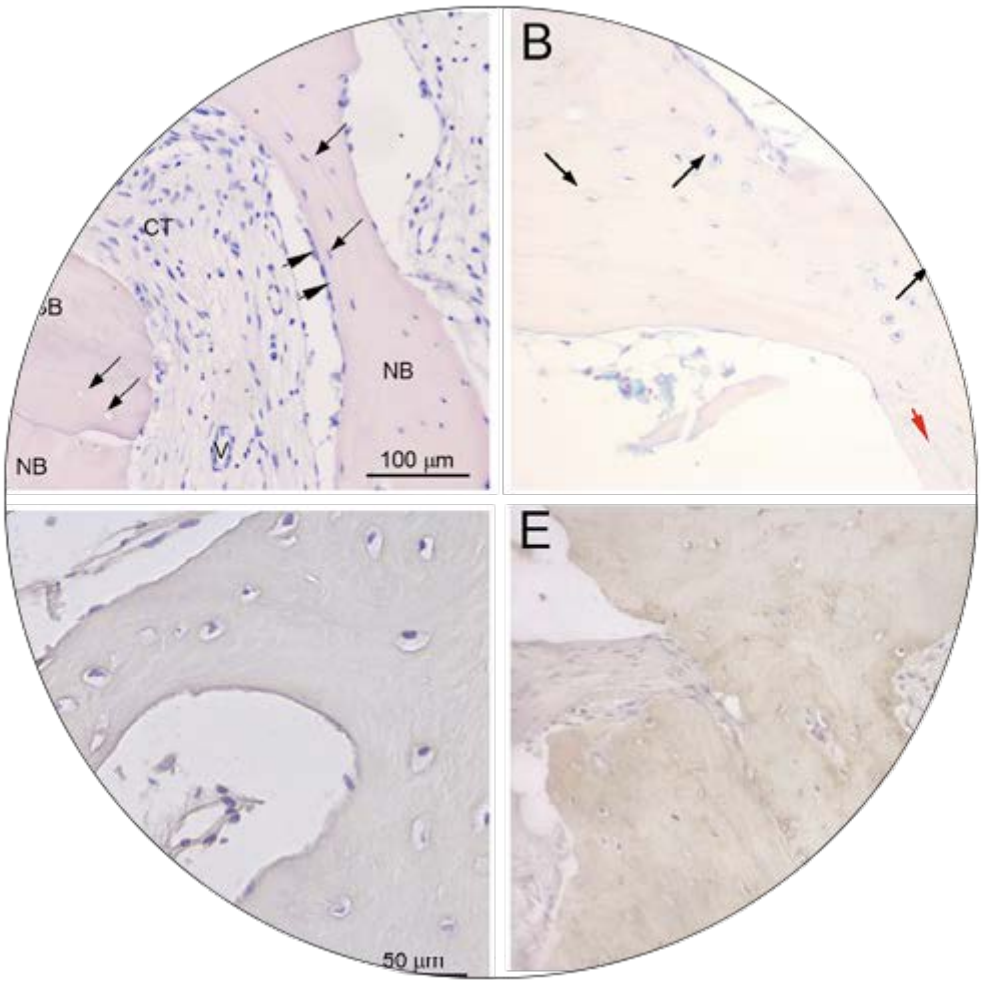

ibi SA industrie biomediche insubri

4 months

Biopsies at 4 months already provide an extensive characterization of the graft substitution, showing a co-existence of SmartBone and newly formed bone. SmartBone is stained with less intensity than new bone and its bone lacunae do not contain any osteocytes, thus allowing its easy identification in the histologic sections, while new bone areas showed osteocytes housed in the bone lacunae and osteoblasts layering at the periphery of new bone grown on SmartBone. Good osteoconductivity is proved also by the presence of well-structured surrounding connective tissue with a rich network of blood vessels, indicating acceptance and integration of the graft material in the recipient site.

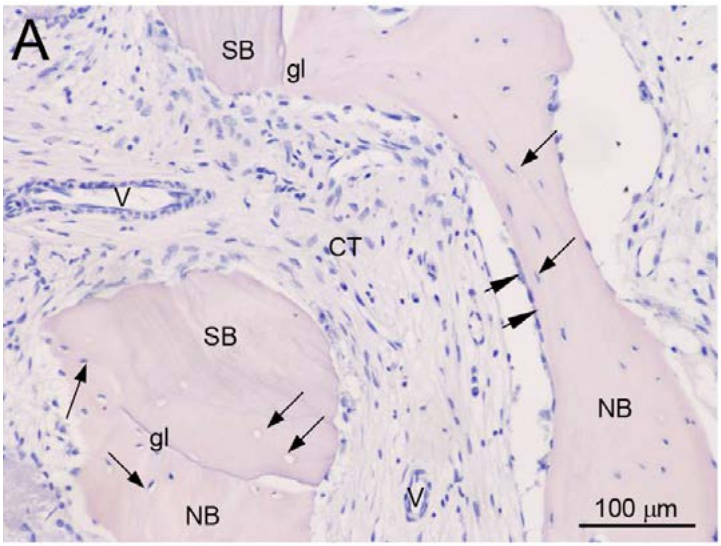

Figure 1: H&E staining of bone biopsy after 4 months from SmartBone grafting. Original magnification 200. NB = new bone; SB = SmartBone; CT = connective tissue; gl = growth line; V = blood vessels; black arrows = bone lacunae; black arrowheads = osteoblasts.

6 months

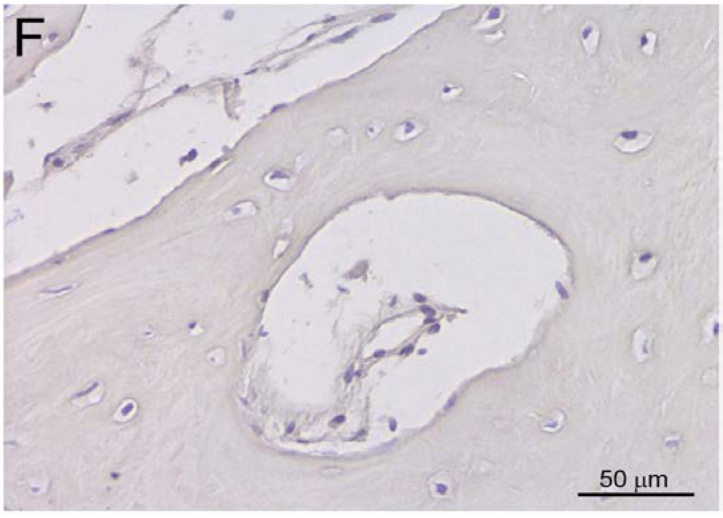

Figure 2: Histological analysis on biopsy after 6 months from SmartBone grafting. Original magnification 400.

From 6 months ahead, SmartBone starts to be completely resorbed and only new bone areas are visible: biopsies clearly show large new bone areas containing osteocytes in bone lacunae, whereas SmartBone particles are extremely rare. In new bone areas, a good positivity for glycoproteins is shown and a strong presence of generic glycosaminoglycans is revealed in the extracellular matrix surrounding the bone lacunae. Comparison with other graft materials indicates that SmartBone is able to accelerate new bone formation.

7 months

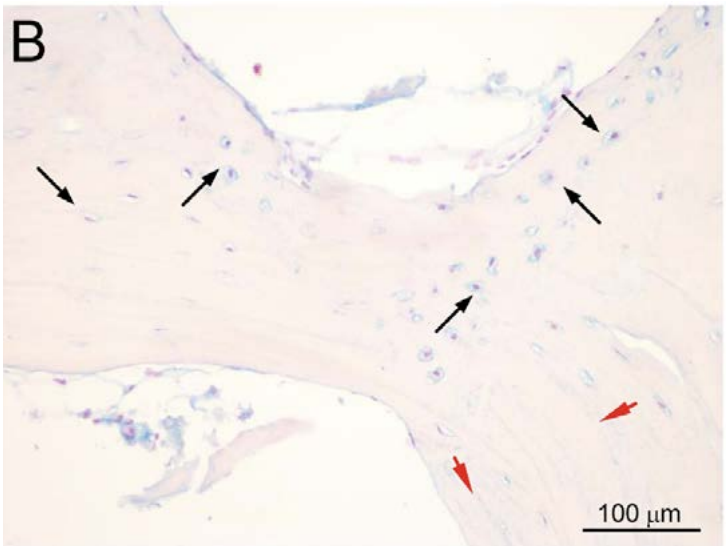

Figure 3: AlcianBlue at pH2.5 on biopsy after 7 months from SmartBone grafting shows generic GAGs in cyan. Original magnification 400. Black arrows=bone lacunae; red arrows = bone scar; black arrowheads = osteoblasts; red arrowheads = bone lamellae.

In the 7-month biopsy, well oriented bone lamellae are visible and the presence of some bone scars, typical of mature bone, can be already seen, much earlier with respect to any other bone substitute. Indeed, SmartBone is already rarely present (1%) as new bone covers almost completely the sample areas with volume percentages of about 80% and connective tissue is reduced to about 19%, proving substitution capabilities similar to those achieved only by using particulate autografts.

9 months

In the 9-month biopsy, new bone areas containing osteocytes in the bone lacunae and many bone scar lines are imaged, while SmartBone is absent: glycoproteins are well expressed mainly in the bone scars, well oriented collagen fibers are detected, collagen type I is observed along the bone lamellae, osteocalcin is well expressed in the bone areas and weak TGF- b1 expression is observed in the cells located along the margin of the bone tissue.

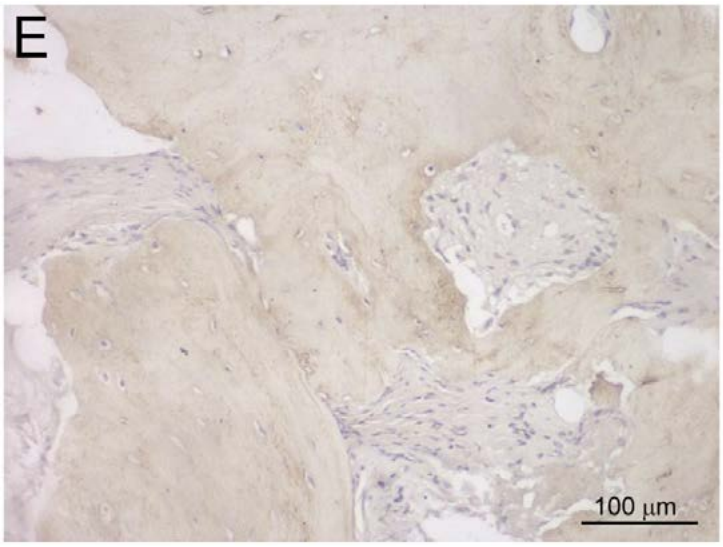

Figure 4: AlcianBlue at pH2.5 on biopsy after 7 months from SmartBone grafting shows generic GAGs in cyan. Original magnification 400. Black arrows=bone lacunae; red arrows = bone scar; black arrowheads = osteoblasts; red arrowheads = bone lamellae.

These findings all confirm complete substitution of SmartBone with new healthy bone that has completed maturity after a fast remodelling process. SmartBone is hence the ideal material for bone regeneration: highly porous, non-immunogenic, biostable until the new tissue formation, bioresorbable and osteoconductive.

All images are taken from: D. D'Alessandro, et al., *Bovine bone matrix/poly(L-lactic-co-ε-caprolactone)/gelatin hybrid scaffold (SmartBone®) for maxillary sinus augmentation: A histologic study on bone regeneration*, Int J Pharmaceut (2016), http://dx.doi.org/10.1016/j.ijpharm.2016.10.036

smartbone®

IBI designed SmartBone following a bottom-up approach: starting from its microstructure that, mimicking natural bone, allows to obtain a device that matches the macroscopic characteristics of a healthy human bone.

KEY FEATURES

A. BIOCOMPATIBILITY

Biocompatibility is a granted feature: all components used in the production of SmartBone are taken only from the market of materials already approved for human use (by both EMEA and US-FDA)!
Furthermore, all the steps of the production process of SmartBone are performed under strict GMP compliance.
All investigations performed under all ISO-10993 standards gave EXCELLENT results, confirming a **VERY HIGH BIOCOMPATIBILITY** of SmartBone.

All *in vivo* investigations and clinical trials gave excellent results, fully confirming the high biocompatibility of SmartBone and its impressive performances.

B. ADEQUATE-SIZED OPEN POROSITY & MICROSTRUCTURE

The first claim of IBI SmartBone is its human-like microstructure, which we evaluated via electron microscopy and microCT scanning.

- **Evaluation Technique and Instruments**

We chose Environmental Scanning Electron Microscopy (E/SEM) as main technique to evaluate SmartBone microstructure and morphology. A top level instrument was chosen to perform these investigations: a Evo 50 EP by Zeiss (Jena, Germany). Furthermore, thanks to the high investigative performances at extended pressure of the available instrument, no metallization nor any other preparatory treatment were needed on the samples prior to investigations.

Thanks to a cooperation with Phoenix|x-ray (a GE company), we performed microCT scans on our SmartBone (applying a VTomEx-s equipment) to investigate geometrical and volumetric properties.

ibi S/A
Via Cantonale 67, CH-6805 Mezzovico Switzerland
t. +41 91 228 01 75 | f. +41 91 220 72 00 | www.ibi-sa.com | info@ibi-sa.com

• Results

The application of our proprietary process produces a composite matrix with a microstructure that, evaluated by E/SEM, has a **strong resemblance with human bone** in terms of open mid-sized porosity.

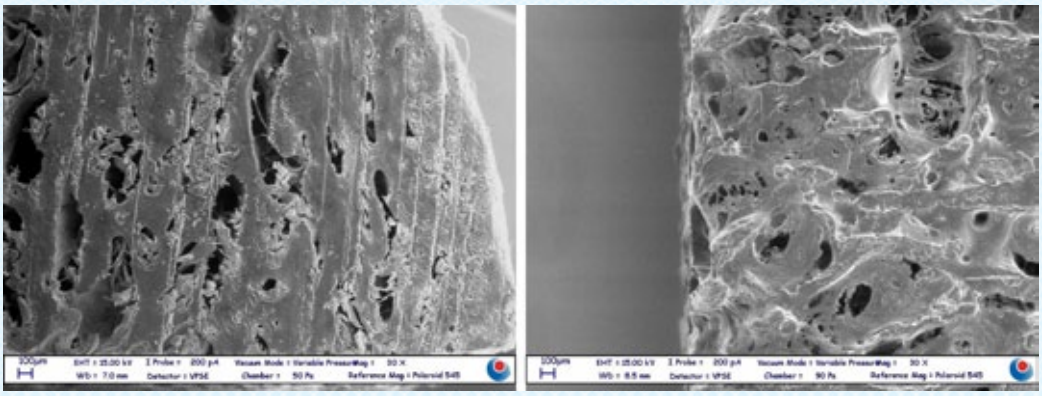

E/SEM images taken at same magnitude of healthy human iliac crest bone sample (left) and IBI SmartBone (right).

Via microCT scanning, we were able to numerically evaluate the average geometrical characteristics of SmartBone: free volume (**ε, i.e. the degree of porosity**) and the surface/volume (s/v) ratio, resulting **ε=27%** and s/v = 4,46mm^{-1}, respectively.

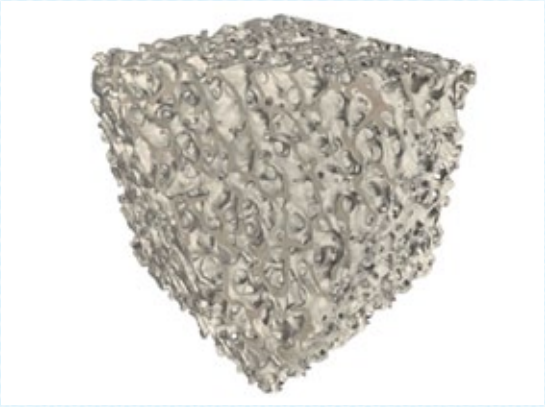

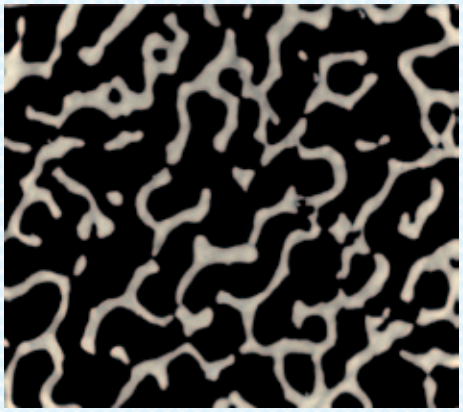

Thanks to microCT scans, a 3D render of an IBI SmartBone was obtained via digital reconstruction (left) and IBI SmartBone open and interconnected porosity was easily confirmed: a typical microCT scan slide of an IBI SmartBone allows also evaluating volumetric parameters (right: a randomly taken scan from a 8x8x8 mm SmartBone block, used to fit the analytic chamber).

• Regularilty of pieces

Many bone substitutes available on the market show an inner variability due to their natural origin. Pieces from the same lot may, indeed, have different microstructure, higher/lower porosity, different density and highly variable physical and mechanical properties.

IBI's process was developed to obtain a smart biomaterial starting from a naturally derived mineral matrix and reinforcing it with biopolymers. Reducing this naturally occurring variability was one of IBI aims: **with SmartBone we now offer regular and homogeneous bone substitutes.**

C. HIGH MECHANICAL PERFORMANCES

Mechanical handling and performances of bone grafts during surgical maneuvering are tremendously essential features! Grafts are, indeed, expected to undergo heavy stresses and loads as far as they need to be shaped and cut before being placed. Furthermore they need to withstand drilling to allow the placement of osteosynthesis screws which must remain toughly in place, offering a solid mechanical bond to host tissue: the better the mechanical stability and the higher the surface contact with the host tissue, the higher and better the integration achieved. Hence, Smartbone mechanical characteristics can be summarised as follows:

- composite mechanical behaviour: both rigid and elastic
- adequately high elastic modulus
- extreme load bearing resistance
- dust and debris free shaping
- capability to withstand precise shaping
- tenacity to fixation screws
- hammering and heavy surgical manoeuvring resistance

• Mechanical testing and instrumentation

A commonly used way to assess the mechanical behaviour of a bone substitute is the monoaxial compression test, which allows calculating maximum stress resistance (breaking stress) and Young's modulus (i.e. elastic module). Vertical compression tests on 10x10x10mm SmartBone blocks were performed using a calibrated MTS 858 MiniBionix.

To make this test more realistic, both dry and deeply wet SmartBone cubes were used, as far as the surgical field is bloody (hence wet) and almost all surgeons tend to dip bone grafts into hot patients' blood for some 20-30 minutes in order to have it absorb as much blood as possible (this widely used surgical practise is based on the evidence that blood starts coagulating inside the graft and thus several growth factors and biochemical signalling molecules are released, finally enhancing and speeding up graft integration once placed into target host site.

• Results

SmartBone showed the typical behaviour of an open porous structure where, under increasing load, a first pseudo-linear and pseudo-elastic behaviour, due to structural resistance, is followed by oscillating behaviour due to progressive breakage of structure and consequent compacting of matrix. Structural breakage is evidently and easily evaluated at maximum load bearing point and this allowed to compute the equivalent maximum stress (about **32MPa**), which was calculated on the full equivalent section (1 sq cm). This behavior is shared with all naturally derived bone grafts, being all of them porous, but with the highly relevant difference of the **tremendously higher performances owned by SmartBone, both at wet and dry state** (no differences were showed in any mechanical performance between dry and wet state)!

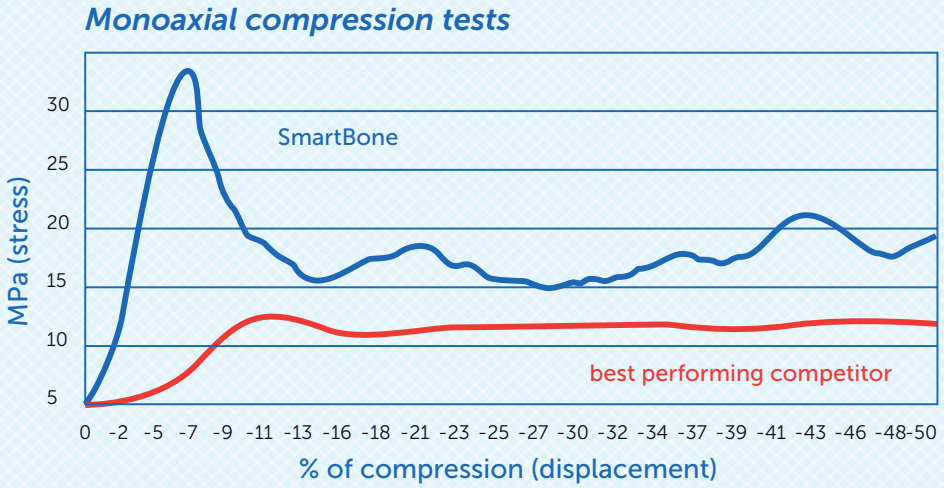

During comparative compression tests, IBI SmartBone (blue plot) showed off all its mechanical performances, being capable to withstand 3 times the maximum load borne by the best performing competitor (red plot) and being 4 times more rigid! (displacement [%] versus stress [MPa] is plotted according to compressive convention).

- **Shaping resistance**

Moreover, further qualitative mechanical investigations showed the capability of **very precisely shaping by common surgical instruments**, the absence of powder and debris formation during handling and a **very high resistance to screws** and fixation maneuvers.

D. HIGH HYDROPHILICITY

Thanks to its microcomposition, SmartBone shows an extremely high hydrophilicity, being capable to quickly (less then 60 mins) reach a **38% $^{w}/_{w}$ swelling ratio** (mass test performed in PBS and dynamic assessed using a Mettler-Toledo 4 decimals calibrated scale).

This extremely good feature was evidently confirmed also during clinical studies where a **very high capability to absorb and retain blood once in situ** was observed.

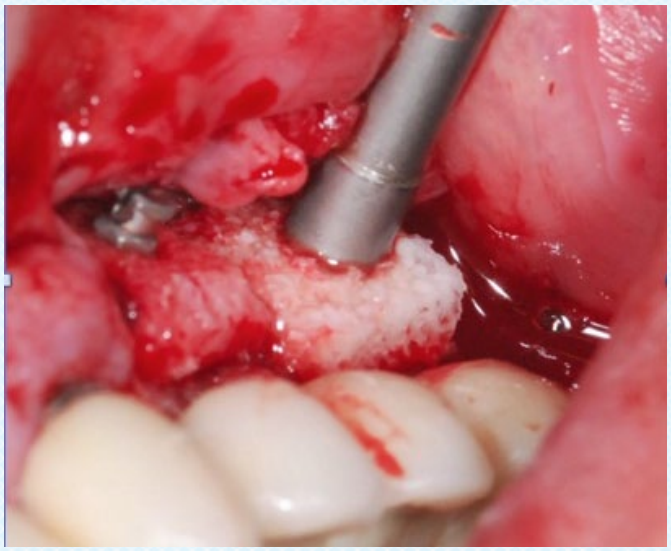

Hydrophilicity is a clinical essential feature: indeed, as said, it is a scientific and clinical evidence that, if the blood is soken up by the graft coagulating inside of it, several growth factors and biochemical signalling molecules are released, hence enhancing and speeding up graft integration once placed into target host site.

A hand-shaped SmartBone block quickly absorbs patients blood once placed in situ in direct contact with a bloody substrate (the graft was, on purpose, placed without having being previously soaked into patients blood).

ibi S/A

Via Cantonale 67, CH-6805 Mezzovico Switzerland
t. +41 91 228 01 75 | f. +41 91 220 72 00 | www.ibi-sa.com | info@ibi-sa.com

E. HIGH TISSUE INTEGRATION

A robust physiological integration into host tissues is an essential feature for a bone substitute. In addition to all ISO10993 compulsory investigations, we assessed *in vitro* citocompatibility and cell viability using both standard line cells and human adipose tissue derived mesenchymal stem cells (HatMSCs). Biological and histological investigations showed how **SmartBone is a very supportive substrate for cell adhesion and growth**; HatMSCs showed *in vitro* capability to properly colonize the scaffold and, once induced, to differentiate!

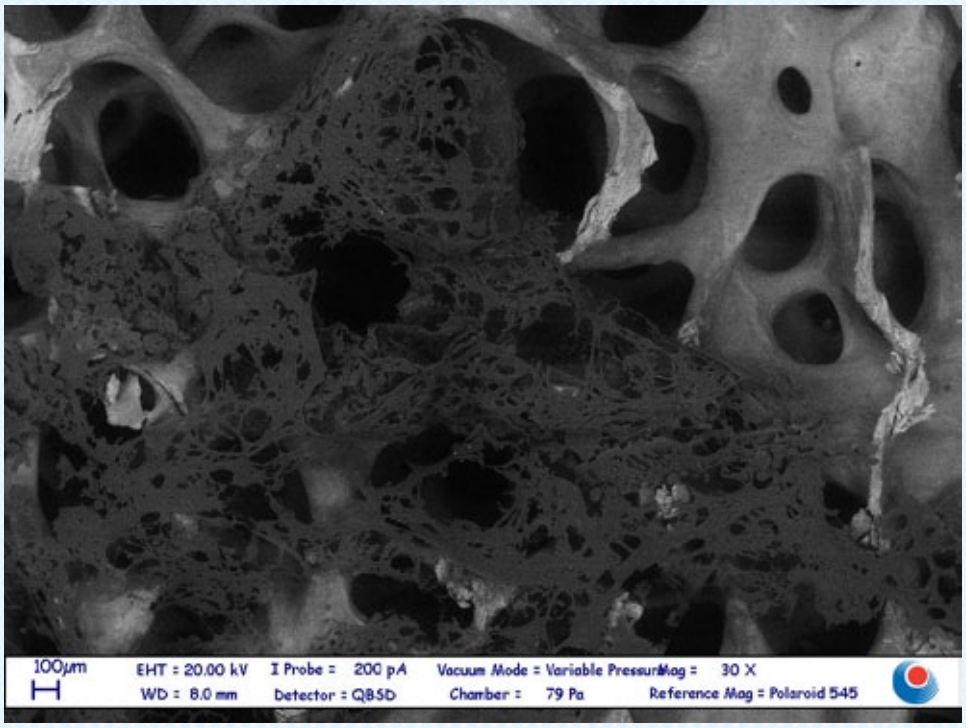

Electronic microscopy image of a "slice" of SmartBone during cell colonization *in vitro* tests. The analysis evidenced the presence of wide and well structured cell formations ins SmartBone, whose micro-structure and composition favor cell colonization already after only 7 days.

In vivo studies were performed to assess osteointegration on a 4 months observation timeframe. Histological analysis proved confirmation of **SmartBone integration, with natural bone formation** and cells and vessels colonizing pores within it during time.

Summarizing, SmartBone main biological features are:

- high cell viability and proliferation support,
- high osteoinduction, conduction and integration.

F. CLINICAL PERFORMANCES

SmartBone is a **bone substituted intended and specifically developed for bone regeneration applications**. SmartBone has been used by surgeons in oral and maxillofacial surgery, allowing **impressive performances** and giving **great results**.

ibi S/A

Via Cantonale 67, CH-6805 Mezzovico Switzerland
t. +41 91 228 01 75 | f. +41 91 220 72 00 | www.ibi-sa.com | info@ibi-sa.com